
**UNIVERSITÀ DEGLI STUDI DI MILANO**

FACOLTÀ DI SCIENZE E TECNOLOGIE

Department of Physics
Bachelor Degree

# Progress towards the reconstruction of the nuclear energy functional from the inverse Kohn Sham method

Supervisor:
**Prof. Gianluca Colò**

Co-supervisor:
**Dr. Francesco Marino**

Candidate:
**Alberto Liardi**

Matriculation number:
**932198**

Academic year 2020-2021

# Contents

**List of Figures** iv

**Introduction** 1

**1 Nuclear Physics fundamentals** 3
- 1.1 Nuclear structure and bulk properties . . . 3
- 1.2 Nuclear models . . . 8
  - 1.2.1 Liquid drop model . . . 8
  - 1.2.2 Harmonic oscillator . . . 9
  - 1.2.3 Shell model . . . 10
  - 1.2.4 Beyond the shell model . . . 11

**2 The direct and inverse problem of the DFT** 13
- 2.1 Density Functional Theory . . . 13
  - 2.1.1 Hohenberg and Kohn theorems . . . 14
  - 2.1.2 $N-$ and $v-$representability . . . 17
  - 2.1.3 Kohn-Sham equations . . . 18
- 2.2 Inverse DFT problem . . . 20
  - 2.2.1 Well-posed problems . . . 20
  - 2.2.2 Kohn Sham inverse problem . . . 22

**3 Nuclear potentials from the Constrained Variational method** 26
- 3.1 CV implementation . . . 26
  - 3.1.1 CV for spherical symmetric systems . . . 26
  - 3.1.2 Radial functions scaling . . . 28
  - 3.1.3 Numerical implementation . . . 30
- 3.2 Nuclear potentials from the Constrained Variational method . . . 31
  - 3.2.1 $^{16}$O . . . 32
  - 3.2.2 $^{40}$Ca . . . 33
  - 3.2.3 $^{208}$Pb . . . 34
- 3.3 Comparison between canonical and non canonical Kohn-Sham orbitals . . . 35

**4 Reconstruction of nuclear Energy Density Functional** 41
- 4.1 A function integration formula: from potential to energy functional . . . 41
  - 4.1.1 Density scalings . . . 42
  - 4.1.2 Stray and non stray potentials . . . 45
- 4.2 Purpose of the work . . . 45
- 4.3 Preliminary tests . . . 46
- 4.4 $\lambda-$scaled orbitals and physical interpretation . . . 50

4.5 EDF from simple nuclear potentials . . . 53
4.5.1 SkX $^{16}$O model . . . 54
4.5.2 $(t_0, t_3)$ $^{16}$O model . . . 57
4.6 Critical discussion . . . 61
4.7 Constrained Hartree-Fock calculations . . . 63

**Conclusions** **66**

**A Elements of Functional Analysis** **68**

**B Detailed calculations of the CV method** **70**
B.1 Kinetic functional . . . 70
B.1.1 Functional with scaled variables . . . 70
B.1.2 Kinetic gradient and Hessian . . . 71
B.2 Constraints . . . 72

**C Relation between $\mu-$ and $\lambda-$scaling** **74**

**Bibliography** **75**

# List of Figures


1.1 Binding energy per nucleon. For nuclear masses above 40-50 the average binding energy shows an almost constant behaviour around 8 Mev; this is related to the saturation of the nuclear force. . . . . 4
1.2 Nuclear SkX densities computed with the Hartree-Fock method. The density first shows a plateau, which ranges from 1 to 5 fm depending on nuclear masses, then decreases exponentially for radii corresponding to the nuclear surface. . . . . 6
1.3 Representation of the energy levels of the shell model. It is possible to see wide gaps between some of the energy levels, which correspond to magic numbers and stable nuclei. . . . . 12

2.1 Example of an inverse crime in a harmonic oscillator simulation. The ground state density of the harmonic oscillator is computed numerically using a fourth-order approximation to the laplacian and zero boundary conditions, and the potential is evaluated using the same laplacian finite difference approximations. This provides an inverse crime. . . . . 21

3.1 $^{16}$O SkX neutron density computed by Hartree Fock method. . . . . 32
3.2 (a) $^{16}$O neutron potential from the inversion of the SkX density (IKS), compared to the Hartree-Fock potential (HF). (b) $^{16}$O neutron difference between IKS and HF potentials. . . . . 33
3.3 (a) $^{40}$Ca neutron potential from the inversion of the SkX density (IKS), compared to the Hartree-Fock potential (HF). (b) $^{40}$Ca neutron difference between IKS and HF potentials. . . . . 34
3.4 $^{208}$Pb proton potential from the inversion of the SOG density (IKS), compared to the Woods Saxon potential (WS). . . . . 35
3.5 $^{16}$O $\{u_k(r)\}$ functions before the diagonalisation of the $(\epsilon_{ij})$ matrix, computed both through IKS and HF method. IKS orbitals are evaluated with two different values of $R_2$: 9.8 and 11 fm. . . . . 36
3.6 $^{16}$O $\{u_k(r)\}$ functions after the diagonalisation of the $(\epsilon_{ij})$ matrix, computed both through IKS and HF method. IKS orbitals are evaluated with two different values of $R_2$: 9.8 and 11 fm. . . . . 37
3.8 $^{40}$Ca $s$ orbitals after the diagonalisation of the $(\epsilon_{ij})$ matrix, computed both through IKS and HF method. IKS orbitals are evaluated with two different values of $R_2$: 11 and 12.1 fm. . . . . 38
3.7 $^{40}$Ca $\{u_k(r)\}$ reduced radial functions before the diagonalisation of the $(\epsilon_{ij})$ matrix, computed both through IKS and HF method. IKS orbitals are evaluated with two different values of $R_2$: 11 and 12.1 fm. . . . . 39

4.1 Energy density functional computed from Eq. (4.21) (Theoretical) and Eq. (4.5) (t-scaling), using a constant density $\rho(r)$. The parameters are: $a = 3000$ MeV fm$^6$ and $b = 3$ fm$^{-3}$. . . . . 48
4.2 Energy density functional computed from Eq. (4.21) (Theoretical) and Eq. (4.5) (t-scaling), using a Fermi function density $\rho(r)$. Chosen parameters are: $a = 5000$ MeV fm$^6$, $b = 50$ fm$^{-3}$ , $c = 0.5$ fm, and $R_c = 10$ fm. . . . . 49
4.3 20-particle HO $\{u_k(r)\}$ reduced radial functions computed from the IKS approach of the non scaled ($\lambda = 1$) and scaled system ($\lambda = 0.6$). *theor* represents the scaling Eq. (4.34) applied directly to the analytical expression of HO wave functions (Eq. (4.36)). . . . . 52
4.4 (a) 20-particle HO potentials of the non scaled system, computed from the IKS approach and the analytical form of the potential. (b) 20-particle HO comparison between potentials of the non scaled and scaled system with $\lambda = 0.6$. These last are evaluated both using the IKS approach (IKS $\lambda = 0.6$) and applying the $\nu-$scaling of the form $\nu_\lambda = \lambda^2\nu$ to the analytical expression of the potential. A comparison is made with the non scaled potential (IKS $\lambda = 1$). . . . . 53
4.5 Simulations regarding $^{16}$O nucleus. In the top panel are presented the system densities $\rho_\lambda(r)$ based on SkX interaction and subjected to the $\lambda-$scaling for different values of $\lambda$. In the bottom panel the scaled potentials associated to such densities are shown. . . . . 54
4.6 $^{16}$O nucleus simulations based on SkX interaction. (a) Potential energy difference $\Delta U$. (b) Kinetic energy difference $\Delta T$, calculated both from the theoretical scaling $T^\lambda = \lambda^2 T$ and from the IKS approach. (c) Total energy difference $\Delta E = \Delta T + \Delta U$. . . . . 56
4.7 $^{16}$O nucleus simulations based on the $(t_0, t_3)$ model without Coulomb interaction. (a) Potential energy difference $\Delta U$ computed with the IKS approach and the theoretical knowledge of the EDF. (b) Kinetic energy difference $\Delta T$, calculated both from the theoretical scaling $T^\lambda = \lambda^2 T$ and from the IKS approach. (c) Total energy difference from the IKS approach. (d) Total energy difference from theoretical calculations by using Eq. (4.44). . . . . 59
4.8 $^{16}$O $(t_0, t_3)$ scaled potentials for different values of $\lambda$. The IKS potentials are evaluated by applying the CV method to the scaled density $\rho_\lambda(r)$ of the system, whereas Theoretical scaled potentials are computed employing $\lambda-$scaling inside the analytical expression of the potential (4.50). . . . . 60
4.9 Comparison between the potential energy difference $\Delta U$ computed from CHF calculations and from Eq. (4.4) for $^{16}$O nucleus with $(t_0, t_3)$ interaction. . . . . 64
4.10 $^{16}$O nucleus CHF simulations based on the $(t_0, t_3)$ model without Coulomb interaction. (a) Potential energy difference $\Delta U$. (b) Total energy difference $\Delta E$ as a function of $\mu$. (c) Total energy difference $\Delta E$ as a function of $\langle r^2 \rangle$. . . . . 65

# Introduction

Nuclear systems have been studied for a long time. However, a unified understanding of structure, reactions and decay properties has not been achieved yet. This is due mainly to the fact that the nucleus is a strongly correlated many-body system, and also to the incomplete knowledge of the interaction which takes place among its constituents. Approximations of such interactions have been suggested and are nowadays used. Nevertheless, they involve numerous terms which still make the treatment of the system an intricate procedure. To make the matter even more complicated, the nucleon-nucleon interaction is also non fundamental, as it derives from QCD. Moreover, there exists a very large number of stable nuclei ($\approx 250$), each displaying many observables associated with their static properties, their excitation spectra, their response to external fields and their decays.

One of the aims of nuclear physics is then to build a model able to properly describe the nucleus; thus, different methods and approaches have been suggested so far. Of great importance are the mean-field models, which describe each nucleon inside the system as if it were an independent particle subject to an effective potential generated by the other particles. Under this perspective the problem is then translated into finding a suitable potential.

Even though the empirical potentials, which are often employed in mean-field methods, are composed of numerous parameters which derive from fits of phenomenological data, this is not the only way to evaluate such potentials. In this work we make use of Density Functional Theory (DFT) in the Kohn-Sham (KS) scheme, as this framework guarantees, in principle, the existence of an exact effective potential for any fermion system.

The core of DFT consists in expressing physical observables as functionals of the one-body density. The mathematical foundations of this approach have been introduced by Hohenberg and Kohn by two theorems that take their names: the former states that there is a one-to-one correspondence between the single-particle potential and the density of the system; from here, every expectation value can be seen as a functional of the density. Instead, the second theorem implies that we can calculate the ground state energy of a system through a variational procedure in terms of the density.

Thanks to the first theorem, DFT can be either employed to find the system density from the knowledge of the potential (direct problem of DFT), or to compute the potential from a given density (inverse problem of DFT). Inverse DFT problems have been somehow less explored that the direct ones, but are becoming increasingly important in recent times. In this case, the density of the system is assumed to be known, be it observed experimentally or computed from *ab initio* methods. The effective potential of the system, and possibly the energy density functional (EDF), is deduced.

The objective of this work is to devise and test an approach along this line, valid for

nuclear systems. The procedure we follow is based on reconstructing the EDF from the knowledge of the system potential, by pursuing a line-integration over a path of scaled densities, which can be physically seen as perturbations of the ground state. The advantage of the approach we present is that the potential taken into consideration does not have to be written in a closed form, but can be found numerically through the inverse problem of the DFT. In particular, we compute such potential using a constrained minimisation procedure called Constrained Variational (CV): in this context the potential arises as the Lagrange multiplier associated to a constraint.
In this work we have focused on the first application of such procedure in the case of nuclei with simplified interactions. In particular, the structure of this work is the following: in Chap. 1 we recall some basic notions of nuclear physics, Chap. 2 is instead focused on the DFT, analysing the two Hohenberg-Kohn theorems and presenting different implementations to solve the inverse DFT problem. In Chap. 3 we describe the CV method implementation for spherical nuclei, and show nuclear potentials computed with this model. Eventually, in Chap. 4 we show our approach by discussing the theoretical background and presenting some preliminary results for real nuclei.

# Chapter 1

# Nuclear Physics fundamentals

In the following sections we briefly recall the main concepts of nuclear physics, focusing in particular on the nuclear structure, the bulk nuclear properties, and the principal nuclear models.

## 1.1 Nuclear structure and bulk properties

The innermost part of the atom is called nucleus: it is a system formed of protons and neutrons, which are generically referred to as nucleons.
Nuclei differ from one another due to their particle compositions: it is then useful to introduce the nuclear mass number $A$, which indicates the total number of nucleons, seen as the sum of $Z$ protons and $N$ neutrons. Although these two kinds of particles are very similar as for their masses and dimensions, they differ in electrical charges: protons have positive charge, while neutrons are neutral.
The practical approach to study nuclear properties is not straightforward: while an atom usually has a radius of $\sim 10^5$ fm, a generic nucleus diameter is of the order of few fm. These extremely small scales make it difficult to probe the nuclear structure as it is otherwise done in atomic physics: if, on the one hand, atomic properties are usually studied through spectroscopic experiments, on the other hand in the nuclear case scattering experiments are the ones which have brought the most important results [1] [2]. It was indeed Rutherford's scattering experiment in 1911 [3] that led to the birth of nuclear physics.

In order to study a nuclear system, theoretically we could apply Schrödinger equation to the $A$ particles which constitute the nucleus, find energies and eigenstates, and from there compute all physical quantities.
Although it looks quite straightforward, this approach is infeasible. The high number of degrees of freedom makes the nucleus a many-body problem that cannot be solved exactly; moreover, interactions among nucleons have numerous terms and are still not fully known. This complexity and the interplay of different energy scales explains why a variety of models has been developed to investigate distinct aspects of the nuclear structure.

In the next paragraphs we introduce some relevant observables for the study of the nucleus.

**Binding energy:** For any nuclear system we can define the binding energy as:

$$B.E. = M(A,Z) - Zm_p - Nm_n \tag{1.1}$$

where M(A,Z) is the mass of the whole nucleus with $A$ nucleons and $Z$ protons, whereas $m_p$ and $m_n$ are the masses of a proton and a neutron, respectively.
Of particular interest is the study of bound states: in such systems the binding energy must be negative, otherwise the system would simply unbind itself in order to minimise its energy. Indeed, looking at Eq. (1.1), we see that the difference between the nucleus mass and the total mass of its components is what gives stability to the system, since the missing mass is converted into energy.
Among all the bound states we will focus on the ground state, the specific configuration which minimises the system energy.

In Fig. 1.1 is shown an important result concerning the average binding energy per nucleon $B/A = -B.E.(A,Z)/A$.

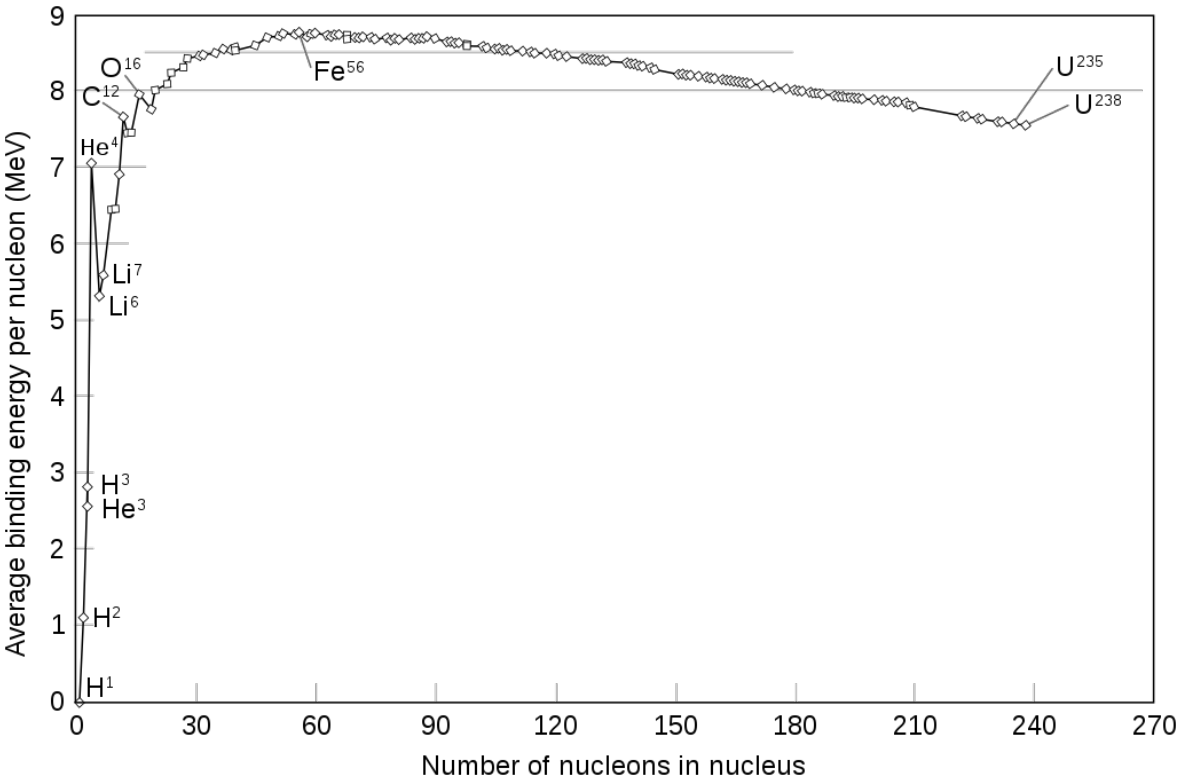


**Figure 1.1:** Binding energy per nucleon. For nuclear masses above 40-50 the average binding energy shows an almost constant value around 8 MeV; this is related to the saturation of the nuclear force. [1]

[1] Source: https://it.wikipedia.org/wiki/File:Binding_energy_curve_-_common_isotopes.svg

We can see that the quantity $B/A$ rapidly increases for small values of $A$, whereas for heavier nuclei is always about 8 MeV. This behaviour explains why light nuclei gain energy in nuclear fusion while heavy nuclei can gain it in fission. Moreover, we will see below how this information helps us to understand the range of nucleon-nucleon interaction.

Using the binding energy definition, we can also introduce the separation energy, that is the energy needed to remove one nucleon from the nucleus.

$$S_p = B.E.(A-1, Z-1) - B.E.(A, Z) \qquad S_n = B.E.(A-1, Z) - B.E.(A, Z) \quad (1.2)$$

$S_p$ and $S_n$ refer to protons and to neutrons, respectively.

**Density:** Since Rutherford's experiment, it was clear that the nucleus was confined in a space much smaller that the size of the atom.
Later on, more accurate electron scattering experiments were able to quantify the nuclear charge distribution as few fm; the first key results were obtained by Robert Hofstadter in 1956 [4], which showed that proton densities are almost constant for the first few fm, then exponentially decreasing as the distance from the nucleus centre increases.
From then, various experiments have been conducted to study the density of several nuclei, confirming the results obtained by Hofstadter.
Here in Fig. 1.2 some nuclear radial densities calculated with Hartree Fock method (Sec. 1.2.4) are presented.

As shown in Fig. 1.2 densities are almost constant inside the nucleus, then rapidly decrease approaching and beyond the nuclear surface. Moreover, we see that heavier nuclei have larger size, as the range in which densities are constant increases with $A$. This is due to a nuclear force property called saturation [5], which is strictly related to the proportionality between the volume $V$ and the atomic mass $A$.

As densities are almost uniform inside the nucleus, we can write:

$$\frac{V}{A} = \frac{4/3\pi R^3}{A} = \text{const.}$$

where $R$ is the radius of the nucleus, here approximated as a sphere. Hence it follows $R \propto A^{1/3}$ [2]. The result is compatible with the experimental findings, which state $R \sim r_0 A^{1/3}$: $r_0$ is a parameter equal to 1.2 - 1.3 fm, depending on the nucleus [6].

Charge nuclear densities are determined experimentally through scattering experiments, which measure the transferred momentum of the particle involved in the scattering. Such information leads to the knowledge of proton densities.
Otherwise, another way to proceed consists in a theoretical study through quantum models such as the DFT (Sec. 2.1), *ab initio* methods, or self-consistent techniques like Hartee-Fock (Sec. 1.2.4).

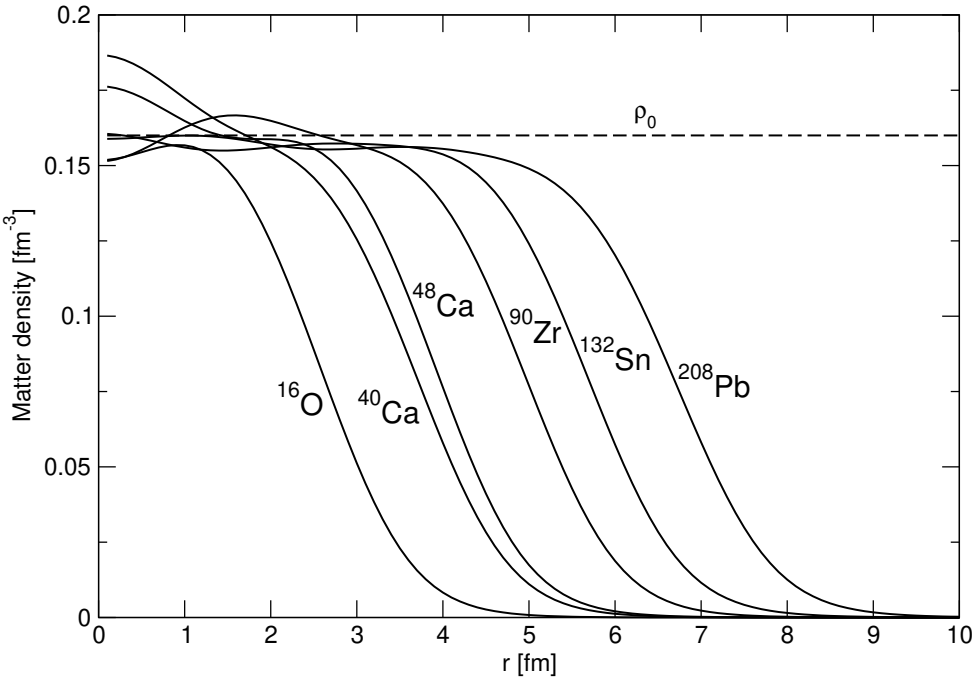


**Figure 1.2:** Nuclear SkX densities computed with Hartree-Fock method [7]. Density first shows a plateau, which ranges from 1 to 5 fm depending on nuclear masses, then decreases exponentially for radii corresponding to the nuclear surface.

The simplest function which represents a nuclear density in spherical simmetry is a Fermi function of the form:

$$\rho(r) = \frac{N}{1 + \exp\left(\frac{r-R}{a}\right)} \tag{1.3}$$

$R$ represents the nuclear radius, and $a$ ($\sim$ 0.5-0.6 fm) describes the behaviour nearby its surface. $N$ is the density saturation, usually equal to 0.16-0.17 fm.
In this work we make use of more kinds of nuclear densities, which are presented in Sec. 3.2.

**Potential:** Now that we have introduced all the necessary quantities, we can focus on the core of nuclear physics.
One of the main challenges in this field consists in finding a potential that correctly takes into account all the features of the nuclear interactions we witness experimentally. The first interaction we consider is the electromagnetic one, originated from charged particles inside the nucleus, the protons. We can write such two-body potential in natural units as:

$$v = \frac{e}{2} \sum_{\substack{i,j=1,\\ i \neq j}}^{Z} \frac{1}{|\mathbf{r}_i - \mathbf{r}_j|} \tag{1.4}$$

where $e$ is the electron charge.
It is important to note that this kind of forces only involves protons, since neutrons do

not bring any charge, implying a breaking in the approximate symmetry between the two particles. Indeed, we see in Chap. 4 that neglecting the Coulomb force allows us to treat the nucleus as if it were made of just $A$ neutrons.
This simplification holds since the Coulomb effect is rather small: generally, it causes a shift on the system energy which can be treated approximately using the first order perturbation theory.

In addition to the Coulomb interaction, there must be another force which involves both protons and neutrons which would explain how the nucleus exists in a stable configuration. We refer to such interaction as the *strong interaction*, since its magnitude is far greater than the electromagnetic one.
The origin of the strong interaction, which is called nucleon-nucleon (NN) interaction in nuclear physics, must be sought in the properties of the quarks that forms nucleons, a topic which is studied in Quantum Chromodynamics (QCD). Still, for the purposes of this work, we can assume the NN interaction as fundamental.

Without any pretence of being exhaustive, we can outline the main properties of the NN interaction from simple considerations and experimental results; for a more complete and deep explanation see [5].
Nucleon-nucleon interaction has to dominate over the Coulomb interaction, otherwise bound states and stable nuclei would not exist. This potential must involve both protons and neutrons, thus being charge independent.

From the almost constant behaviour of nuclear binding energies per nucleon (Fig. 1.1), at least for nuclei with $A > 30$, we can infer the short-ranged nature of the NN interaction: if each nucleon is interacting only with its nearest neighbours, the energy scales as $E \propto A$, instead of the typical $E \propto A\,(A-1)/2$ for long-range interactions. Experimental results provide an interaction range of $\sim 1.5$ fm.
A central role in NN interaction is also played by its spin dependence, in keeping with Pauli principle. Moreover, there are other terms which include spin-orbit coupling, as it is needed to describe magic numbers (see Sec. 1.2.1), and tensor components, as manifested in the deuteron quadrupole moment [5].
The presence of such several terms which involve two or three bodies, and their non-trivial dependency on position, spin, and momentum, hinders the exact knowledge of the nuclear interaction.
Nevertheless, especially for light nuclei, it is still possible to compute realistic potentials from *ab initio* calculations or phenomenological fit procedures (Sec. 1.2.4).

However, in order to study properties of nuclei, it is still useful to employ models which do not account for the complexity of the real nuclear interaction, and that can provide interesting information as for nuclear structure. The most common nuclear models are presented in Sec. 1.2.

## 1.2 Nuclear models

As we have said, the NN interaction is not completely known. This prevents us from having a general nuclear model able to explain the behaviour of all nuclei, as happens in particle physics and the Standard Model. Still, we can employ different nuclear models, each of which focuses on different aspects of the same problem, in order to obtain information regarding nuclear quantities.

In the following sections we consider the Liquid drop model, which accurately describes nuclear binding energies but fails in explaining spectroscopy experiments, the harmonic oscillator, that is a rough approximation of nuclear model, but it is still useful for later simulations (Chap. 4), and the shell model, which reflects the fact that in many experiments one clearly sees particles in shell-model orbitals (for instance, when making spectroscopy around magic nuclei).
Eventually, in the last section more advanced model are presented.

### 1.2.1 Liquid drop model

We first start looking at a macroscopical model called Liquid drop model [6]. In this context binding energies are described by the semi-empirical Bethe-Weizsäcker formula (BW):

$$B.E.(A,Z) = -a_1 A + a_2 A^{\frac{2}{3}} + a_3 \frac{Z^2}{A^{1/3}} + a_4 \frac{(N-Z)^2}{A} \pm a_5 A^{-\frac{3}{4}} \tag{1.5}$$

where $a_i$ are constants with energy dimensions and approximate values between 0.6 and 20 MeV.
The first two terms are related to volume and surface respectively: as for volume dependence, we see that $B.E. \propto A$, as we have already observed before. The presence of a surface term can be understood if we see the nucleus as a liquid drop: this peculiarity gives name to the model.
The third term is due to the Coulomb interaction and corresponds to the energy of an uniformly charged sphere. This is indeed named Coulomb term.
The fourth and fifth ones do not have any classical interpretation. The former, called asymmetry term, follows from Pauli's principle and the presence of neutrons and protons: it could be understood even in a Fermi gas model as the energy spent to change protons into neutrons respecting the Pauli principle, although it also takes contribution from the difference between pp and pn interactions. The latter, the pairing term, depends on nucleon spins, as it captures the effects of spin-coupling: it represents the fact that even-even nuclei gain binding energies as nucleons tend to form "pairs".
Through the liquid drop model different phenomena can be understood: fission process, for instance, is seen as a drop which splits into two lighter nuclei by a low-energy neutron.

To conclude, nuclear binding energies and certain reactions can be explained by seeing the nucleus as a liquid drop; however, there are other properties which cannot be interpreted by such model [6].

The leading result suggesting that there must be more to BW formula is the presence of magic numbers, specific numbers of nucleons that result in highly stable nuclei. As BW suggests that physical quantities vary continuously or monotonically as function of the mass and atomic numbers, it cannot account for the existence of shell structures and discontinuities in nuclear properties [6]. In order to describe more precisely the nucleus, we are now focusing on microscopic models.

### 1.2.2 Harmonic oscillator

The simplest microscopic nuclear system we can think of is a set of nucleons inside an harmonic oscillator (HO) well.
Since we will focus only on closed-shell nuclei, thus spherically symmetric systems, we look at the isotropic harmonic oscillator as it preserves such symmetry. It is a model which describes particles trapped inside a quadratic potential of the form:

$$v(r) = \frac{1}{2} m\omega^2 r^2 \tag{1.6}$$

where $m$ is the particle mass, $r$ is the distance from the HO center, and $\omega$ is the oscillation frequency of the system. For the nuclear case we have $\hbar\omega \approx 41/A^{1/3}$, which is expressed in MeV units.
Each spherically symmetric system in the neighbourhood of a stable minimum can be interpreted as an isotropic harmonic oscillator. Here a three-dimensional harmonic oscillator is considered.

The greatest advantage of considering such system dwells in the analytical knowledge of its eigenfunctions and eigenvalues. In fact the problem can be factorised into a radial and an angular term, and Schrödinger equations can be solved exactly.
Using uncoupled basis and proceeding with spherical coordinates, HO eigenfunctions read:

$$\psi_\lambda(\mathbf{r}) = \psi_\lambda(r,\theta,\phi) = R(r)\,Y(\theta,\phi) \tag{1.7}$$

$$R_{kl}(r) = N_{kl} r^l e^{-\nu r^2} L_k^{(l+\frac{1}{2})}(2\nu r^2) \tag{1.8}$$

$$N_{kl} = \sqrt{\sqrt{\frac{2\nu^3}{\pi}} \frac{2^{k+2l+3}\; k!\; \nu^l}{(2k+2l+1)!!}} \tag{1.9}$$

$$\nu \equiv \frac{\mu\omega}{2\hbar}, \qquad n \equiv 2k + l \tag{1.10}$$

$R$ are radial functions and $Y$ spherical harmonics; ${L_k}^{(l+\frac{1}{2})}$ inside the radial function are generalized Laguerre polynomials.

Energies are instead expressed as

$$E = \hbar\omega(N + \frac{3}{2}) \tag{1.11}$$

where $N$ is the principal quantum number, defined as $N = 2(n-1) + l$.

The harmonic oscillator alone is not adequate to explain magic numbers obtained by the experiments [6], only predicting 8 and 20. The first improvement we can make on the HO model is adding the spin-orbit coupling, which introduces an Hamiltonian of the form $H_{SO} = v_{SO}\,\mathbf{L}\cdot\mathbf{S}$. From a comparison with experimental results, it is found that $v_{SO} < 0$: spin-orbit interaction has opposite sign than the corresponding one in atomic physics, and it is also much more intense.
Even though the composition of HO and spin-orbit model is a better approximation of the HO only, it still does not capture all the interactions inside the nucleus.

### 1.2.3 Shell model

Although the harmonic oscillator approximation can be suitable for simple estimates around the ground state of particular nuclei, we still need a model which predicts more generic nuclear properties: the HO potential of Eq. (1.6) indeed cannot properly describe the nucleus nearby its surface, as the nuclear potential should vanish for $r \to \infty$, whereas the harmonic oscillator one diverges. Moreover, we have seen in the previous section that the HO model, even considering the spin-orbit coupling, does not reproduce the correct magic numbers.
Therefore a new model is needed: the Shell model.

Within the Shell model nucleons are assumed as independent particles inside an effective potential generated by the other nucleons. Although it is not an exact approach, it is possible to do such simplification as the interaction between nucleons spans ∼1.5 fm, whereas the mean distance between nucleons is ∼ 2 fm: "collisions" between nucleons are rare, thus, although the interaction is strong, a mean field picture, with nucleons moving in an average potential, does make sense. Interactions are then slightly attractive and only rarely strongly repulsive [5].
Moreover, since magic-number nuclei have spherical symmetry, it is useful to build the nuclear shell model in analogy with the atomic model, introducing shells which are related to energy levels.
The shell model energy levels are presented in Fig. 1.3[2].

The problem now consists in finding a suitable effective potential which is able to describe nucleon interactions.
A reasonable choice could be a Fermi-like function which accounts for the short-range character of nuclear interaction. A possible representation of such potential for a spherical nucleus is the following:

$$v(r) = -\frac{v_0}{1 + \exp\left(\frac{r-R}{a}\right)} \tag{1.12}$$

where $v_0$ is the potential well depth, $R$ is the nucleus radius, and $a$ represents the surface width.
This family of potentials resembles the potential generated by a density of the form (1.3), and are called Woods-Saxon potentials (WS). Typical values are: $v_0 \sim 50$ MeV,

[2]Source: http://www0.mi.infn.it/jroca/doc/thesis/thesis-alberto-scalesi.pdf

$R \sim r_0 A^{1/3}$ and $a \sim$ 0.5-0.7 fm. In general, $v_0$ for realistic WS potentials shows a non-trivial dependence on $N$ and $Z$.

The WS potential alone predicts some magic numbers which do not exist and, on the other hand, misses some which are obtained experimentally [6]. To reproduce the correct numbers (2, 8, 20, 28, 50, 82, 126, and 184), we must also include the spin-orbit interaction which was introduced in the previous section: thanks to this term the correct magic numbers, shown in Fig. 1.3, are obtained.

### 1.2.4 Beyond the shell model

Even if the shell model succeeds in the explanation of magic numbers, it is still based on a mean field theory and therefore not exact; it also does not suggest any way to find or to approximate the nuclear potential.
To further improve the study of nuclear properties, different models have been developed, such as the Hartee Fock approach (HF), the *ab initio* techniques, as well as the Density Functional Theory (DFT).

The former is a self-consistent method which approximates the wave function of a N-particle system with a single Slater determinant of N orbitals; eventually a variational procedure that minimises the energy leads to N-coupled differential equations for the N orbitals [8]. From here, both nuclear densities and potentials can be evaluated.

In contrast, *ab initio* methods adopt a more fundamental approach, seeking to describe the atomic nucleus by solving the non-relativistic Schrödinger equation for all constituent nucleons, using an Hamiltonian which describes nuclear interactions in the vacuum. However, both the interacting Hamiltonian, due to the partial knowledge of the nuclear potential, and the many-body techniques used to define such interactions are not unique; this gives birth to various *ab initio* models.
Sophisticated methods to find the Hamiltonian are based on chiral effective field theory (EFT), which takes into account all interactions compatible with the symmetries of the QCD [9]. Among the computational methods to solve Schrödinger equations, we can cite Diffusion Monte Carlo (DMC) and Self Consistent Green Function Theory (SCGFT) [10] [11].
Although in principle these techniques are exact and can describe all nuclei, the computational costs of such models increase exponentially with the number of nucleons. Thus, *ab initio* methods are only applicable to light nuclei, whereas for heavier nuclei approximations are needed.

Eventually, another way to deal with nuclear problems is the DFT, which has brought accurate results regarding nuclear as well as electronic systems in the last decades. As the present work is based on such functional approach, this model is deepened in Chap. 2.

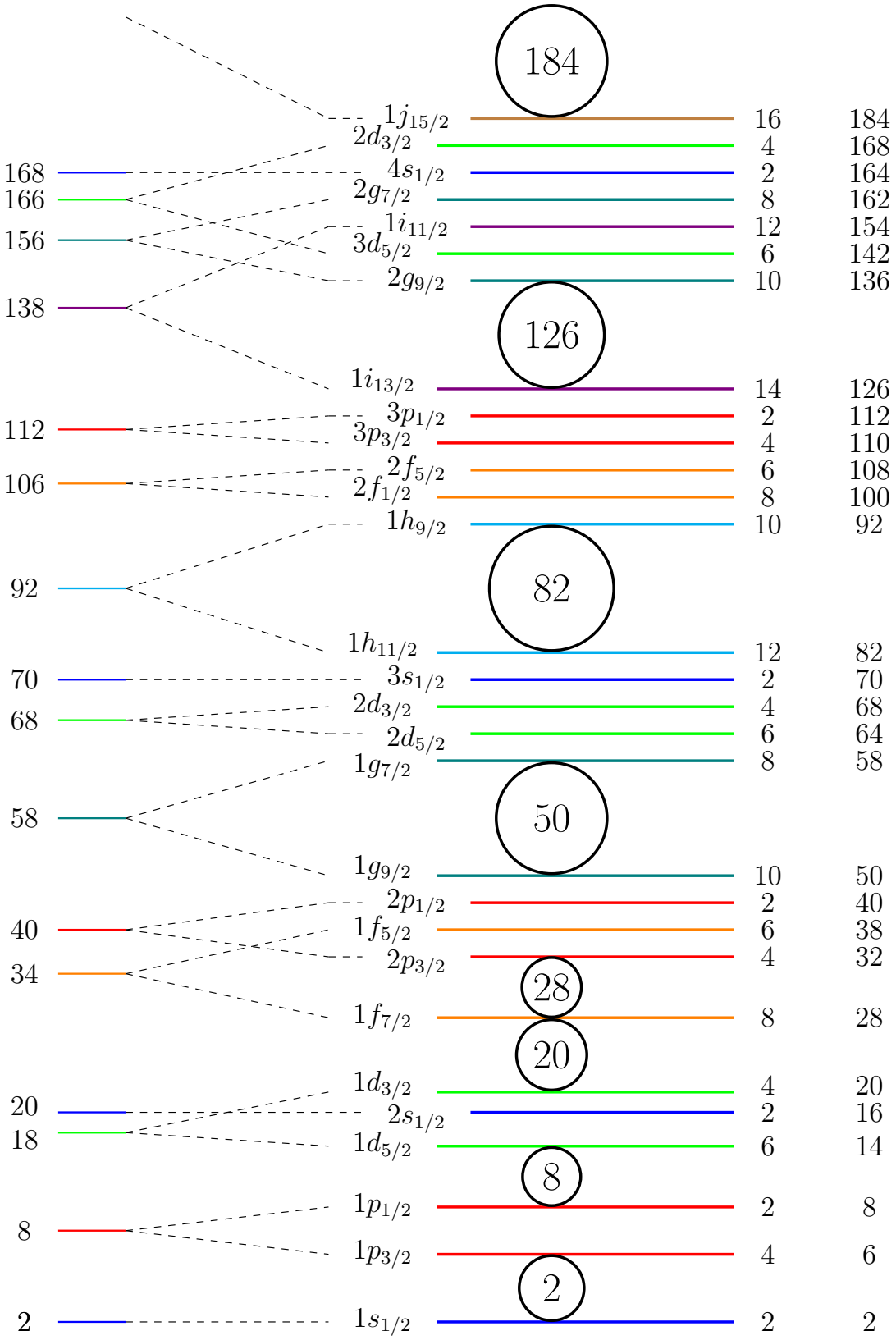


**Figure 1.3:** Representation of the energy levels of the shell model. It is possible to see wide gaps between some of the energy levels, which correspond to magic numbers and stable nuclei.

# Chapter 2

# The direct and inverse problem of the DFT

In this chapter we introduce the mathematical model used throughout this work to study nuclear structure: this approach is known as the Density Functional Theory (DFT).
We first discuss the main characteristics of the DFT and the direct problem for electronic systems (Sec. 2.1), then focusing more thoroughly on the inverse problem (Sec. 2.2) and the Kohn-Sham approach (Sec. 2.2.2). The DFT applications on nuclear systems are treated in Chap. 3 and 4.
The approach to the theory presented below resembles the one of classic manuals as [12] and [13]. For a more rigorous and extended study on the subject we refer to such works.

## 2.1 Density Functional Theory

The DFT is a theoretical and computational model which is widely popular in physics and chemistry as it was proposed to study electronic systems and molecules [13] [14]. As a theory, it is actually applicable to any system of fermions so that nuclear DFT also exists and can be employed to find nuclear properties of complex many-body problems [15] [16].
The main idea of the theory is to express all physical quantities as functionals of the density of the system $\rho(\mathbf{r})$: this approach leads to a huge conceptual as well as computational simplification, as the information of a N-particle system is contained into a three-variable function, rather than an eigenfunction $\psi(\mathbf{r}_1, \sigma_1; ...; \mathbf{r}_N, \sigma_N)$ of 3N space variables plus any spin degrees of freedom. This model allows to study complex systems which cannot be solved otherwise, as computational costs of exact numerical methods, in which the number of degrees of freedom scales exponentially with particles number $N$, are extremely high.

The assumption of characterising a quantum ground state solely in terms of the system density is not straightforward. Martin and Schwinger [17] showed it is possible

to describe a ground state with one- and two-particle Green functions which can be derived from a set of coupled differential equations, including time as well as space variables, that involve a number $n < N$ of particles. Thus it was not clear how the one-particle density alone could be enough to express the ground state energy; the first models by Thomas and Fermi were indeed seen as oversimplifications in order to avoid the many-particle computational problems.
The turning point for the DFT, which involved both its mathematical foundations and the interest within the scientific community, consisted in the publication in 1964 of the two Hohenberg-Kohn theorems (HK) [18]: the first grants the possibility to express the system energy as a functional of the system density only, avoiding any possible ambiguity in the choice of such functional. The latter suggests instead a procedure useful to calculate the ground energy through a minimisation principle.
With the theorems at hand, every expectation value of physical observables can be see as a functional of the density. This aspect is actually a part of the original proof of the theorem.

### 2.1.1 Hohenberg and Kohn theorems

The approach to HK theorems presented below regards electronic systems with non degenerate ground states. We refer to [12] and [13] for generalisations of such theorems, and to [15] and [16] for the specific treatment of the DFT in nuclear systems.

**First HK theorem**
The first Hohenberg-Kohn theorem assures there is a one to one correspondence between the external potential of the system and the ground state density; the ground state of the system can then be expressed as a functional of the density. Thus, the expectation value of any observable can be seen as a density functional.

We start considering a system of N interacting fermions subjected to a two-body known potential $\hat{W}$, e.g. Coulomb interaction, and an external potential $\hat{V}$. We can write the non-relativistic Hamiltonian as:

$$\begin{aligned}\hat{H} = \hat{T} + \hat{V} + \hat{W} = -\frac{h^2}{2m}\sum_{i=1}^{N}\nabla_i^2 + \sum_{i=1}^{N}\hat{v}(\mathbf{r}_i) + \frac{1}{2}\sum_{\substack{i,j=1,\\ i\neq j}}^{N}\hat{w}(\mathbf{r}_i,\mathbf{r}'_j) = \\ = -\frac{h^2}{2m}\sum_{\alpha}\int d^3r\,\hat{\psi}^+_\alpha(\mathbf{r})\nabla^2\hat{\psi}_\alpha(\mathbf{r}) + \sum_{\alpha}\int d^3r\,\hat{\psi}^+_\alpha(\mathbf{r})v(\mathbf{r})\hat{\psi}_\alpha(\mathbf{r}) + \\ + \frac{1}{2}\sum_{\alpha\,\beta}\int d^3r\int d^3r'\,\hat{\psi}^+_\alpha(\mathbf{r})\hat{\psi}^+_\beta(\mathbf{r}')w(\mathbf{r},\mathbf{r}')\hat{\psi}_\beta(\mathbf{r}')\hat{\psi}_\alpha(\mathbf{r})\end{aligned} \tag{2.1}$$

where $(i, j)$ are particle indexes, whereas $(\alpha, \beta)$ are spin indexes. In the last step the second quantised notation was used [19].
Given an eigenfunction $|\Phi\rangle$, we can write the eigenvalue equation for the Hamiltonian (2.1):

$$\hat{H}\,|\Phi\rangle = (\hat{T} + \hat{V} + \hat{W})\,|\Phi\rangle = E_{gs}\,|\Phi\rangle \tag{2.2}$$

The external potential $\hat{V}$ was chosen from a particular set $\mathcal{V}$ so that Eq. (2.2) provides a unique value of the energy $E_{gs}$, that is, a non-degenerate ground state.
Since energies can be defined up to an additive constant, we construct a new set of potentials by applying the equivalence relation *"equal up to ad additive constant"* to $\mathcal{V}$. With abuse of notation we refer to such set again with $\mathcal{V}$, which now does not contain external potentials that differ by a constant.
Considering a set of ground states $\mathbf{\Psi}$ and a ket $|\Psi\rangle \in \mathbf{\Psi}$, the system density $\rho(\mathbf{r})$ reads:

$$\begin{aligned}\rho(\mathbf{r}) = \langle\Psi|\hat{\rho}(\mathbf{r})|\Psi\rangle &= \langle\Psi|\sum_{\alpha}\hat{\psi}^{+}_{\alpha}(\mathbf{r})\hat{\psi}_{\alpha}(\mathbf{r})|\Psi\rangle \\ &= N\sum_{\alpha}\int dx_2 ... \int dx_N |\Psi(\mathbf{r},\alpha,x_2,...,x_N)|^2\end{aligned} \tag{2.3}$$

where, again, second quantised notation was introduced. We can now define the set of ground state densities $\mathcal{N}$, which contains all the densities $\rho(\mathbf{r})$ of the form (2.3).

Looking at Eq. (2.1) we can define the map $\mathcal{X} : \mathcal{V} \to \mathbf{\Psi}$, which associates a potential to a ground state wave function. Analogously, referring to Eq. (2.3), we introduce the function $\mathcal{Y} : \mathbf{\Psi} \to \mathcal{N}$, which relates a ground state wave function to a density. Both maps are surjective by definition.
To prove the injectivity we have to consider their domains of definition, that are $\mathcal{V}$ and $\mathbf{\Psi}$, respectively. If we show that there is a one to one correspondence between $\mathcal{V}$ and $\mathbf{\Psi}$, $\mathbf{\Psi}$ and $\mathcal{N}$, then the relation linking $\mathcal{V}$ and $\mathcal{N}$ must be bijective either. We achieve that in two separate steps [12].
The following proof holds for non degenerate ground states, but can be generalised to other systems (Sec. 2.1.2).

**$\mathcal{V} \to \mathbf{\Psi}$ Injectivity**

We start considering two external potentials $\hat{V}, \hat{V}' \in \mathcal{V}$ such that $\hat{V} \neq \hat{V}'$; from the definition of $\mathcal{V}$, they differ by more than a constant. Applying (2.1) to ground state eigenfunctions for different Hamiltonians we have:

$$\hat{H}\,|\Psi\rangle = (\hat{T} + \hat{V} + \hat{W})\,|\Psi\rangle = E_{gs}\,|\Psi\rangle \tag{2.4}$$

$$\hat{H}'\,|\Psi'\rangle = (\hat{T} + \hat{V}' + \hat{W})\,|\Psi'\rangle = E'_{gs}\,|\Psi'\rangle \tag{2.5}$$

Taking $|\Psi'\rangle = |\Psi\rangle$ and subtracting the two above we obtain $(V - V')\,|\Psi\rangle = (E_{gs} - E'_{gs})\,|\Psi\rangle$; thus, as $V$ and $V'$ are multiplicative operators, we have $(V - V') = (E_{gs} - E'_{gs}) = \text{const.}$, contradicting the statement above. Last equation holds at least for $|\Psi\rangle$ regular enough, which comprehends all physical situations.
Hence any external potential is in a one-to-one correspondence to a ground state wave function.

**$\mathbf{\Psi} \to \mathcal{N}$ Injectivity**

Considering now two Hamiltonians $\hat{H}, \hat{H}'$ and their eigenstates $|\Psi\rangle, |\Psi'\rangle$, we want to prove that their ground state densities $\rho(\mathbf{r}), \rho'(\mathbf{r})$ are different. Proceeding with a *reductio ad absurdum*, we assume $\rho(\mathbf{r}) = \rho'(\mathbf{r})$.
From the ground state definition we have:

$$E_{gs} = \langle\Psi|\hat{H}|\Psi\rangle < \langle\Psi|\hat{H}'|\Psi\rangle \tag{2.6}$$

since we assumed not-degenerate ground states. We can rewrite the right hand side by using (2.1) and linearity property:

$$E_{gs} < \langle\Psi|\hat{H}'|\Psi\rangle = \langle\Psi|\hat{H}' + \hat{V} - \hat{V}'|\Psi\rangle = E'_{gs} + \int d^3r(\rho'(\mathbf{r})\,(v(\mathbf{r}) - v'(\mathbf{r}))) \tag{2.7}$$

Repeating the same steps for $E'_{gs}$, we obtain the following analogous inequality:

$$E'_{gs} < \langle\Psi|\hat{H}|\Psi\rangle = \langle\Psi|\hat{H} + \hat{V}' - \hat{V}|\Psi\rangle = E_{gs} + \int d^3r(\rho'(\mathbf{r})\,(v'(\mathbf{r}) - v(\mathbf{r}))) \tag{2.8}$$

Addition of (2.7) and (2.8) leads to an absurd:

$$E_{gs} + E'_{gs} < E'_{gs} + E_{gs} \tag{2.9}$$

Thus, any ground state corresponds to one and only one density.

We can now state the first Hohenberg-Kohn theorem as follows: given a system whose Hamiltonian is of the kind (2.1), with a not-degenerate ground state, there is a bijective relation between the system density $\rho(\mathbf{r})$ and the external potential $\hat{V}$. Hence, any ground state expectation value can be expressed in terms of the ground state density only: $O[\rho] = \langle\Psi[\rho]|\hat{O}|\Psi[\rho]\rangle$, where $\Psi[\rho]$ is a functional of the density. The expectation value of the Hamiltonian is then a functional of the density $\rho(\mathbf{r})$.

**Second HK theorem**

The second HK theorem derives directly from the former. The theorem establishes the variational character of the energy functional, which can be defined as:

$$E_{v_0}[\rho] = \langle\Psi[\rho]|\hat{T} + \hat{W} + \hat{V}_0|\Psi[\rho]\rangle \tag{2.10}$$

The ground state energy is then $E_0 = E_{v_0}[\rho_0] < E_{v_0}[\rho]$ for any $\rho \neq \rho_0$, where $\rho_0$ is the ground state density. Thus the ground state energy can be obtained through a process of minimisation of the energy functional (2.10):

$$E_0 = \min_{\rho\in\mathcal{N}} E_{v_0}[\rho] \tag{2.11}$$

where $\mathcal{N}$ contains all the grounds state densities which are in bijective correspondence with an external potential in $\mathcal{V}$. We can explicitly show the external potential dependence of the energy introducing $F_{HK} \equiv \langle\Psi[\rho]|\hat{T} + \hat{W}|\Psi[\rho]\rangle$ and rewriting (2.10) as below:

$$E_{v_0}[\rho] = F_{HK}[\rho] + \int d^3r\, v_0(\mathbf{r})\rho(\mathbf{r}) \tag{2.12}$$

$F_{HK}$ is a universal functional, that is a quantity not depending on $V_0$ but only on kinetic and the two-body terms; $F_{HK}$ has indeed the same expression when applied to atoms, molecules, and solids, in which $\hat{W}$ is the Coulomb interaction.

Although the great simplifications this approach is bringing, especially avoiding the treatment of 3N degrees of freedom in favour of only 3, the two HK theorems do not suggest any way to construct both the map $\mathcal{N} \to \mathcal{V}$ and the functional $F_{HK}$. This is in fact one of the main challenges the DFT has to face.

### 2.1.2 $N-$ and $v-$representability

Both theorems can be extended to degenerate ground states, spin-polarised, relativistic and finite temperature systems. However, Eq. (2.11) holds as long as $\rho(\mathbf{r}) \in \mathcal{N}$; we call these densities $v-$representable.
It is now natural to ask whether all the densities of physical interest are $v-$representable. The answer, unfortunately, is negative: indeed, there exist even well behaved functions $\rho(\mathbf{r})$, normalised to the number of particles $N$, that do not correspond to a ground state density for any potential $v(\mathbf{r})$. Examples of such densities are presented in Sec. 2.3 of [12] and 3.3 of [13].
This result makes the variational approach we previously introduced more difficult to pursue, since it may happen that during the minimisation procedure we find some non $v-$representable densities.

To overcome the $v-$representability problem we must extend the domain of the functional $F_{HK}[\rho]$, as a characterization of $v-$representable functions has not been found yet. Levy [20] and Lieb [21] suggested to consider a wider set of densities, which are called $N-$representable: such densities derive from some antisymmetric wave function $\Psi(x_1, ..., x_N)$ of a $N-$particle system, which does not need to be the eigenstate of an Hamiltonian of the form (2.1). We indicate the set of $N-$representable functions with $\widetilde{\mathcal{N}}$, in order to differentiate it from $\mathcal{N}$ of the previous section.
In analogy with $F_{HK}$, we can define a new universal functional $F_{LL}$ as:

$$F_{LL}[\rho] \equiv \inf_{\Psi \to \rho \in \widetilde{\mathcal{N}}} \langle \Psi | \hat{T} + \hat{W} | \Psi \rangle \tag{2.13}$$

Moreover, the infimum is actually a minimum [21].
To prove that the functional $F_{LL}[\rho]$ is a reasonable extension of $F_{HK}[\rho]$, we first look at what happens for a density $\rho(\mathbf{r}) \in \mathcal{N}$: substituting in (2.13) we obtain the exact definition of $F_{HK}[\rho]$. Thus:

$$F_{HK}[\rho] = F_{LL}[\rho]\Big|_{\widetilde{\mathcal{N}}} \tag{2.14}$$

As for non $v-$representable densities, we must prove that the energy functional

$$E_{v_0}[\rho] = F_{LL}[\rho] + \int d^3r \, v_0(\mathbf{r})\rho(\mathbf{r}) \tag{2.15}$$

assumes its unique minimum at the ground state density $\rho_0(\mathbf{r})$, which corresponds to an external potential $v_0(\mathbf{r})$. We do that by considering the infimum over the N-particle $\Psi$ functions as a sequence of infima over $\rho(\mathbf{r}) \in \widetilde{\mathcal{N}}$ and $\Psi \to \rho$:

$$\begin{aligned} E_0 &= \inf_{\Psi} \langle \Psi | \hat{T} + \hat{W} + \hat{V}_0 | \Psi \rangle = \inf_{\rho \in \widetilde{\mathcal{N}}} \left( \inf_{\Psi \to \rho \in \widetilde{\mathcal{N}}} \langle \Psi | \hat{T} + \hat{W} + \hat{V}_0 | \Psi \rangle \right) \\ &= \inf_{\rho \in \widetilde{\mathcal{N}}} \left( \inf_{\Psi \to \rho} \langle \Psi | \hat{T} + \hat{W} | \Psi \rangle + \int d^3r \, \rho(\mathbf{r}) v_0(\mathbf{r}) \right) \\ &= \inf_{\rho \in \widetilde{\mathcal{N}}} \left( F_{LL}[\rho] + \int d^3r \, \rho(\mathbf{r}) v_0(\mathbf{r}) \right) \end{aligned} \tag{2.16}$$

Using (2.15) we conclude the proof:

$$E_0 = \inf_{\rho \in \widetilde{\mathcal{N}}} E_{v_0}[\rho] \tag{2.17}$$

where the infimum is also a minimum.

Shortly said, the Levy and Lieb approach extends the formalism first introduced by Hohenberg and Kohn, solving problems related to density representability without affecting its variational nature.

### 2.1.3 Kohn-Sham equations

Despite the huge simplifications achieved so far, the system taken into consideration is made of $N-$interacting fermions, which makes the problem non trivial; moreover, the variational approach suggested by the second HK theorem is rather difficult to implement. Thus, further work is still needed so as to find a practical technique to evaluate nuclear properties.
In 1965 Kohn and Sham showed [22] it is possible to formulate HK as a problem of independent particles in a suitable effective one-body potential. In particular, their work allows to consider an auxiliary problem of $N$ non-interacting particles whose single-particle potential $v_s(\mathbf{r})$ provides a ground state density which is the same one of the interacting system. This approach is achieved by introducing $N$ single-particle orbitals.

More in detail, we can write the energy functional of a non-interacting particle system as :

$$E_s[\rho] = T_s[\rho] + V_s[\rho] \tag{2.18}$$

From the second HK theorem the ground state density $\rho_0(\mathbf{r})$ leads to the condition $\delta E[\rho_0] = 0$.
We introduce the single-particle orbitals $\phi_k(\mathbf{r})$, for which the following relation holds:

$$\rho(\mathbf{r}) = \sum_{k=1}^{\mathrm{N_{orb}}} |\phi_k(\mathbf{r})|^2 \tag{2.19}$$

Employing the first HK theorem we can see the orbitals $\phi_k(\mathbf{r})$ as density functionals $\phi_k(\mathbf{r}) = \phi_k([\rho], \mathbf{r})$.

Expressing $T$ and $V$ introduced in the previous section in terms of $\phi_k(\mathbf{r})$ we have:

$$T_s[\rho] = \sum_{k=1}^{\mathrm{N_{orb}}} \int d^3r\, \phi_k^*(\mathbf{r}) \left(-\frac{\hbar^2}{2m}\nabla^2\right) \phi_k(\mathbf{r}) \tag{2.20}$$

$$V_s[\rho] = \int d^3r\, v_s(\mathbf{r})\rho_s(\mathbf{r}) = \sum_{k=1}^{\mathrm{N_{orb}}} \int d^3r\, v_s(\mathbf{r})\, |\phi_k(\mathbf{r})|^2 \tag{2.21}$$

where $\mathrm{N_{orb}}$ is the total number of orbitals of the nucleus.
The work by Kohn and Sham [22] guarantees the existence of a single-particle potential $v_s(\mathbf{r})$ such that the ground state density of the interacting system and auxiliary problem are the same, that is $\rho_s(\mathbf{r}) = \rho_0(\mathbf{r})$.

Following Sec. 4.1 of [12], we introduce Hartree and exchange-correlation functionals:

$$E_H[\rho] = \int d^3r\, v_H(\mathbf{r})\rho(\mathbf{r}) \tag{2.22}$$

$$v_H(\mathbf{r}) = \frac{1}{2}\int d^3r'\, w(\mathbf{r},\mathbf{r}')\rho(\mathbf{r}') \tag{2.23}$$

$$E_{XC}[\rho] \equiv F_{HK}[\rho] - T[\rho] - E_H[\rho] \tag{2.24}$$

Rewriting the functional $E_{v_0}$ (Eq. (2.10)) with the information above we obtain:

$$E_{v_0}[\rho] = T_s[\rho] + \int d^3r\, v_0(\mathbf{r})\rho(\mathbf{r}) + \frac{1}{2}\iint d^3r\, d^3r'\, \rho(\mathbf{r})w(\mathbf{r},\mathbf{r}')\rho(\mathbf{r}) + E_{XC}[\rho] \tag{2.25}$$

From the definition of functional derivative we have:

$$v_0([\rho],\mathbf{r}) = \frac{\delta E_{v_0}}{\delta\rho(\mathbf{r})} \tag{2.26}$$

$$v_H([\rho],\mathbf{r}) = \frac{\delta E_H}{\delta\rho(\mathbf{r})} \tag{2.27}$$

$$\tag{2.28}$$

By analogy, we define $v_{XC}$ as:

$$v_{XC}([\rho],\mathbf{r}) = \frac{\delta E_{XC}}{\delta\rho(\mathbf{r})} \tag{2.29}$$

Applying variational principle (Eq. (2.11)) to both $E_{v_0}$ and $T$ we find:

$$v_{KS} = v_H + v_{XC} + v_0 \tag{2.30}$$

$v_{KS}$ is the Kohn-Sham (KS) potential, which represents the single particle potential of the non-interacting system.

From the variational principle and employing the orbitals introduced above, we finally obtain Schrödinger equations for a particle with a self-consistent potential:

$$-\frac{\hbar^2}{2m}\nabla^2\phi_k(\mathbf{r}) + v_{KS}([\rho],\mathbf{r})\phi_k(\mathbf{r}) = \epsilon_k\phi_k(\mathbf{r}) \qquad \forall\, k = 1,...,\mathrm{N_{orb}} \tag{2.31}$$

Once orbitals are known, densities can be calculated from (2.19).
Kohn Sham equations must be solved self-consistently as $v_{KS}$ depends on the density. The procedure to follow can resemble the one used to solve Hartree Fock equations, but the KS approach is more general and potentially accurate, since correlation effects can be included. Moreover, the HF procedure is complicated by the non-local exchange term, whereas in DFT the exchange-correlation potential can be suitably approximated with a local contribution.

To conclude, HK theorems have shown how 3N degrees of freedom of a $N-$interacting fermion system can be reduced to only 3, using the ground state density. Furthermore, the Kohn-Sham approach allowed to translate the original problem in a much easier one, consisting in a non-interacting particle system, in which we know the explicit form of the kinetic energy term.
This last step brings great advantages: computationally speaking, solving KS equations is simpler than proceeding with the HK minimisation, as the problem now consists in solving Schrödinger equations. In addition, the available approximations for the functional $E_{XC}$ in (2.24), are better than the $F_{HK}$ ones.

## 2.2 Inverse DFT problem

Within the DFT, a direct or forward problem consists in evaluating ground state densities from the knowledge of the energy density functional (EDF). The exact one unfortunately is not known, although several valid approximations do exist. In spite of this lack of information, such approximations lead to accurate results.
On the other hand, in the previous section we showed it is possible to express physical observables as functionals of the density, thus we can use the one-to-one correspondence assured by HK theorems to find the energy functionals: such approach is called the inverse problem of the DFT. In other words, as long as the inverse problem is well defined (see Sec. 2.2.1 below), we can calculate the Kohn-Sham potential $v_{KS}$ starting from the knowledge of the system density.
While the direct DFT problem has a great history of success, being hugely studied since decades, the inverse problem has attracted attention more recently. Several works have been devoted to this topic in recent years, from studies on numerical methods employed to solve inverse problems [23], to practical applications both on electronic systems [24] [25], and on nuclear physics [26] [27] [28] [29].
The inverse DFT technique is indeed suggesting a new way to approach nuclear problems that can give precious insights on the subject. It is now mainly used to benchmark the many approximate exchange-correlation functionals currently available, but its possible applications are much wider. In fact, in this work we make use of the inverse problem as a way to find new energy density functionals.

Moreover, this approach allows to find the potential avoiding the usage of techniques based on fitting experimental data, which are common procedures in nuclear physics, albeit they are often rather complex and can occasionally lead to ambiguities [30].

### 2.2.1 Well-posed problems

In accordance with Hadamard definition, a well-posed problem must fulfill the following properties [31]:

- the existence of a solution of the problem;
- the uniqueness of the solution;
- the continuous dependence of the solution on the input data.

Last condition assures that small enough changes in the initial conditions entail small changes in the solution. Indeed this is a typical property of weak solutions of a differential equation [32]. If one (or more) of the three is not satisfied, the problem is said ill-posed.

In contrast to direct problems, which are generally well-posed, inverse problems are usually ill-posed [33]; this requires extra care, as unphysical results and numerical errors may appear.

Moreover, numerical methods for inverse problem can lead to the so-called "inverse crimes", in which the results obtained by the method are said to be overfitting the input data. That is, rounding and approximations depict the inverse problem less ill-posed than it actually is, ending in a model which contains more information than that given in input.

To show an example of an inverse crime, we report a simulation from [23], which describes the ground state density of the harmonic oscillator numerically computed with box-type boundary conditions and a fourth-order finite difference approximation for the laplacian. If the same finite difference approximation is used while evaluating the potential from orbitals, the resulting potential is almost exact everywhere, as seen in Fig. 2.1.

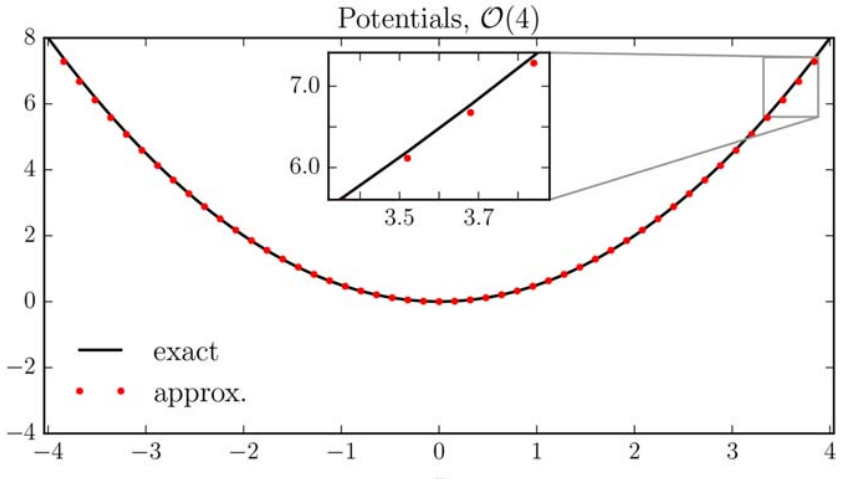


**Figure 2.1:** Example of an inverse crime in a harmonic oscillator simulation. The ground state density of the harmonic oscillator is computed numerically using a fourth-order approximation to the laplacian and zero boundary conditions, and the potential is evaluated using the same laplacian finite difference approximations. This provides an inverse crime.

In this case the inverse crime is due to cancellation of errors between the data simulation and reconstruction methods. This usually happens in DFT inversions, when the same numerical methods are used to solve both the direct and the inverse problems.

To avoid inverse crimes while making the model robust, regularisation techniques are usually taken into consideration [34] [35]. These procedures allow to substitute the original problem with a slightly different one which is well-posed and has unique solution.

HK theorems make the DFT direct and inverse problem well-defined, as there is a one-to-one correspondence between $\rho(\mathbf{r})$ and $v([\rho], \mathbf{r})$. Nonetheless, for the inverse problem, non-exact input data (affected by errors or approximations), may result in a violation of Hadamard's conditions. To overcome such difficulty and find numerically

valid solutions to the problem, it is therefore necessary to use regularisation techniques or to construct the inverse model with caution.

### 2.2.2 Kohn Sham inverse problem

As we have seen in Sec. 2.1.3, the Kohn Sham approach yields the following Schrödinger equations for the single-particle orbitals $\phi_k(\mathbf{r})$:

$$-\frac{\hbar^2}{2m}\nabla^2\phi_k(\mathbf{r}) + v_{KS}([\rho],\mathbf{r})\phi_k(\mathbf{r}) = \epsilon_k\phi_k(\mathbf{r}) \qquad \forall\, k = 1, ..., \mathrm{N_{orb}} \tag{2.32}$$

where

$$v_{KS} = v_H + v_{XC} + v_0 \tag{2.33}$$

$$\rho(\mathbf{r}) = \sum_{k=1}^{\mathrm{N_{orb}}} |\phi_k(\mathbf{r})|^2 \tag{2.34}$$

These equations hold both for the forward and the inverse problem, however they differ in the unknown quantities: in the direct problem we know the Kohn-Sham potential $v_{KS}(\mathbf{r})$, whereas orbitals $\phi_k(\mathbf{r})$, eigenvalues $\epsilon_k$ and density $\rho(\mathbf{r})$ must be found through a self-consistent method. In the inverse problem $\rho(\mathbf{r})$ is known, and $v_{KS}(\mathbf{r})$, $\phi_k(\mathbf{r})$, and $\epsilon_k$ are the unknowns.
Such differences lead to the development of completely different algorithms to face the two problems.

Below two different techniques for solving Eq. (2.32) with the inverse approach are presented: the vLB and CV methods.

**vLB method**
The first model we look at was suggested by van Leeuwen and Baerends [36]. It is a self-consistent procedure based on solving Schrödinger Eq. (2.32) with different potentials, until the target density is correctly reproduced.
More in detail, starting from Eq. (2.32), multiplying by $\phi_k^*(\mathbf{r})$ and summing over $k$ index we have:

$$-\frac{\hbar^2}{2m}\sum_{k=1}^{\mathrm{N_{orb}}}\phi_k^*(\mathbf{r})\nabla^2\phi_k(\mathbf{r}) + v_{KS}([\rho],\mathbf{r})\sum_{k=1}^{\mathrm{N_{orb}}}|\phi_k(\mathbf{r})|^2 = \sum_{k=1}^{\mathrm{N_{orb}}}\epsilon_k|\phi_k(\mathbf{r})|^2 \tag{2.35}$$

Employing Eq. (2.19) the potential $v_{KS}$ reads:

$$v_{KS}([\rho],\mathbf{r}) = \frac{1}{\rho(\mathbf{r})}\frac{\hbar^2}{2m}\sum_{k=1}^{\mathrm{N_{orb}}}\left(\phi_k^*(\mathbf{r})\nabla^2\phi_k(\mathbf{r}) + \epsilon_k|\phi_k(\mathbf{r})|^2\right) \tag{2.36}$$

The problem can now be solved self-consistently: choosing an initial potential $v(\mathbf{r})$, we compute the system density $\rho^k(\mathbf{r})$ associated to such potential through Schrödinger equation (2.32); if $\rho^k(\mathbf{r})$ is close enough to the target density $\rho(\mathbf{r})$ then $v_{KS} \simeq v$, otherwise the potential must be modified and the procedure starts over.

Different criteria both for the convergence of the density and for the modification of the potential have been suggested. Choosing a percentage threshold $\epsilon$, Jensen and Wasserman [23] suggest to stop iterations when the condition given by Eq. (2.37) is satisfied:

$$\max_{\mathbf{r}} \left| 1 - \frac{\rho^k(\mathbf{r})}{\rho(\mathbf{r})} \right| < \epsilon \tag{2.37}$$

where $\rho^k(\mathbf{r})$ is the density obtained during the k-th step the iterations.
On the other hand, one the most straightforward way to change the potential after each step is:

$$v^{k+1}(\mathbf{r}) = \frac{\rho^k(\mathbf{r})}{\rho(\mathbf{r})} v^k(\mathbf{r}) \tag{2.38}$$

The k-th potential is decreased where the computed density is smaller than the target one, whereas if $\rho^k(\mathbf{r}) > \rho(\mathbf{r})$ then the potential is increased. Alternatives to this formula are presented in [23].

The vLB method greatest advantage consists in the simplicity of its implementation, as it only requires to solve Schrödinger equations repeatedly. Nevertheless, it shows a strong dependence on the choice of the initial potential: the algorithm does not explore a wide range of parameters, thus the information obtained by this approach is rather limited.

**CV method**

Another way to solve the inverse problem consists in the constrained-variational (CV) method, first introduced by Wasserman and Jensen [23]. The problem is set as a constrained optimisation procedure: we first consider a set of orbitals under the constraint that a certain target density must be reproduced, also requiring the orthonormality among such orbitals. The ground state wave functions are obtained by the constrained minimisation of the kinetic energy which satisfies the conditions above. In this context the Kohn-Sham potential arises as the Lagrange multiplier associated to the density constraint, i.e. the requirement that the single-particle orbitals obtained from the minimisation must reproduce the ground state density given in input.
The functional to be minimised is the expectation value of the kinetic energy of a system with non-interacting particle, as we are employing KS formalism. Referring to Eq. (2.20), integrating by parts and using the divergence theorem, we can rewrite such functional:

$$T_s[\{\phi_k\}] = \frac{\hbar^2}{2m} \sum_{k=1}^{\mathrm{N_{orb}}} d_k \int d^3r \; |\nabla \phi_k(\mathbf{r})|^2 \tag{2.39}$$

where $d_k$ is the degeneracy of the orbital, that is, the number of particles that occupy the k-th shell.
The term $\int d^3r \, \nabla \cdot (\phi_k^*(\mathbf{r}) \nabla \phi_k(\mathbf{r}))$, which appears while integrating by parts, vanishes as $\phi \to 0$ for $r \to \infty$, since orbitals must be normalised.
The energy minimum can be found, according to Eq. (2.16), through a minimisation first over the eigenfunctions, $\Psi$ which generate a density $\tilde{\rho}(\mathbf{r})$, and then over the $N-$representable densities (Sec. 2.1.2).
Thus we obtain the following constraint from the first minimisation:

$$\rho(\mathbf{r}) = \sum_{k}^{\mathrm{N_{orb}}} d_k \, |\phi_k(\mathbf{r})|^2 = \tilde{\rho}(\mathbf{r}) \tag{2.40}$$

$\tilde{\rho}(\mathbf{r})$ is called target density, that is the ground state density given in input.

A constrained optimisation can be equivalently cast as a free minimization of a certain cost functional, making use of Lagrange multipliers techniques. We can indeed introduce the Lagrange multiplier $v(\mathbf{r})$ of the constraint (2.40), and define:

$$G_d[\{\phi_k\}; v(\mathbf{r})] \equiv \int d^3r\, v(\mathbf{r})(\rho(\mathbf{r}) - \tilde{\rho}(\mathbf{r})) = 0 \tag{2.41}$$

Likewise we introduce the constraint on the orthonormality between orbitals as:

$$G_{ij}[\{\phi_k\}] \equiv \int d^3r\, \phi_i^*(\mathbf{r})\phi_j(\mathbf{r}) = \delta_{ij} \qquad \forall i = 1, ..., \mathrm{N_{orb}},\ j \leq i \tag{2.42}$$

$G$ is symmetric, thus $G_{ij} = G_{ji}$ and the sum extends over the lower triangle of the matrix. Lagrange multipliers of $G_{ij}$ are the quantities $-d_i\epsilon_{ij}$.
It is now possible to define the cost functional $J$:

$$\begin{aligned} J[\{\phi_j\}, v(\mathbf{r}), \{\epsilon_{ij}\}] &\equiv T_s[\{\phi_j\}] + G_d[\{\phi_j\}; v(\mathbf{r})] - \sum_{i=1}^{\mathrm{N_{orb}}} \sum_{j=1}^{i} d_i\epsilon_{ij} G_{ij}[\{\phi_j\}] \\ &= \frac{\hbar^2}{2m} \sum_{j=1}^{\mathrm{N_{orb}}} d_j \int d^3r\ |\nabla\phi_j(\mathbf{r})|^2 + \int d^3r\, v(\mathbf{r})(\rho(\mathbf{r}) - \tilde{\rho}(\mathbf{r})) + \\ &\quad - \sum_{i=1}^{\mathrm{N_{orb}}} \sum_{j=1}^{i} d_i\epsilon_{ij} \int d^3r\, \phi_i^*(\mathbf{r})\phi_j(\mathbf{r}) \end{aligned} \tag{2.43}$$

In the second step definitions (2.39) (2.41) (2.42) were used.

The constrained minimisation of the functional $T$ is then replaced by the free minimisation of $J$, as long as the constraint equations are satisfied.
Applying the functional derivatives $\delta/\delta\phi_k^*(\mathbf{r})$ to the functional $J$ and evaluating at the minimum, which gives $\delta J = 0$, we have:

$$\frac{\delta J(\{\phi_j\})}{\delta\phi_k^*(\mathbf{r})} = \left( -\frac{\hbar^2}{2m}\nabla^2\phi_k(\mathbf{r}) + v([\rho], \mathbf{r})\phi_k(\mathbf{r}) - \sum_{i=1}^{k} \epsilon_{ki}\phi_i(\mathbf{r}) \right) d_i = 0 \tag{2.44}$$

Hence:

$$-\frac{\hbar^2}{2m}\nabla^2\phi_k(\mathbf{r}) + v([\rho], \mathbf{r})\phi_k(\mathbf{r}) = \sum_{i=1}^{k} \epsilon_{ki}\phi_i(\mathbf{r}) \tag{2.45}$$

Eq. 2.45 is a non-canonical Schrödinger equation, as in the right hand side a sum over different orbitals and eigenvalues is present. However, the left hand side term is a self-adjoint operator, that is the single-particle Hamiltonian, we can then apply a canonical transformation to 2.45 and obtain:

$$-\frac{\hbar^2}{2m}\nabla^2\phi_k(\mathbf{r}) + v(\mathbf{r})\phi_k(\mathbf{r}) = \epsilon_k\phi_k(\mathbf{r}) \tag{2.46}$$

which is exactly the Schrödinger equation we obtained in (2.32).
The meaning of Lagrange multiplier $v(\mathbf{r})$ is now clear: it is the single-particle external

potential $v_{KS}$ introduced in Sec. 2.1.3, which is specific for the problem taken into consideration.

The implications of this model are of great importance: using only the ground state density, which can be measured experimentally or computed with other methods, e.g. Hartree-Fock direct problem (Sec. 1.2.4), we are able to evaluate the single-particle orbitals $\phi_k(\mathbf{r})$, the specific effective potential $v(\mathbf{r})$ for the system taken into consideration, and the ground state kinetic energy $T$.
From the knowledge of this quantities we can take the next step and find the total energy functional of the system (Chap. 4).

# Chapter 3

# Nuclear potentials from the Constrained Variational method

In this chapter we first proceed to implement the CV method introduced in Chap. 2, specialising it for spherical systems. In the second part we make use of such model and run simulations to find nuclear potentials for stable magic nuclei. We consider the $^{16}$O, $^{40}$Ca, and $^{208}$Pb nuclei.

## 3.1 CV implementation

The Constrained Variational equations characterising the method, that are Eq. (2.41) and Eq. (2.42) for the constraints, and Eq. (2.44) which states the variational nature of the approach, involve a variety of terms, each one depending on three spatial variables. This makes solving the problem rather complex.
To overcome such computational difficulties, we restrict our studies to spherical symmetric systems: this way we only have to treat the radial coordinate, translating the original problem into a 1-dimensional one. From a physical point of view, we are focusing on closed-shell nuclei [34] [35].

The first step is then to write the problem defined in Sec. 2.2.2 in spherical coordinates; later on, new variables and functions are introduced to make the algorithm more accurate and stable.

### 3.1.1 CV for spherical symmetric systems

Recalling Eq. (2.19), we can write the system density in the coupled basis $\alpha = (n\,l\,s\,j\,m_j)$ as:

$$\rho(\mathbf{r}) = \sum_{\alpha\,\sigma} |\psi_\alpha(\mathbf{r},\sigma)|^2 \tag{3.1}$$

The sum extends over all the possible values of $(\alpha, \sigma)$.
Due to symmetry reasons, it is possible to show that the density of a spherical sym-

metric system only depends on the radial coordinate. Thus, Eq. (3.1) becomes:

$$\rho(r) = \sum_{k=1}^{\mathrm{N_{orb}}} d_k \frac{|u_k(r)|^2}{4\pi\, r^2} \tag{3.2}$$

where $d_k$ stands for the occupancy of the k-th shell; as we are focusing on closed-shell nuclei, it always assumes its maximum value. We choose to work in the coupled basis, in which the degeneracy reads $d_k = 2j_k + 1$: thus, orbitals are characterised by $(n,\, l,\, j)$ quantum numbers.

Proceeding to write CV equations in spherical coordinates, we first look at the kinetic term. The laplacian operator in the new $(r, \theta, \varphi)$ coordinates reads:

$$\nabla^2 = \frac{1}{r}\frac{\partial^2}{\partial r^2} r + \frac{\Lambda^2}{r^2} \tag{3.3}$$

in which $\Lambda$ is the Legendre operator, that in 3D can be written as:

$$\Lambda^2 = \frac{1}{\sin(\theta)}\frac{\partial}{\partial\theta}\left(\sin(\theta)\frac{\partial}{\partial\theta}\right) + \frac{\partial^2}{\partial\varphi^2} \tag{3.4}$$

It is possible to show that $\Lambda \propto \mathbf{L}$, in particular we have:

$$\mathbf{L}^2 = -\hbar^2\Lambda^2 \tag{3.5}$$

Thus, we can insert the orbital angular momentum in the laplacian operator and, therefore, in the kinetic term.
Using the information above we have:

$$\begin{aligned}\nabla^2\phi(\mathbf{r},\sigma) &= \frac{1}{r}\frac{\partial^2}{\partial r^2}(r\,\phi(\mathbf{r},\sigma)) + \frac{\Lambda^2}{r^2}\phi(\mathbf{r},\sigma) = \\ &= \frac{1}{r}\frac{\partial^2 u(r)}{\partial r^2}\,Y(\theta,\varphi,\sigma) + \frac{\Lambda^2\,u(r)}{r^2}\,Y(\theta,\varphi,\sigma)\end{aligned} \tag{3.6}$$

where we used that $\phi(\mathbf{r},\sigma) = u(r)/r\; Y(\theta,\varphi,\sigma)$. $u(r)$ is the reduced radial function and $Y(\theta,\varphi,\sigma)$ is the generalised spherical harmonic function, which contains both the spherical harmonic and the spinor term. Employing the relation between $\Lambda^2$ and $L^2$ we eventually obtain:

$$\nabla^2\phi(\mathbf{r},\sigma) = \left(\frac{\partial^2 u(r)}{\partial r^2} - \frac{l(l+1)}{r^2}\,u(r)\right)\frac{Y(\theta,\varphi,\sigma)}{r} \tag{3.7}$$

Using the jacobian transformation $d\mathbf{r} = r^2 dr d\Omega$ we can write:

$$\begin{aligned}\sum_\sigma \int d^3r\,\phi^*(\mathbf{r},\sigma)\nabla^2\phi(\mathbf{r},\sigma) &= \sum_\sigma \int |Y(\theta,\varphi,\sigma)|^2 d\Omega \int \frac{u^*(r)}{r}\frac{1}{r}\left(\frac{\partial^2 u(r)}{\partial r^2} - \frac{l(l+1)}{r^2}u(r)\right) r^2 dr \\ &= \int u^*(r)\left(\frac{\partial^2 u(r)}{\partial r^2} - \frac{l(l+1)}{r^2}u(r)\right) dr\end{aligned} \tag{3.8}$$

In the last step the normalisation of generalised spherical harmonic functions has been used.
Hence, the kinetic energy now reads:

$$\begin{aligned} T_s[\{u_k\}] &= -\frac{\hbar^2}{2m}\sum_{k=1}^{\mathrm{N_{orb}}} d_k \int u^*(r)\left(\frac{\partial^2 u(r)}{\partial r^2} - \frac{l(l+1)}{r^2}u(r)\right)dr \\ &= \frac{\hbar^2}{2m}\sum_{k=1}^{\mathrm{N_{orb}}} d_k \int \left(|u_k'(r)|^2 + \frac{l(l+1)}{r^2}|u(r)|^2\right)dr \end{aligned} \tag{3.9}$$

As the Hamiltonian of the system is time independent, reduced radial functions $u(r)$ can be chosen to be real, thus the module symbol can be omitted.

Repeating the same procedure for the constraint on density (2.41), we obtain:

$$G_d[\{u_k\}, v(r)] = \int v(r)\left(\left(\sum_{k=1}^{\mathrm{N_{orb}}} d_k u_k^2(r)\right) - 4\pi r^2 \tilde{\rho}(r)\right) = 0 \tag{3.10}$$

In contrast, the condition relating the orthonormality between orbitals is not straightforward, as it involves different generalised spherical harmonics:

$$\sum_{\sigma}\left(\int Y_i^*(\theta,\varphi,\sigma)Y_j(\theta,\varphi,\sigma)d\Omega\right)\left(\int u_i(r)u_j(r)dr\right) = \delta_{ij} \tag{3.11}$$

The first integral which contains angular variables is equal to $\delta_{l_i l_j}\delta_{j_i j_j}$ due to generalised spherical harmonics properties. If $l_i \neq l_j$ or $j_i \neq j_j$, then Eq. (3.11) is trivially satisfied. Otherwise, even the orthonormality between radial functions must hold:

$$G_{ij}[\{u_i\}] = \int u_i(r)u_j(r)dr = \delta_{ij} \quad \text{if } l_i = l_j, j_i = j_j; \quad \forall i = 1, ..., \mathrm{N_{orb}},\ j \leq i \tag{3.12}$$

Equations (3.9), (3.10), and (3.11) contain all the information regarding the CV method for spherical symmetric systems; in principle, it is possible to solve this problem in terms of the $u(r)$ radial functions. However, this approach provides large errors in the region in which wave functions are close to zero: that is why more regular functions are needed.

### 3.1.2 Radial functions scaling

As the authors of [23] point out, the finite difference method used to represent the laplacian operator may lead to numerical errors when wave functions are exponentially decreasing. Therefore, they suggest to introduce some scaled orbitals $\{f_k(\mathbf{r})\}$ which have a smoother behaviour than $\{u_k(r)\}$, defined as:

$$f_k(\mathbf{r}) \equiv \frac{\phi_k(\mathbf{r})}{\sqrt{\tilde{\rho}(\mathbf{r})}} \tag{3.13}$$

Since from Eq. (2.19) we know that $\tilde{\rho}(\mathbf{r}) \sim |\phi(\mathbf{r})|^2$, $\{f_k\}$ orbitals have a far less steep behaviour than the original ones. Moreover, this approach also avoids numerical errors

arising from the treatment of numbers with different orders of magnitude, as $\{f_k(\mathbf{r})\}$ functions usually range from 0 to 1.
For the spherical symmetric case we use the scaling formula suggested by [35], which slightly differs from the original Eq. (3.13). It reads:

$$f_k(r) = \frac{u_k(r)}{\sqrt{4\pi\tilde{\rho}(r)}\, r} \tag{3.14}$$

We can now express the equations obtained above in terms of the scaled radial functions $\{f_k(\mathbf{r})\}$.

Starting from Eq. (3.14), the following expression holds:

$$\rho(r) = \tilde{\rho}(r) \sum_{k=1}^{\mathrm{N_{orb}}} d_k f_k^2(r) \tag{3.15}$$

Thus, it is convenient to write the density constraint $\rho(r) = \tilde{\rho}(r)$ as:

$$g_d(\{f_k\}, r) \equiv \sum_{k=1}^{\mathrm{N_{orb}}} d_k f_k^2 = 1 \tag{3.16}$$

It is also possible to express the constraints in the integral form by using Eq. (3.10), (3.11), and (3.14). For the density constraint we have:

$$G_d[\{f_k\}, v(r)] = \int v(r) \left( \left( \sum_{k=1}^{\mathrm{N_{orb}}} d_k f_k^2(r) \right) - 1 \right) 4\pi\tilde{\rho}(r) r^2 dr = 0 \tag{3.17}$$

Instead, the orthonormality condition becomes:

$$G_{ij}[\{f_k\}] = \int 4\pi\tilde{\rho}(r) r^2 f_i(r) f_j(r) dr = 1 \quad \text{if } l_i = l_j, j_i = j_j; \quad \forall i = 1, ..., \mathrm{N_{orb}},\ j \leq i \tag{3.18}$$

The calculations regarding the kinetic term are slightly more demanding, as the $u(r)$ derivatives must be evaluated in terms of $f(r)$. However, proceeding by substitution we eventually obtain:

$$T_s[\{f_k\}] = \sum_{k=1}^{\mathrm{N_{orb}}} d_k \int dr \left( -\frac{\hbar^2}{2m} 4\pi \right) \left( C_0(r,k) f_k^2(r) + C_1(r) f_k(r) \dot{f}_k(r) + C_2(r) f_k(r) \ddot{f}_k(r) \right) \tag{3.19}$$

in which we introduced the following functions:

$$C_0(r,k) \equiv -l_k(l_k+1)\tilde{\rho}(r) + r\dot{\tilde{\rho}}(r) + \frac{r^2}{2}\ddot{\tilde{\rho}}(r) - \frac{r^2}{4}\frac{(\dot{\tilde{\rho}}(r))^2}{\tilde{\rho}(r)} \tag{3.20}$$

$$C_1(r) \equiv r^2\dot{\tilde{\rho}}(r) + 2r\tilde{\rho}(r) = \dot{C}_2(r) \tag{3.21}$$

$$C_2(r) \equiv r^2\tilde{\rho}(r) \tag{3.22}$$

where we used the dot $\dot{}$ notation to represent the derivative with respect to the radial coordinate. Full derivation is presented in App. B.

### 3.1.3 Numerical implementation

The CV method expressed with the $\{f_k(r)\}$ functions can now be implemented. In order to find the Kohn Sham potential associated to the density given in input, a constrained minimisation of the kinetic functional (3.19), or, in other words, a free minimisation of the objective functional $J[\{u_k(r)\}]$ (2.43), must be pursued.
This way we evaluate the scaled orbitals $\{f_k(r)\}$ which corresponds to the ground state of the system. From here, it is possible to compute both the potential $v(r)$ and the eigenvalues $\epsilon_{ij}$ employing Euler-Lagrange equations which derive from the condition $\delta J = 0$; we see that this approach is equivalent to solve a system of non-canonical Schrödinger equations, in which we know the orbitals from the previous minimisation procedure.

For the procedure presented above Jensen and Wasserman [23] suggest to use IPOPT (Interior Point OPTimizer), a library specialised in solving large-scale non-linear optimisation problems. IPOPT[1] requires the knowledge of the kinetic functional, as well as the constraint equations; moreover, it also needs the kinetic gradient, the constraint jacobian, and the hessian of the whole objective functional (see App. B). IPOPT also stores only the non zero elements of jacobian and hessian matrices, making the algorithm faster. Especially in our case, in which there are only very few non zero terms inside such matrices, this implementation reduces the number of steps needed to reach convergence.
Another essential information IPOPT requires is the orbital starting point. As IPOPT only explores a limited part of the phase space, it converges to the first local minimum it finds, having no way to discern different local minima from one another. Thus, the choice of the initial condition deeply influences which solution the algorithm finds.
E.g., if the starting orbital is close to the minimum, the convergence occurs rapidly; on the other hand, if the initial guess is too far from the solution, the convergence may never be achieved.
Therefore, a careful study on how the choice of the starting point affects the results obtained is of great importance. However, as harmonic oscillator orbitals have been shown to provide a reasonably good guess for nuclear problems [34], in this work we always employ such wave functions as the initial orbitals.

In order to implement the program we first have to discretise the CV equations: considering a radial mesh of $N_{points}$ evenly spaced in a closed interval $[R_1, R_2]$, the possible radial values are:

$$r_k = R_1 + hk \quad 0 \leq k \leq N_{points} \tag{3.23}$$

in which $h$ is the grid step, defined as $h = (R_2 - R_1)/N_{points}$.
Coding the CV equations means that we also need to discretise integrals and derivatives. For this purpose we make use of Python libraries, such as SciPy[2] and FinDiff[3], in order to minimise the numerical errors committed during integration and differenti-

[1] https://projects.coin-or.org/Ipopt
[2] https://www.scipy.org/
[3] https://pypi.org/project/findiff/

ation, respectively.

Eventually, once $\{f_k(r)\}$ are known, it is possible to compute the potential. Although in principle IPOPT already returns the value of the Lagrange multipliers, that are, $v(r)$ and $\epsilon_{ij}$ (Sec. 2.2.2), the scaling procedure we have applied (Eq. (3.14)) makes it difficult to reconstruct the real quantities with physical meaning from the scaled ones.
Hence, it is more convenient to start from Eq. (2.43), define a Lagrangian which describes the system, and then compute both the potential and the eigenvalues from the Euler - Lagrange (EL) equations, since we now know the orbitals $\{f_k(r)\}$, and, from Eq. (3.14), the $\{u_k(r)\}$ as well. In formula we have:

$$\mathcal{L} = \frac{\hbar^2}{2m}\sum_{k=1}^{\mathrm{N_{orb}}} d_k \left(\dot{u}_k(r)^2 + \frac{l(l+1)}{r^2}u(r)^2\right) + v(r)\sum_{k=1}^{\mathrm{N_{orb}}} d_k u_k^2 - \sum_{i=1}^{\mathrm{N_{orb}}}\sum_{j=1}^{i}\epsilon_{ij}u_i(r)u_j(r) \quad (3.24)$$

The EL equations then read:

$$-\frac{\hbar^2}{2m}2d_k\left(\ddot{u}_k(r) - \frac{l_k(l_k+1)}{r^2}u_k(r)\right) + 2d_k v(r)u_k(r) = \sum_{j=1}^{\mathrm{N_{orb}}} d_j\epsilon_{jk}(1+\delta_{jk})u_j(r) \quad (3.25)$$

Eq. (3.25) holds for any $k = 1, ..., \mathrm{N_{orb}}$, making it a system of linear equations with $v(r)$ and $\epsilon_{ij}$ as unknowns. To solve such problem, we use a linear algebra package, Sparse matrix[4], which is part of the bigger SciPy library introduced above.

At last, we underline another reason for which the resolution of EL equations is needed: when the IPOPT optimisation finds the orbitals $\{f_k(r)\}$ such that the density of the system is, in principle, equal to the target one, such orbitals are not unique, being defined up to a unitary transformation. Indeed, unitary transformations on wave functions $\{f_k(r)\}$ do not affect the physical quantities of the system, that are, the potential $v(r)$ and the eigenvalues $\epsilon_{ij}$.
Hence, the only way to remove this ambiguity originated by such gauge invariance is to choose a specific gauge in which to work. This is exactly what happens when we translate the Lagrange constrained minimisation problem into one of linear algebra, defining matrices to represent the information contained in Eq. (3.25).

## 3.2 Nuclear potentials from the Constrained Variational method

Now that we have described what the Constrained Variational method consists in and how to implement it, we can move on and analyse the results obtained from simulations.
We remind that the whole inverse DFT problem (Sec. 2.2) aims to calculate the potential from the knowledge of the density of the system. Thus, we are going to look at

[4]https://docs.scipy.org/doc/scipy/reference/sparse.html

some magic closed-shell nuclei, which are $^{16}$O, $^{40}$Ca and $^{208}$Pb.
Even if various tests have been pursued, as the ultimate purpose of this work is to construct the energy functional (Chap. 4), we only report the results obtained with suitable choices of the radial interval and of the wave function starting points. For a more in-depth study we refer to [26] [34] [35].
For $^{16}$O and $^{40}$Ca nuclei we run simulations using neutron densities. However, same results could be obtained by using proton ones. The calculation with the SkX interaction considered below includes the spin-orbit term, whereas the Coulomb term can be omitted as we look at chargeless particles.

### 3.2.1 $^{16}$O

We first look at $^{16}$O nucleus, composed of 8 protons and 8 neutrons, making it a stable double magic nucleus.
The density we focus on is computed using a Skyrme interaction (SkX) [7], and its behaviour for neutrons is shown in Fig. 3.1.

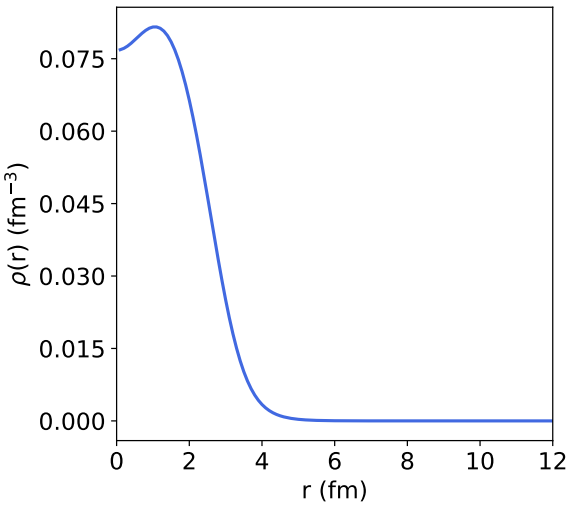


**Figure 3.1:** $^{16}$O SkX neutron density computed by Hartree Fock method.

As seen in Chap. 1, the density shows an initial plateau, while it exponentially decreases as the radius becomes greater.

Applying the CV method, we pursue the inversion considering the interval $[0.1, 11.0]$ fm and a radial step $h = 0.1$ fm. Proceeding with the simulations, we obtain the results shown in Fig. 3.2.

IKS and HF potentials show good agreement with one another: the difference between the two quantities is always smaller than 2 MeV. For $r \sim 8$ fm we see the IKS potential is weakly decreasing: this is caused by the finite length of the interval used in the inversion and has no physical explanation.

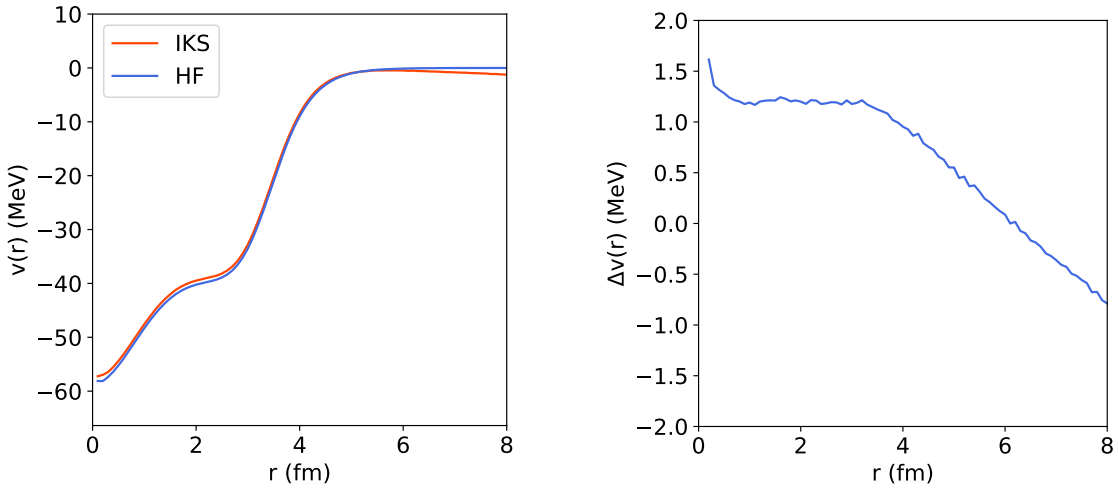


**(a)** **(b)**

**Figure 3.2:** (a) $^{16}$O neutron potential from the inversion of the SkX density (IKS), compared to the Hartree-Fock potential (HF). (b) $^{16}$O neutron difference between IKS and HF potentials.

It can be seen that, unlike previous implementations [34] [35], it is not necessary to remove the potential values in the first points of the mesh, as they do not deviate from the expected behaviour. This is an advantage of the new Python code and could be due to different libraries used for interpolations and higher precision in the derivative calculations.
However, the code still depends on the choice of the interval upper bound, as it does not converge for values of $R_2$ which are too small or too big. Therefore caution must be paid while choosing such parameter: a possible way to set a suitable value of $R_2$ consists in choosing a cutoff value with which to compare the density $\rho(r)$; in this perspective $R_2$ is chosen as the radius for which the density becomes smaller than the cutoff. For radii $r > R_2$ the density is indeed negligible. Reasonable choices of such threshold, which we employ in Chap. 4, are either $10^{-8}$ or $10^{-9}$ fm$^{-3}$. Eventually this also avoids numerical errors that arise when functions are too close to zero.

### 3.2.2 $^{40}$Ca

$^{40}$Ca is also a double magic nucleus, formed by 20 protons and 20 neutrons. Even in this case we consider the SkX interaction and compute the density associated to neutrons.

This time for the density inversion we use a radial grid with endpoints $R_1 = 0.1$ fm and $R_2 = 12.0$ fm, and step $h = 0.1$ fm. The result of the simulation is presented in Fig. 3.3.
Likewise what we previously obtained with $^{16}$O nucleus, the IKS and HF potentials show similar behaviours, with a difference smaller than 1 MeV everywhere. This time

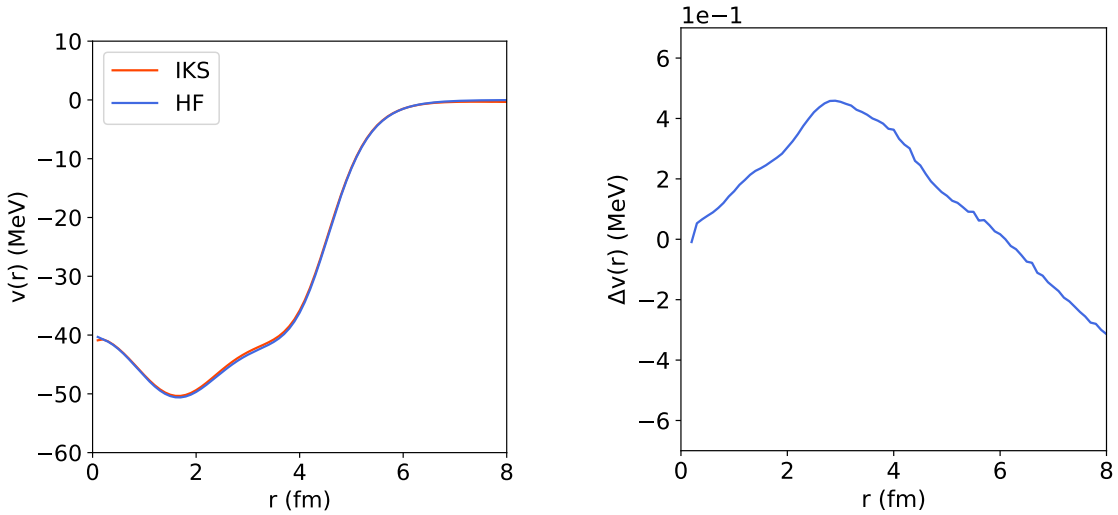


**(a)** **(b)**

**Figure 3.3:** (a) $^{40}$Ca neutron potential from the inversion of the SkX density (IKS), compared to the Hartree-Fock potential (HF). (b) $^{40}$Ca neutron difference between IKS and HF potentials.

the results are even better than the $^{16}$O ones, as the $^{40}$Ca is heavier and displays a weaker dependence on the interval endpoints.

### 3.2.3 $^{208}$Pb

The $^{208}$Pb nucleus has 82 protons and 126 neutrons, both 82 and 126 are magic numbers. Although this nuclide is not treated in further simulations in Chap. 4, we look at the behaviour of its potential because the density is computed with the Sum Of Gaussian parametrisation, showing different characteristics from the cases previously discussed. Moreover, we can benchmark the results with the ones of other works, such as [26].
SOG, standing for Sum Of Gaussian, as its name states, consists in a sum of different Gaussian functions with different centres and widths. This approach allows to predict accurate densities as long as a great number of parameters are employed, for instance, Zenihiro in [37] uses 12.

Proceeding with simulations for protons in the interval $[0.1, 12.0]$ fm with step $h = 0.1$ fm, we obtain the potential shown in Fig. 3.4. The proton SOG density used in this context was taken from [38].
We can note that, at the beginning of the interval, $v(r)$ calculated from the inverse problem presents great oscillations whose amplitude cannot be ignored; this behaviour does not have any physical meaning and it is due to the gaussian parametrisation of the SOG density. From 4 to 8 fm we see qualitatively agreement between the IKS and WS potentials, whereas for $r > 8$ fm the IKS potential loses any physical interpretation, as it diverges. We can again understand this fact by looking at how the SOG density is

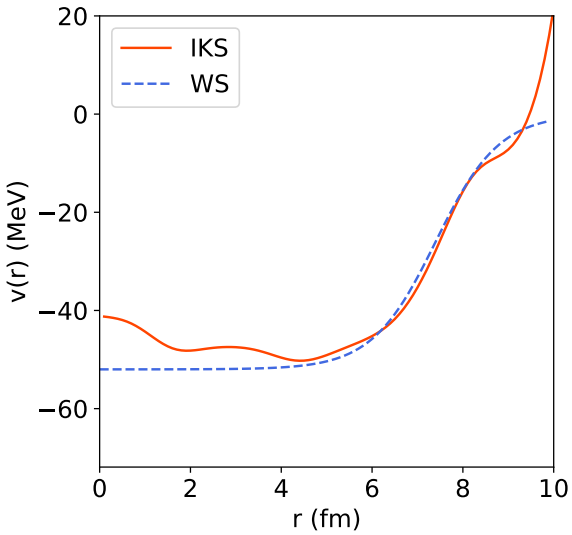


**Figure 3.4:** $^{208}$Pb proton potential from the inversion of the SOG density (IKS), compared to the Woods Saxon potential (WS).

constructed: any gaussian wave function corresponds to a harmonic potential, which is unbounded as it scales with $\sim r^2$. We indeed saw in Sec. 1.2.2 that the harmonic approximation is suitable only in the nuclear innermost region. This problem regarding Gaussian tails is largely known in nuclear physics and has already been treated in [26].

In contrast to what we have seen before, further simulations prove that the potential only weakly depends on the upper bound of the interval: this could be understood remembering that our first orbital guess consisted in harmonic oscillator wavefunctions (Sec. 3.1.3), which are, indeed, Gaussians. This explains why, different choices of $R_2$ notwithstanding, the convergence occurs rapidly.

## 3.3 Comparison between canonical and non canonical Kohn-Sham orbitals

We previously said (Sec. 3.1.3) that the orbitals $\{f_k(r)\}$ are determined up to a unitary transformation, which does not affect the physics of the problem. Nevertheless, if one wants to study the behaviour of the orbitals themselves, it is important to understand which unitary transformation must be applied to such wave functions, that is, which choice of the gauge leads to physically meaningful orbitals.
Thus, during the solution of Eq. (3.25), we can apply unitary transformations to the matrix representing the linear problem.

To understand which transformation of physical interest could be considered, we note that the Hamiltonian commutes with the system density $[H, \rho] = 0$, hence it can be simultaneously diagonalised with the matrix of the $\epsilon_{ij}$ eigenvalues. This fact sug-

gests to apply the specific unitary transformation that diagonalises the matrix which represents the linear problem.
To prove this ansatz, we look at $^{16}$O and $^{40}$Ca orbitals, studying what happens when we diagonalise the $(\epsilon_{ij})$ matrix.

### $^{16}$O

The $^{16}$O has 8 neutrons, which are distributed in 3 orbitals: $1s_{1/2}$, $1p_{3/2}$, and $1p_{1/2}$. We first compare the orbitals obtained by the minimisation procedure conducted by IPOPT using two different values or $R_2$ for the inversions, which are 9.8 and 11 fm. The potentials associated to such wave functions are identical, nevertheless, as we have seen before, in general it is not true that also the orbitals must be the same. We also consider orbitals computed with HF method, using these results as a benchmark.
Proceeding with the simulation we obtain what is presented in Fig. 3.5.

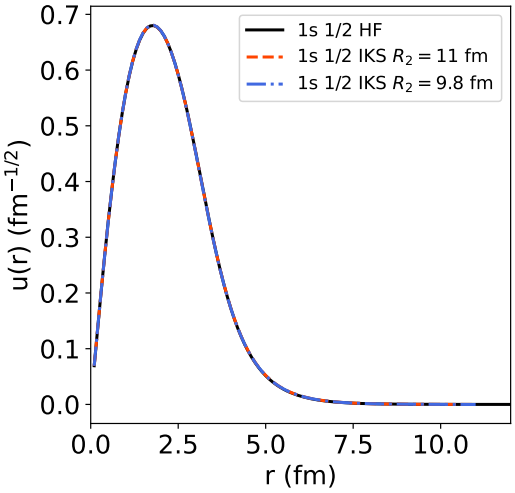


**(a)** $1s_{1/2}$ $^{16}$O radial functions

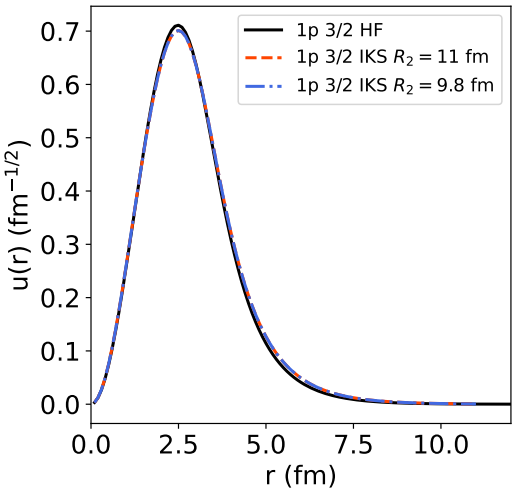


**(b)** $1p_{3/2}$ $^{16}$O radial functions

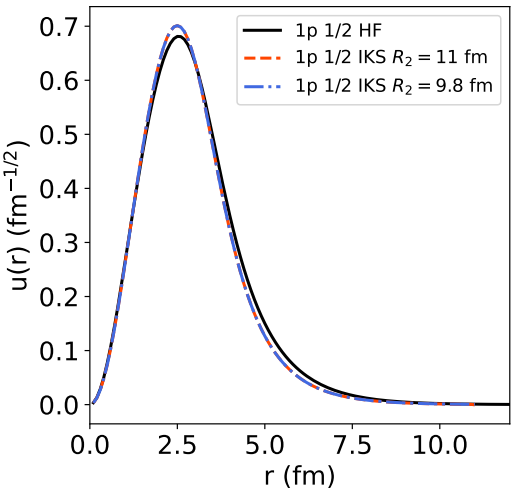


**(c)** $1p_{1/2}$ $^{16}$O radial functions

**Figure 3.5:** $^{16}$O $\{u_k(r)\}$ functions before the diagonalisation of the $(\epsilon_{ij})$ matrix, computed both through IKS and HF method. IKS orbitals are evaluated with two different values of $R_2$: 9.8 and 11 fm.

We see that the two IKS orbitals coming from different calculations show exactly the very same behaviour. Also HF radial functions are in great agreement with the IKS ones, being slightly different only nearby $r \sim 6$ fm in the case of the $1p_{1/2}$ orbital.

We now look at what happens to those orbitals if we diagonalise the $(\epsilon_{ij})$ matrix. The results are shown in Fig. 3.6.

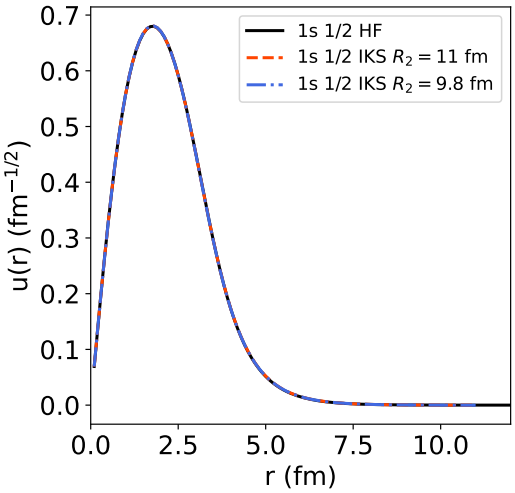


**(a)** $1s_{1/2}$ $^{16}$O radial functions

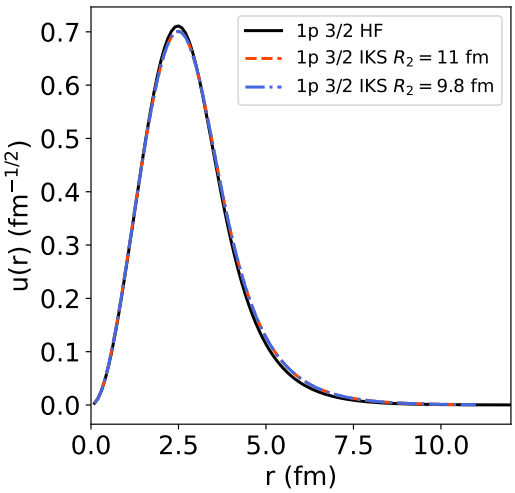


**(b)** $1p_{3/2}$ $^{16}$O radial functions

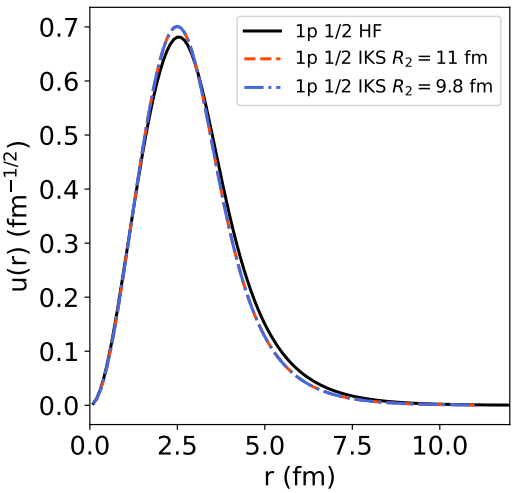


**(c)** $1p_{1/2}$ $^{16}$O radial functions

**Figure 3.6:** $^{16}$O $\{u_k(r)\}$ functions after the diagonalisation of the $(\epsilon_{ij})$ matrix, computed both through IKS and HF method. IKS orbitals are evaluated with two different values of $R_2$: 9.8 and 11 fm.

Contrary to what we were expecting, the orbitals do not change at all. We see below that this result is actually a particular case, in which the matrix $(\epsilon_{ij})$ is already diagonalised.

More interesting are the simulations regarding $^{40}$Ca nucleus; these are presented below.

### $^{40}$Ca

$^{40}$Ca includes 20 neutrons, that are distributed in 6 orbitals. We can proceed as we did before, comparing two IKS orbital sets, inverted using $R_2 = 11$ and 12.1 fm, with the HF ones. What is obtained is illustrated in Fig. 3.7.

Unlike the $^{16}$O case, we see that the $s$ orbitals of the two IKS problems have different behaviours, even though they produce the same potential. All the other IKS orbitals are in agreement both with one another and with the HF ones, thus we expect they are not influenced by the application of the unitary transformation that makes $(\epsilon_{ij})$ diagonal.
Moreover, not only have $s$ orbitals distinct behaviours from one another, but they also have a different number of radial nodes, which is unphysical.

Diagonalising the eigenvalue matrix we obtain the results in Fig. 3.8.

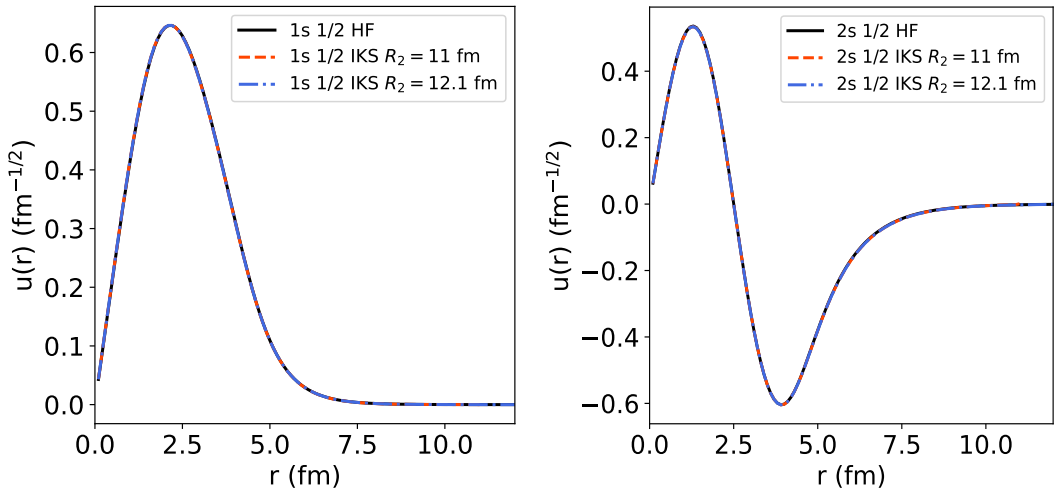


**(a)** $1s_{1/2}$ $^{40}$Ca radial functions **(b)** $2s_{1/2}$ $^{40}$Ca radial functions

**Figure 3.8:** $^{40}$Ca $s$ orbitals after the diagonalisation of the $(\epsilon_{ij})$ matrix, computed both through IKS and HF method. IKS orbitals are evaluated with two different values of $R_2$: 11 and 12.1 fm.

All the *non-s* orbitals do not change after the diagonalisation, hence their graphs were omitted.
As for $s$ orbitals, we see that the unitary transformation that diagonalises the problem provides IKS orbitals with the same behaviour, even though they were computed with different $R_2$. Moreover, they also show great agreement with the HF wave functions.

We can sum up what we obtained stating that only $s$ orbitals need to be diago-

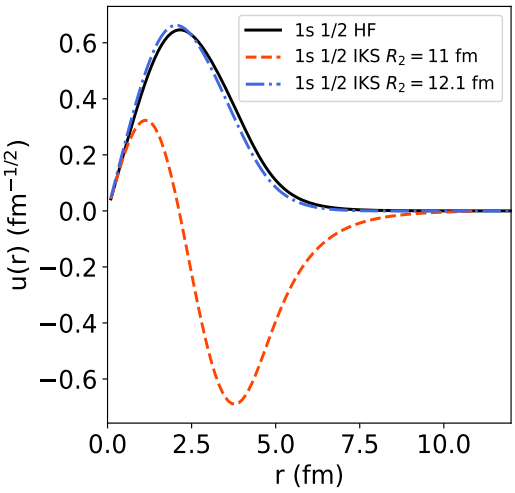


**(a)** $1s_{1/2}$ $^{40}$Ca radial functions

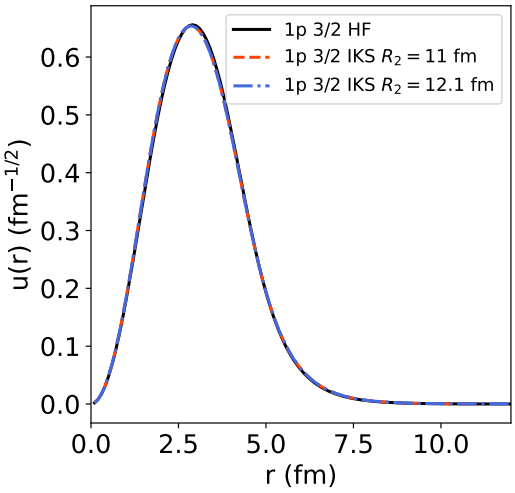


**(b)** $1p_{3/2}$ $^{40}$Ca radial functions

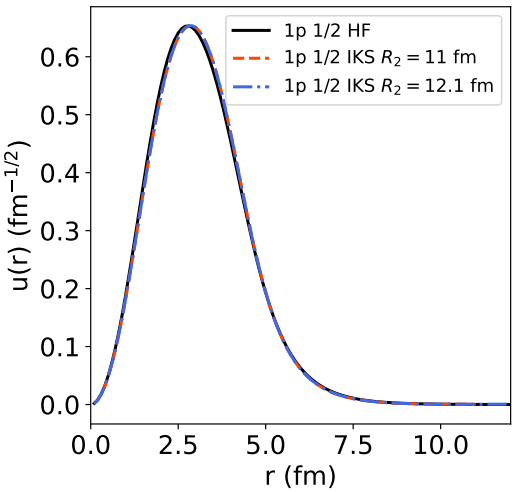


**(c)** $1p_{1/2}$ $^{40}$Ca radial functions

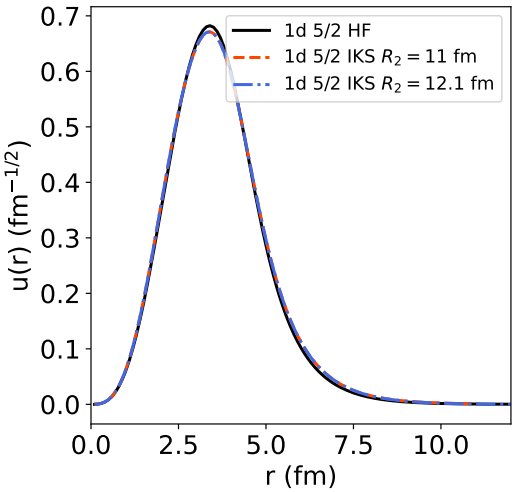


**(d)** $1d_{5/2}$ $^{40}$Ca radial functions

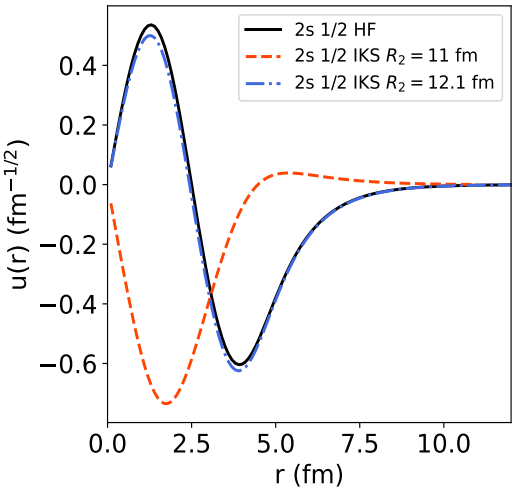


**(e)** $2s_{1/2}$ $^{40}$Ca radial functions

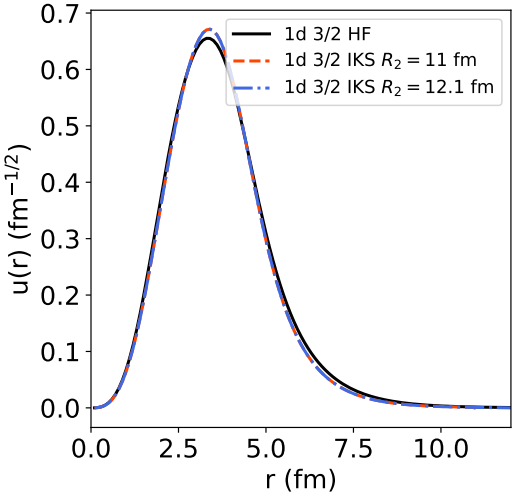


**(f)** $1d_{3/2}$ $^{40}$Ca radial functions

**Figure 3.7:** $^{40}$Ca $\{u_k(r)\}$ reduced radial functions before the diagonalisation of the $(\epsilon_{ij})$ matrix, computed both through IKS and HF method. IKS orbitals are evaluated with two different values of $R_2$: 11 and 12.1 fm.

nalised, as they are the only wave functions which mix with each other. This is due to the different principal quantum number $n$ of the two orbitals. Thus, the $(\epsilon_{ij})$ matrix can then be interpreted as a block matrix, in which the only non-diagonal terms regard $s$ orbitals.
In the $^{16}$O case we did not see any transformation among orbitals, as there were orbitals with only $n = 1$. Instead, considering $^{40}$Ca, we saw that $1s_{1/2}$ and $2s_{1/2}$ radial wave functions can be disentangled by the diagonalisation procedure, which also gives the right number of radial nodes and good compatibility with the HF orbitals.
Further simulations (e.g. harmonic oscillator with 20 particles) have demonstrated that this always happen when we deal with a system which includes orbitals with same $(l, j)$ but different $n$. From now on, this approach is employed throughout the whole work. If not explicitly specified, we always refer to the diagonalised orbitals while studying wave functions in Chap. 4.

# Chapter 4

# Reconstruction of nuclear Energy Density Functional

The purpose of this chapter is to reconstruct the nuclear energy density functional (EDF) from the knowledge of the potential of the system, which is evaluated through the Kohn Sham inverse (IKS) problem (Sec. 2.2.2). We first introduce the theoretical approach we use to face the problem (Sec. 4.1 and 4.2), applying then such model to analytical potentials for which we can compute the exact expression of the EDF and compare the results (Sec. 4.3).
The next step is to focus on the harmonic oscillator (Sec. 4.4), which is a particularly suitable test as its wave functions are known analytically. We eventually specialise our study on proper nuclear interactions (Sec. 4.5), namely SkX and $(t_0, t_3)$ models, analysing both their orbitals as well as potentials and pursuing the reconstruction of the EDF using the IKS procedure shown in Chap. 3.

## 4.1 A function integration formula: from potential to energy functional

We have seen that one of the main quantities which characterises a nucleus is its binding energy (Sec. 1.1). Thanks to the first HK theorem we know it is possible to express the system energy as a density functional (EDF); however, the expression of such EDF is usually unknown.
In this passage we study a method to evaluate the energy functional starting from the knowledge of the potential $v_{KS}(\mathbf{r})$ (Eq. (2.33)), calculated from the DFT inverse problem (Sec. 2.2). The approach we follow throughout this section is presented by Gaiduk in [39] and [40].
The main idea of this model consists in reconstructing the energy functional $U[\rho]$ through some sort of functional "integration" of a model potential $v(\mathbf{r})$. We first discuss the method for a general potential, treating the Kohn-Sham potential later.

By definition, we can write the potential as a functional derivative of the energy:

$$v(\mathbf{r}) = \frac{\delta U[\rho]}{\delta \rho(\mathbf{r})} \tag{4.1}$$

If we consider a local potential, that is, a potential which only depends on $\rho$, and not on $\nabla\rho$ or higher derivatives of $\rho$, then the energy functional can be found simply through an integral of the potential:

$$U_{loc}[\rho] = \int d\mathbf{r}\, v_{loc}(\mathbf{r})\rho(\mathbf{r}) \tag{4.2}$$

This simple formula is not valid if the potential is semilocal, i.e. if $\nabla\rho$ and higher derivatives of the density appear inside $v(\mathbf{r})$ expression, as the functional derivative takes the form Eq. (A.5).
To overcome such limitation, van Leeuwen and Baerends [41] suggested to introduce an additional parameter $t$ into the density $\rho(\mathbf{r})$ to create a path of densities $\rho_t(\mathbf{r})$ parametrised by $t$: this way we can see the energy functional as a function of the parameter $t$, $U[\rho_t] = U(t)$. The derivative of this newly-made function reads:

$$\frac{\partial U(t)}{\partial t} = \int d\mathbf{r}\, \frac{\delta U[\rho_t]}{\delta \rho_t(\mathbf{r})} \frac{\partial \rho_t(\mathbf{r})}{\partial t} = \int d\mathbf{r}\, v([\rho_t];\mathbf{r}) \frac{\partial \rho_t(\mathbf{r})}{\partial t} \tag{4.3}$$

Integrating the above equation from $t = A$ to $t = B$ we obtain:

$$U[\rho_B] - U[\rho_A] = \int_A^B dt\, \frac{\partial U(t)}{\partial t} = \int_A^B dt \int d\mathbf{r}\, v([\rho_t(\mathbf{r})];\mathbf{r}) \frac{\partial \rho_t(\mathbf{r})}{\partial t} \tag{4.4}$$

This is the most general form of the line integral over $t$, which holds for any path connecting $\rho_A$ and $\rho_B$.

Choosing a parametrisation of $\rho_t(\mathbf{r})$ so that $U[\rho_A] = 0$ and $\rho_B(\mathbf{r}) = \rho(\mathbf{r})$, Eq. (4.4) becomes:

$$U[\rho] = \int_0^1 dt \int d\mathbf{r}\, v([\rho_t(\mathbf{r})];\mathbf{r}) \frac{\partial \rho_t(\mathbf{r})}{\partial t} \tag{4.5}$$

Thus, once the potential of the system is known, it is possible to find the EDF expression through Eq. (4.5).

As the path $\rho_t(\mathbf{r})$ is arbitrary, we can choose any *reasonable* parametrisation of the density in order to perform the line integral, that is, any path whose derivative $\partial\rho_t/\partial t$ is well defined for all values of $t$. In practice, it is useful to integrate along paths with physical meaning, such as magnitude- or coordinate-scaled density paths.
We now focus on the three different scalings introduced in [40].

### 4.1.1 Density scalings

The three scalings considered below are called $q-$scaling, $\lambda-$scaling and $\zeta-$scaling.

**q-scaling**

The first transformation we take into consideration is the linear density scaling [42] [43] [44], which reads:

$$\rho_q(\mathbf{r}) = q\rho(\mathbf{r}) \tag{4.6}$$

The derivative of the scaled density with respect to the parameter gives:

$$\frac{\partial \rho_q(\mathbf{r})}{\partial q} = \frac{\partial [q\rho(\mathbf{r})]}{\partial q} = \rho(\mathbf{r}) \tag{4.7}$$

Thus, we can write the integral in Eq. (4.5) explicitly for the q-scaling:

$$\begin{aligned} U[\rho] &= \int_0^1 dq \int d\mathbf{r}\ v([\rho_q(\mathbf{r})], \mathbf{r})\ \frac{\partial \rho_q(\mathbf{r})}{\partial q} \\ &= \int_0^1 dq \int d\mathbf{r}\ v([q\rho(\mathbf{r})], \mathbf{r})\ \rho(\mathbf{r}) \\ &= 4\pi \int_0^1 dq \int dr\ r^2\ v([q\rho(r)], r)\ \rho(r) \end{aligned} \tag{4.8}$$

In the last step spherical coordinates have been used: this last term holds as long as the system is spherically symmetric and the density depends exclusively on the radius $r$.
Normalisation of the scaled density $\rho_q$ leads to:

$$\int d\mathbf{r}\, \rho_q(\mathbf{r}) = \int d\mathbf{r}\, q\rho(\mathbf{r}) = qN \tag{4.9}$$

Where we used the normalisation of the ground state density $\rho(\mathbf{r})$ to the number of particles have been used.
Eq. (4.9) states that this scaling does not keep the system particle number constant, changing as $qN$.

**$\lambda$-scaling**

Another choice of the path transformation is the uniform density scaling, which we call $\lambda$-scaling:

$$\rho_\lambda(\mathbf{r}) = \lambda^3 \rho(\lambda \mathbf{r}) \tag{4.10}$$

Calculating the scaling derivative we have:

$$\frac{\partial \rho_\lambda(\mathbf{r})}{\partial \lambda} = \frac{\partial [\lambda^3 \rho(\lambda \mathbf{r})]}{\partial \lambda} = \lambda^2 [3\rho(\lambda \mathbf{r}) + (\lambda \mathbf{r}) \cdot \nabla_{\lambda \mathbf{r}}\, \rho(\lambda \mathbf{r})] \tag{4.11}$$

Eventually Eq. (4.5) takes the form:

$$\begin{aligned} U[\rho] &= \int_0^1 d\lambda \int d\mathbf{r}\ v([\rho_\lambda(\mathbf{r})], \mathbf{r})\ \frac{\partial \rho_\lambda(\mathbf{r})}{\partial \lambda} \\ &= \int_0^1 d\lambda \int d\mathbf{r}\ v([\lambda^3 \rho(\lambda \mathbf{r})], \mathbf{r})\ \lambda^2\, [3\rho(\lambda \mathbf{r}) + (\lambda \mathbf{r}) \cdot \nabla_{\lambda \mathbf{r}}\, \rho(\lambda \mathbf{r})] \\ &= \int_0^1 d\lambda \int d\mathbf{x}\ v([\lambda^3 \rho(\mathbf{x})], \mathbf{x}/\lambda)\ \frac{3\rho(\mathbf{x}) + \mathbf{x} \cdot \nabla_{\mathbf{x}}\, \rho(\mathbf{x})}{\lambda} \\ &= 4\pi \int_0^1 d\lambda \int dx\ x^2\ v([\lambda^3 \rho(x)], x/\lambda)\ \frac{3\rho(x) + x\, \frac{\partial \rho(x)}{\partial x}}{\lambda} \end{aligned} \tag{4.12}$$

This particular scaling plays a major role as it has strict relations with the Levy-Perdew virial relation [41] [45], which reads:

$$U_v[\rho] = \int d\mathbf{r}\, v_v(\mathbf{r})[3\rho(\mathbf{r}) + \mathbf{r}\cdot\nabla\rho(\mathbf{r})] \tag{4.13}$$

Eq. (4.12) and (4.13) are indeed the same as long as the following condition holds:

$$v([\rho_\lambda];\mathbf{r}) = \lambda v([\rho];\lambda\mathbf{r}) \tag{4.14}$$

Eq. (4.14) is always valid for any exchange potential, as they are homogeneous of degree one [46].

Moreover $\lambda$-scaling conserves the particle number of the system:

$$\int d\mathbf{r}\,\rho_\lambda(\mathbf{r}) = \int d\mathbf{r}\,\lambda^3\rho(\lambda\mathbf{r}) = \int d\mathbf{x}\,\rho(\mathbf{x}) = N \tag{4.15}$$

Physical interpretation of such transformation is straightforward: we see from Eq. (4.10) that as $\lambda$ increases, the system is getting narrower. This has important consequences both on the density and on the potential behaviour, which are studied later in Sec. 4.4 and 4.5.

**$\zeta$-scaling**

The last scaling we focus on is the $\zeta$-scaling:

$$\rho_\zeta(\mathbf{r}) = \zeta^2\rho(\zeta^{1/3}\mathbf{r}) \tag{4.16}$$

whose derivative reads:

$$\frac{\partial\rho_\zeta(\mathbf{r})}{\partial\zeta} = \frac{\partial[\zeta^2\rho(\zeta^{1/3}\mathbf{r})]}{\partial\zeta} = \zeta\left[2\rho(\zeta^{1/3}\mathbf{r}) + \frac{\zeta^{1/3}\mathbf{r}}{3}\cdot\nabla_{\zeta^{1/3}\mathbf{r}}\,\rho(\zeta^{1/3}\mathbf{r})\right] \tag{4.17}$$

Eq. (4.5) then becomes:

$$\begin{aligned} U[\rho] &= \int_0^1 d\zeta \int d\mathbf{r}\; v([\rho_\zeta(\mathbf{r})],\mathbf{r})\;\frac{\partial\rho_\zeta(\mathbf{r})}{\partial\zeta} \\ &= \int_0^1 d\zeta \int d\mathbf{r}\; v([\zeta^2\rho(\zeta^{1/3}\mathbf{r})],\mathbf{r})\;\zeta\left[2\rho(\zeta^{1/3}\mathbf{r}) + \frac{\zeta^{1/3}\mathbf{r}}{3}\cdot\nabla_{\zeta^{1/3}\mathbf{r}}\,\rho(\zeta^{1/3}\mathbf{r})\right] \\ &= \int_0^1 d\zeta \int d\mathbf{x}\; v([\zeta^2\rho(\mathbf{x})],\mathbf{x}/\zeta^{1/3})\;\left[2\rho(\mathbf{x}) + \frac{\mathbf{x}}{3}\cdot\nabla_{\mathbf{x}}\,\rho(\mathbf{x})\right] \\ &= 4\pi\int_0^1 d\zeta \int dx\; x^2\; v([\zeta^2\rho(x)],x/\zeta^{1/3})\;\left[2\rho(x) + \frac{x}{3}\frac{\partial\rho(x)}{\partial x}\right] \end{aligned} \tag{4.18}$$

$\zeta$-scaling was introduced by Perdew [47] in order to study a system in which the number of particle changes as $\zeta N$, in fact:

$$\int d\mathbf{r}\,\rho_\zeta(\mathbf{r}) = \int d\mathbf{r}\,\zeta^2\rho(\zeta^{1/3}\mathbf{r}) = \int d\mathbf{x}\,\zeta\rho(\mathbf{x}) = \zeta N \tag{4.19}$$

### 4.1.2 Stray and non stray potentials

It is now natural to ask whether the choice of the scaling, that is, the density path $\rho_t$, may influence the EDF obtained by Eq. (4.5).
The answer to the question is found in functional analysis: if the model potential $v([\rho(\mathbf{r})];\mathbf{r})$ is a functional derivative, then it admits a parent functional $U[\rho]$ such that Eq. (4.1) holds, producing the same result for any choice of $\rho_t$. Otherwise the potential is called *stray* and the integral (4.5) is path-dependent.

The treatment of stray potential is a delicate topic and closely recalls the problem of incomplete differentials from the ordinary calculus. Although we do not address such difficulties, referring to [39] for a deeper study, we report a condition which is both necessary and sufficient for a potential to be non stray:

$$\frac{\delta v([\rho];\mathbf{r})}{\delta\rho(\mathbf{r}')} = \frac{\delta v([\rho];\mathbf{r}')}{\delta\rho(\mathbf{r})} \tag{4.20}$$

In the present work we focus on the model potential $v_{KS}(\mathbf{r})$ which is calculated through the Kohn Sham approach. In this case, path-dependence of the line integral is not the only problem of stray model potentials: in fact, if the potential is not a functional derivative, then the Kohn-Sham equations do not represent a solution to any energy minimisation problem (Sec. 2.2.2), and the density computed from the orbitals $\phi_k(\mathbf{r})$ does not correspond to the real minimum of the energy.
Nevertheless, other works [26] [34] [48] have showed the great agreement between the potential calculated from the IKS method and other models, e.g. Hartee-Fock and van Leeuwen e Baerends procedure, proving the accuracy of the minimum found through the IKS procedure.
Therefore we can assume that $v_{KS}(\mathbf{r})$ is a functional derivative and admits a parent functional. Every scaling presented above must then lead to the same EDF.

## 4.2 Purpose of the work

Having introduced the theoretical model we use to reconstruct the energy density functional, we now outline the practical approach, explaining how we evaluate physical quantities using the IKS and to which nuclear systems we apply the method.

The original work [40] focused on the application of this density scaling technique to analytical potentials expressed as density functionals (e.g. local density approximation (LDA) potentials [39]); thus, even the EDF expression could be found explicitly using Eq. (4.5), at least as long as the solution of such integral could be written analytically. In contrast, in this work the ultimate purpose is to apply the theory presented above to evaluate the EDF of nuclear systems whose potential is not known, since they make up the majority of nuclear cases, as we widely discussed in Chap. 1. To do so, if we still want to use Eq. (4.5), not only the potential of the original system must be evaluated, but we also need to compute the potential $v([\rho_t];\mathbf{r})$ of the scaled systems, that are

systems whose density is subjected to a scaling induced by the generic parameter $t$. This way we are able to perform the line integration of the potential over the density path $\rho_t(\mathbf{r})$ and find the energy functional.

In this perspective the IKS approach comes in aid: indeed, to find the potential of scaled and non scaled systems, we could apply the CV method. As for the non scaled problem, the approach is identical to what has been done in Sec. 3.2: we start calculating the orbitals by minimising the kinetic functional subjected to the constrains on density and orthonormality, then by solving EL equations to find the potential $v_{KS}(\mathbf{r})$. However, the very same procedure can be applied to the scaled system, paying attention that now a scaling is applied to the system density which now is $\rho_t(\mathbf{r})$. Using such density in the IKS technique, one first obtains the scaled orbitals, then finds the scaled potential of the system. We focus on the physical meaning of such transformations in Sec. 4.4.
Once the potentials have been evaluated, we can finally compute the energy functional from Eq. (4.5) or, more generally, from Eq. (4.4).

## 4.3 Preliminary tests

We verify the correctness of the line-integral formula (Eq. (4.5)) in a simple case of a local energy functional, both from the analytical and the numerical point of view. The results obtained are seen as benchmarks for the calculations of the following sections.
We start considering an energy density functional of the form:

$$U = \int_0^{\mathbf{R}_{max}} d\mathbf{r}\ \frac{a}{\alpha+1}[\rho(\mathbf{r})]^{\alpha+1} = 4\pi \int_0^{R_{max}} dr\ r^2 \frac{a}{\alpha+1}[\rho(r)]^{\alpha+1} \tag{4.21}$$

where spherical symmetry of the system has been used in the last step. $a$ and $\alpha$ are arbitrary values, $R_{max}$ is the volume radius in which the particles are confined. We use $R_{max}$ as the integration upper bound in order to study how the energy depends on the system size.
Calling $\mathcal{E}$ the energy density, defined as:

$$\mathcal{E} = \frac{a}{\alpha+1}[\rho(\mathbf{r})]^{\alpha+1} \tag{4.22}$$

potentials can then be evaluated from a functional derivative (Eq. (4.1)):

$$v([\rho(\mathbf{r})], \mathbf{r}) = \frac{\delta U}{\delta \rho} = \frac{\partial \mathcal{E}}{\partial \rho} = a[\rho(\mathbf{r})]^{\alpha} \tag{4.23}$$

Using this approach we can compute the system energy both from Eq. (4.21) and from Eq. (4.5), which was derived from considerations of functional analysis in Sec. 4.1. This way we compute the EDF with two different methods so as to compare the results.
However, before showing what simulations yield, it is interesting to explicitly prove that Eq. (4.5), with a potential of the form (4.23), leads to Eq. (4.21) from which we

started. We do that in the case of $\lambda-$ scaling (Sec. 4.1.1).
Applying the scaling $\rho_\lambda(\mathbf{r}) = \lambda^3\rho(\lambda\mathbf{r})$ to Eq. (4.23) we have:

$$v[\rho_\lambda] = a\lambda^{3\alpha}\rho^\alpha(\lambda\mathbf{r}) = a\lambda^{3\alpha}\rho^\alpha(\mathbf{x}). \tag{4.24}$$

Then, from Eq. (4.5):

$$\begin{aligned} U[\rho] &= \int_0^1 d\lambda \int d^3r\ v[\rho_\lambda]\frac{\partial\rho_\lambda}{\partial\lambda} \\ &= a\int_0^1 d\lambda\ \lambda^{3\alpha-3+2}\int d^3x\ \rho^\alpha(\mathbf{x})\left[3\rho(\mathbf{x}) + \mathbf{x}\cdot\nabla_{\mathbf{x}}\rho(\mathbf{x})\right]. \end{aligned} \tag{4.25}$$

Employing the divergence theorem and integration by parts, we take into account that:

$$\begin{aligned} &\int d^3x\ \nabla\cdot(\mathbf{x}\rho^{\alpha+1}(\mathbf{x})) = 0 = \int d^3x\ \left[3\rho^{\alpha+1}(\mathbf{x}) + (\alpha+1)\,\rho^\alpha(\mathbf{x})\mathbf{x}\cdot\nabla\rho\right], \\ &\int d^3x\ \ (\alpha+1)\,\rho^\alpha(\mathbf{x})\mathbf{x}\cdot\nabla\rho = -\int d^3x\ 3\rho^{\alpha+1}(\mathbf{x}). \end{aligned} \tag{4.26}$$

Thus, Eq. (4.25) becomes

$$\begin{aligned} U[\rho] &= a\frac{\lambda^{3\alpha}}{3\alpha}\Big|_0^1 \int d^3x\ \left(1 - \frac{1}{\alpha+1}\right)3\rho^{\alpha+1}(\mathbf{x}) \\ &= \frac{a}{\alpha+1}\int d^3x\ \rho^{\alpha+1}(\mathbf{x}). \end{aligned} \tag{4.27}$$

Eq. (4.27) is exactly the EDF (4.21) we started from.

Focusing now to some specific cases, we study the EDF in Eq. (4.21) with $\alpha = 2$ varying the radius $R_{max}$. The choice of $\alpha = 2$ allows to interpret the system energy as stemming from a two-body interaction [16]. Physically speaking, we are analysing what happens to the energy of a system which is increasing in size, keeping its number of particles constant.
Once the form of the potential energy functional has been chosen, we analyse some specific cases with suitably chosen densities. We start from a constant density:

$$\rho(\mathbf{r}) = \begin{cases} bN, & \text{if } 0 < r < R_{max} \\ 0, & \text{otherwise.} \end{cases}$$

where $N$ is the normalisation constant and $b$ an arbitrary constant, we can compute the system energy in the two ways said before, obtaining the results shown in Fig. 4.1.

All the scalings presented in Fig. 4.1 show great agreement to the theoretical one and, therefore, to each other. Indeed, as discussed in Sec. 4.1.2, the potential taken into consideration is a functional derivative (from definition of Eq. (4.22)), thus, the $q-$, $\lambda-$, and $\zeta-$ scaling must lead to the same result.
Moreover, the monotonic decreasing behaviour of the energy can be understood as, when the system becomes bigger, particles inside it are on average more distant to each other; thus the interaction is weaker and the energy lessens, vanishing as $R_{max} \to \infty$.

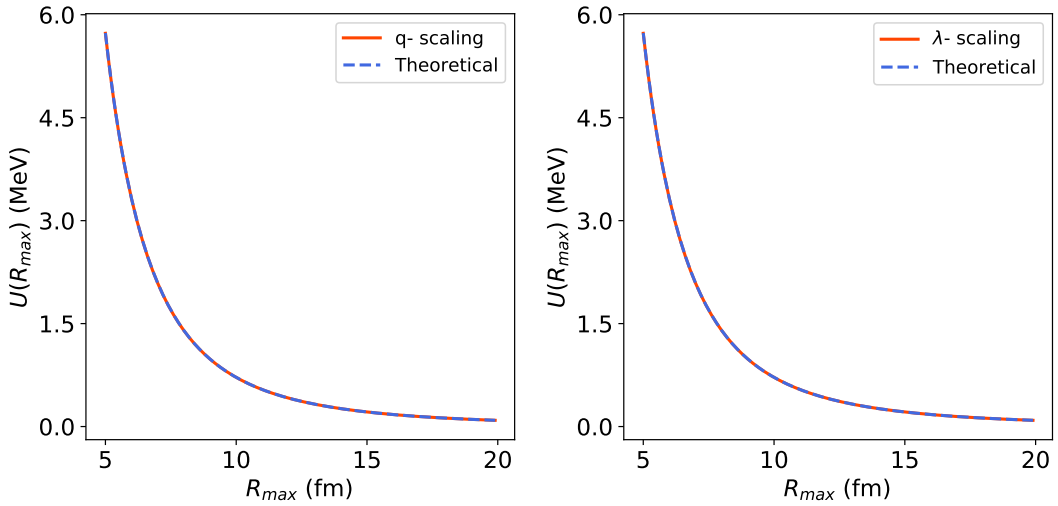


**(a)** q-scaling **(b)** $\lambda$-scaling

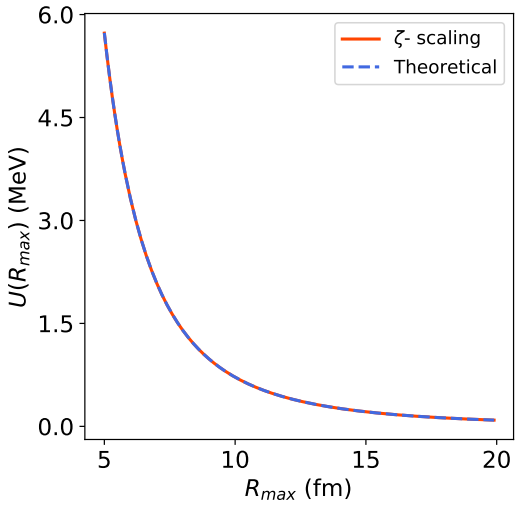


**(c)** $\zeta$-scaling

**Figure 4.1:** Energy density functional computed from Eq. (4.21) (Theoretical) and Eq. (4.5) (t-scaling), using a constant density $\rho(r)$. The parameters are: $a = 3000$ MeV fm$^6$ and $b = 3$ fm$^{-3}$.

Addressing now to a more physical density, we consider a Fermi function (Sec. 1.1) written as:

$$\rho(\mathbf{r}) = \rho(r) = \frac{bN}{1 + \exp(\frac{r - R_c}{c})} \tag{4.28}$$

$N$ is the normalisation constant, $b$ and $c$ arbitrary constants, $R_c$ the cut-off radius. In Fig. 4.2 we show the results obtained by simulations with such density.

Again, results obtained by different scalings are compatible both with the theoretical behaviour and with each other for the same reasons we said above. We see that the system energy converges to a constant value when $R_{max} > R_c + c$ : in fact, particles are confined inside a specific region which is determined by the exponential function in Eq. (4.28). Even though we expand the system, as the distance between particles does not change, the system energy remains constant.

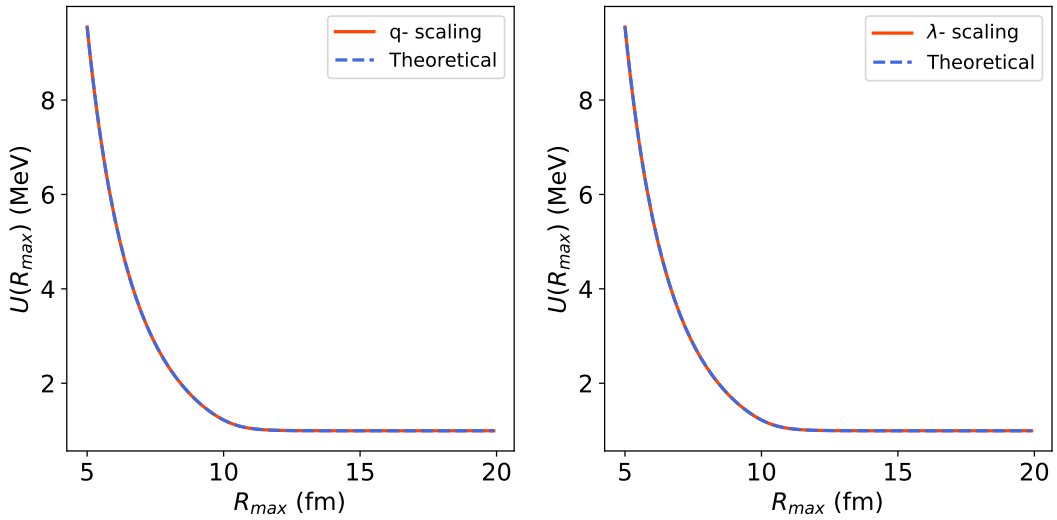


**(a)** q-scaling **(b)** $\lambda$-scaling

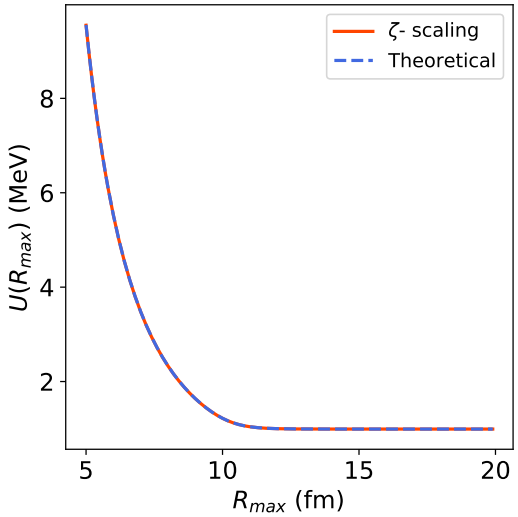


**(c)** $\zeta$-scaling

**Figure 4.2:** Energy density functional computed from Eq. (4.21) (Theoretical) and Eq. (4.5) (t-scaling), using a Fermi function density $\rho(r)$. Chosen parameters are: $a = 5000$ MeV fm$^6$, $b = 50$ fm$^{-3}$ , $c = 0.5$ fm, and $R_c = 10$ fm.

Even though in this section we used all the three scalings to make it clear that they lead to the very same quantities (at least for potential which are functional derivatives, see Sec. 4.1.2), from now on we only consider the $\lambda-$scaling, as it is the only one which maintains the number of particles of the system constant and has a clear physical interpretation.

## 4.4 $\lambda-$scaled orbitals and physical interpretation

In this section we pursue a more in-depth study on the physical meaning of the $\lambda-$scaling presented in Sec. 4.1.1.

We could ask what happens to the set of orbitals $\phi_k(\mathbf{r})$ when a scaling of the form (4.10) is applied to the density of the system. In particular, the objective is to understand how radial functions scale.
We start by writing down the density as

$$\rho(\mathbf{r}) = \sum_{j=1}^{\mathrm{N_{orb}}} d_j \, |\phi_j(\mathbf{r})|^2 \tag{4.29}$$

where $d_j$ the degeneracy of each orbital. Applying Eq. (4.10) we obtain:

$$\rho_\lambda(\mathbf{r}) = \lambda^3 \rho(\lambda\mathbf{r}) = \lambda^3 \sum_{j=1}^{\mathrm{N_{orb}}} d_j \, |\phi_j(\lambda\mathbf{r})|^2 = \sum_{j=1}^{\mathrm{N_{orb}}} d_j \, |\phi_{\lambda_j}(\mathbf{r})|^2 \tag{4.30}$$

$$\phi_\lambda(\mathbf{r}) = \lambda^{3/2} \phi(\lambda\mathbf{r}) \tag{4.31}$$

While Eq. (4.30) always holds, as it represents the $\lambda-$scaling applied to orbitals, the scaling of Eq. (4.31) is found under the assumption that every wave function scales in the same way as the others. In principle, each $\phi_j(r)$ could scale on its own and thus Eq. (4.31) may not hold. However, from a physical point of view, the condition that radial functions are subjected to the very same scaling is a reasonable ansatz.
Eventually, changing into spherical coordinates and introducing reduced radial functions $u(r)$ and spherical harmonics $Y(\theta, \varphi)$, we obtain the scaling of the former wave functions:

$$\phi_\lambda(\mathbf{r}) = \phi_\lambda(r, \theta, \varphi) = \frac{u_\lambda(r)}{r} \, Y(\theta, \varphi) \tag{4.32}$$

$$\phi_\lambda(\mathbf{r}) = \lambda^{3/2} \phi(\lambda\mathbf{r}) = \lambda^{3/2} \frac{u(\lambda r)}{\lambda r} \, Y(\theta, \varphi) = \lambda^{1/2} \frac{u(\lambda r)}{r} \, Y(\theta, \varphi) \tag{4.33}$$

$$u_\lambda(r) = \lambda^{1/2} \, u(\lambda r) \tag{4.34}$$

Therefore, aims of the following simulations are to prove the validity of the assumption made on the $\phi$ scaling in Eq. (4.31), as well as to study the potential generated by the scaled orbitals, that is, the potential of the scaled system with density $\rho_\lambda(\mathbf{r})$.

Throughout the whole section we focus on the harmonic oscillator model, whose wave functions and potential are known analytically, allowing a comparison with the theoretical behaviours.

We start considering a 20-particle harmonic oscillator, applying the scaling (4.10) with a parameter $\lambda = 0.6$ to the system. 0.6 is a suitable value for $\lambda$ as it is far enough from $\lambda = 1$ to allow the distinction between wave functions of the scaled and non scaled system, while not being too close to $\lambda = 0$, for which numerical errors arise (see Sec.

4.5).
The orbitals of the scaled system can be computed either by following the IKS approach or by using the theoretical knowledge of the HO wave functions. The former consists in employing the scaled density in the IKS procedure (Sec. 2.2.2) when the system density is $\rho_\lambda(\mathbf{r})$. Indeed, from the IPOPT optimisation we obtain the ground state orbitals related to the scaled system.
Otherwise, it is possible to evaluate the scaled orbitals directly from HO wave functions presented in Sec. 1.2.2: we do that by applying Eq. (4.34) to Eq. (1.8), remembering that, since $u(r) = r\,R(r)$, the scaling is of the form $u_\lambda(r) = \lambda^{3/2}\, r\, R(\lambda r)$. In formula we have:

$$R_\lambda(r) = \lambda^{3/2} R(\lambda r) \tag{4.35}$$

$$R_{\lambda_{kl}}(r) = \lambda^{3/2}\, N_{kl} (\lambda r)^l e^{-\nu(\lambda r)^2} L_k^{(l+\frac{1}{2})}(2\nu(\lambda r)^2) \tag{4.36}$$

Eq. (4.36) expresses the theoretical scaled wave functions.
We can now run the simulations: results are presented in Fig. 4.3. We also remind that $(\epsilon_{ij})$ diagonalisation of Sec. 3.3 is taken into account.

Comparing the scaled orbitals of Fig. 4.3 we see that the two methods employed provide the same results. Moreover, as we discussed in Sec. 4.1.1, we understand that $\lambda-$scaling with a parameter $\lambda < 1$ consists in an expansion of the original system, as the wave functions of the scaled problem are wider than the non scaled ones. Eventually, we have also found that the scaling (4.34) is a reasonable assumption, as it properly describes the orbital scaling behaviour.

We now concentrate on the study of the harmonic oscillator potential when the same $\lambda-$scaling is applied to the system. These potentials are generated by the orbitals shown in Fig. 4.3.
We both compute the potential of the non scaled system and the scaled one: as for the non scaled potential, we compare the theoretical potential of Eq. (1.6) with the one obtained by the IKS method which uses the original non scaled system density; instead, for the scaled potential, we follow a different approach. From Eq. (4.36) we note that we can interpret the $\lambda-$ scaling as if it were applied to the system frequency $\nu$, modifying it as $\nu_\lambda = \lambda^2\nu$. Indeed, writing down again Eq. (4.36) and using the definition of $N_{kl}$ (Eq. (1.9)), we have:

$$\begin{aligned} R_{\lambda_{kl}}(r) &= \lambda^{3/2}\, N_{kl} (\lambda r)^l e^{-\nu(\lambda r)^2} L_k^{(l+\frac{1}{2})}(2\nu(\lambda r)^2) \\ &= \sqrt{\sqrt{\frac{2\nu^3\lambda^6}{\pi}} \frac{2^{k+2l+3}\; k!\; \nu^l \lambda^{2l}}{(2k+2l+1)!!}}\, r^l e^{-\nu\lambda^2 r^2} L_k^{(l+\frac{1}{2})}(2\nu\lambda^2 r^2) \\ &= \sqrt{\sqrt{\frac{2\nu_\lambda^3}{\pi}} \frac{2^{k+2l+3}\; k!\; \nu_\lambda^l}{(2k+2l+1)!!}}\, r^l e^{-\nu_\lambda r^2} L_k^{(l+\frac{1}{2})}(2\nu_\lambda r^2) \end{aligned} \tag{4.37}$$

The physical interpretation is straightforward: for $\lambda < 1$, varying on $\lambda$, the potential decreases as $v(r) = \frac{1}{2} m(\lambda^2\omega)^2 r^2$, making the system less confined. This is indeed what is happening, since the system density is wider.
It is now possible to compare this result with the one obtained by the scaled potential

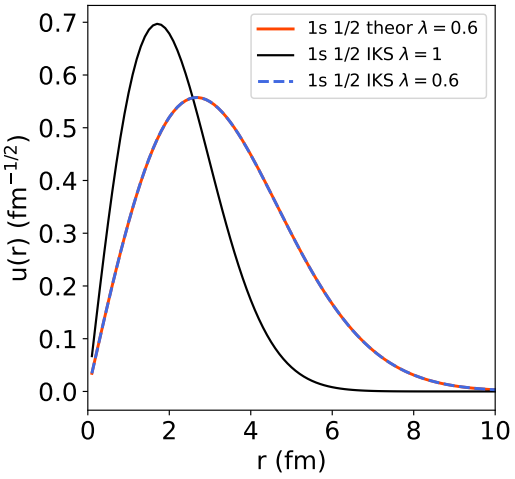


**(a)** $1s_{1/2}$ 20-particle HO radial functions

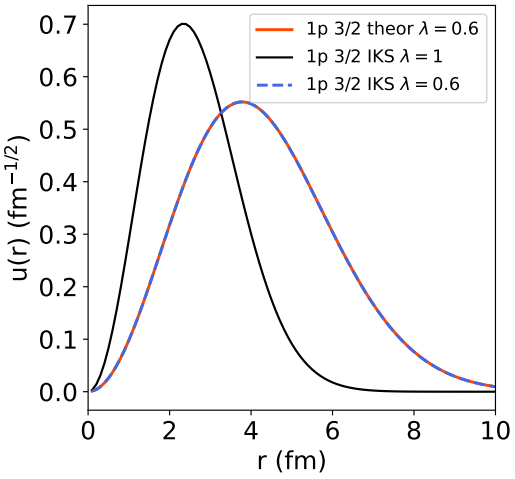


**(b)** $1p_{3/2}$ 20-particle HO radial functions

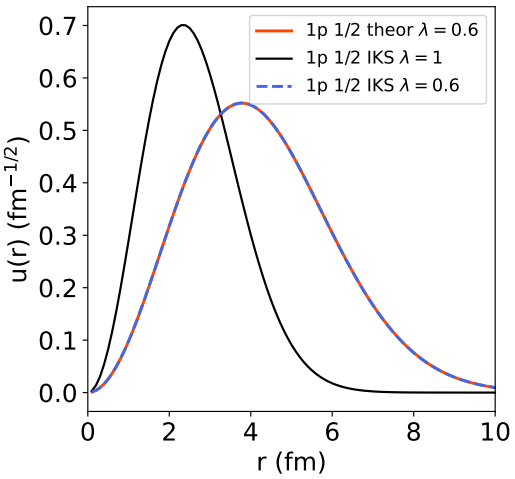


**(c)** $1p_{1/2}$ 20-particle HO radial functions

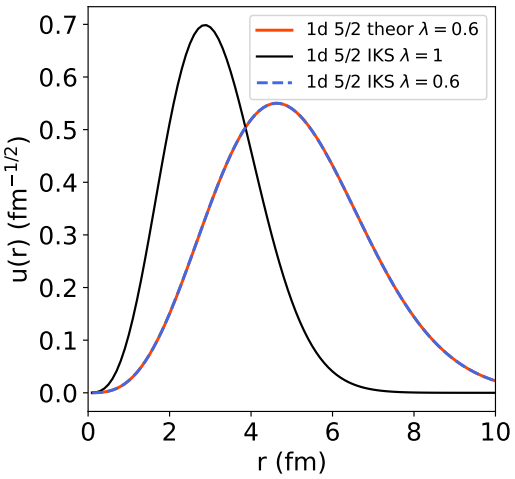


**(d)** $1d_{5/2}$ 20-particle HO radial functions

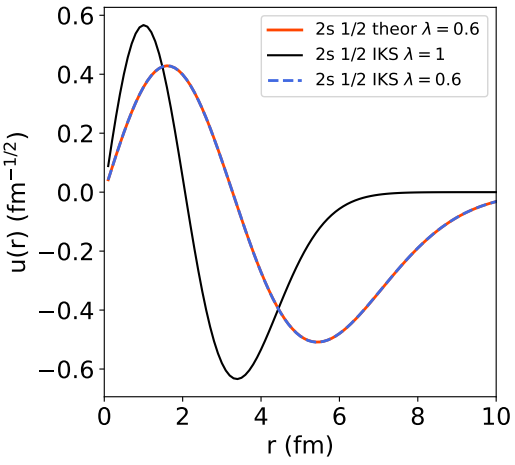


**(e)** $2s_{1/2}$ 20-particle HO radial functions

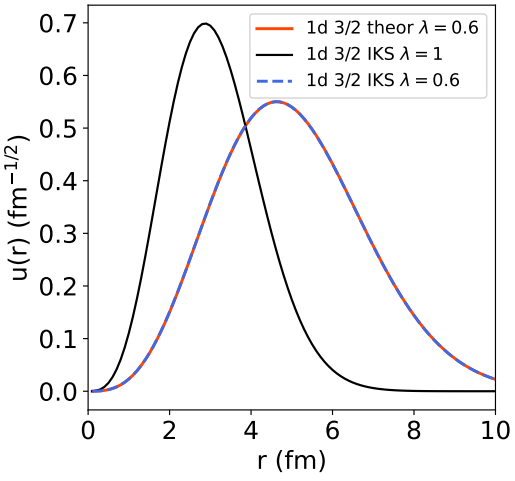


**(f)** $1d_{3/2}$ 20-particle HO radial functions

**Figure 4.3:** 20-particle HO $\{u_k(r)\}$ reduced radial functions computed from the IKS approach of the non scaled ($\lambda = 1$) and scaled system ($\lambda = 0.6$). *theor* represents the scaling Eq. (4.34) applied directly to the analytical expression of HO wave functions (Eq. (4.36)).

generated by the IKS approach, which employs the scaled system density $\rho_\lambda(r)$. Potentials are presented in Fig. 4.4.

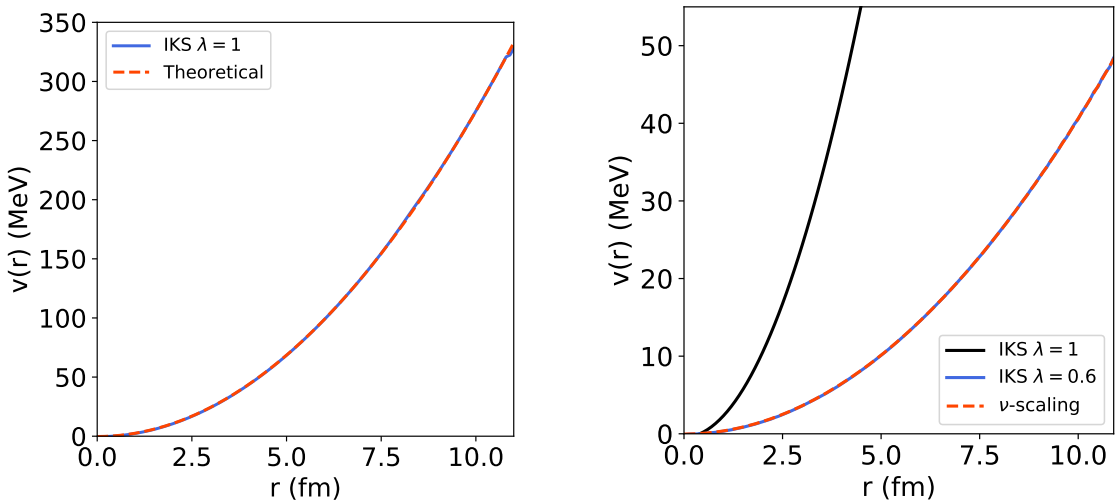


**(a)** Potentials of the original system

**(b)** Potentials for $\lambda = 0.6$

**Figure 4.4:** (a) 20-particle HO potentials of the non scaled system, computed from the IKS approach and the analytical form of the potential. (b) 20-particle HO comparison between potentials of the non scaled and scaled system with $\lambda = 0.6$. These last are evaluated both using the IKS approach (IKS $\lambda = 0.6$) and applying the $\nu-$scaling of the form $\nu_\lambda = \lambda^2\nu$ to the analytical expression of the potential. A comparison is made with the non scaled potential (IKS $\lambda = 1$).

The results obtained are consistent with the theoretical behaviours, therefore proving the considerations made above. In addition, as suggested before, we see that for $\lambda < 1$ the scaled potentials are wider than the ones of the original system.

In conclusion, we have seen how $\lambda-$scaling of Eq. (4.10) influences both the orbitals and the potential of a system. Although we made this analysis for the HO case, the physical interpretation of such transformations should not depend on the model taken into consideration. Indeed, we obtain qualitatively similar results when applying the scalings on nuclear models in Sec. 4.5.

## 4.5 EDF from simple nuclear potentials

In this section we finally apply the method introduced in Sec. 4.1 to proper nuclear systems so as to evaluate the energy functional. The models taken into account are SkX first (Sec. 4.5.1) and then $(t_0, t_3)$ (Sec. 4.5.2).
However, before pursuing such objective, we recall that Eq. (4.4) only provides the potential energy of the system; thus, to calculate the total energy, the kinetic term must be taken into account as well.
To understand how $\lambda-$scaling affects the kinetic functional, we start from its definition in Eq. (2.39) and apply the orbital scaling we found in Eq. (4.31). Proceeding with

the calculations we have:

$$\begin{aligned} T_s^{\lambda}[\{\phi_k\}] &= \frac{\hbar^2}{2m}\sum_{k=1}^{\mathrm{N_{orb}}} d_k \int d^3r \ |\nabla_{\mathbf{r}}\phi_{\lambda_k}(\mathbf{r})|^2 = \\ &= \frac{\hbar^2}{2m}\sum_{k=1}^{\mathrm{N_{orb}}} d_k \int d^3r \ \left|\nabla_{\lambda\mathbf{r}}\lambda^{3/2}\phi_k(\lambda\mathbf{r})\right|^2 = \\ &= \lambda^2 \frac{\hbar^2}{2m}\sum_{k=1}^{\mathrm{N_{orb}}} d_k \int d^3x \ |\nabla_{\mathbf{x}}\phi_k(\mathbf{x})|^2 = \\ &= \lambda^2 \, T_s[\{\phi_k\}] \end{aligned} \tag{4.38}$$

Where in the third step we introduced the new variable $\mathbf{x} = \lambda^3\mathbf{r}$.
We are now ready to compute the total energy of the system employing the IKS method as presented in Sec. 4.2.

### 4.5.1 SkX $^{16}$O model

The first system we focus on is the $^{16}$O nucleus with SkX interaction [7]. Before computing the energy, it is interesting to look at the scaled density and potentials of such model. Calculating those quantities for different values of $\lambda$ we obtain the results shown in Fig. 4.5.

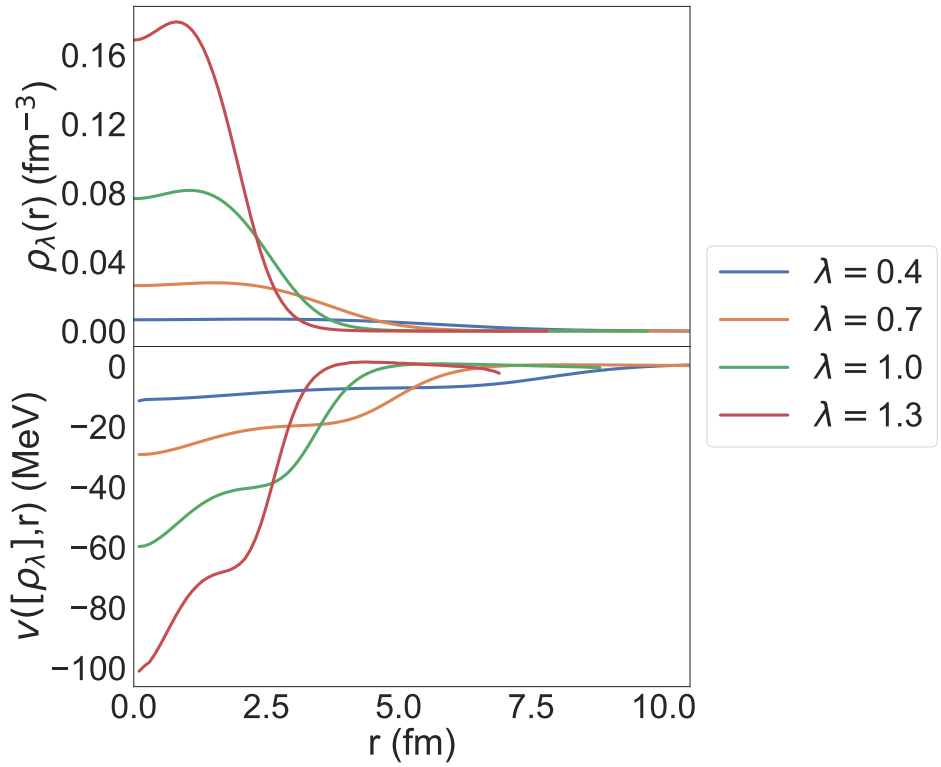


**Figure 4.5:** Simulations regarding $^{16}$O nucleus. In the top panel are presented the system densities $\rho_\lambda(r)$ based on SkX interaction and subjected to the $\lambda-$scaling for different values of $\lambda$. In the bottom panel the scaled potentials associated to such densities are shown.

All potentials presented above have been shifted so as to vanish at infinity, that is, $v([\rho(r)], r) \to 0$, for $r \to \infty$. From the behaviour of the density we see that, as $\lambda$ decreases, the system size becomes bigger. This is also coherent with the transformation to which the potential is subjected: when the density is wide, that is, for small values of $\lambda$, the potential is shallow as the system is indeed less confined. For scaling with higher $\lambda$ we see the opposite trend: narrower densities lead to greater potentials, and the system is strongly confined.

Turning now on the energy calculations, we write the full energy of the system as a sum of the kinetic and the potential part $E = T + U$. We proceed by steps, considering each term on its own.
As for the potential energy, we said it can be evaluated from Eq. (4.5) once the potentials of the scaled systems, whose density is $\rho_\lambda(r)$, have been computed through the IKS method (Sec. 4.2). Following this approach, we note an issue right away, as Eq. (4.5) has been found under the assumption that there is a density $\rho^*(r)$ such that $U[\rho^*] = 0$. Such condition could be given by the choice of the parameter $\lambda = 0$, however, the IKS method fails when applied to problems with density $\rho_\lambda(r)$ with $\lambda \to 0$, as the system becomes too wide and the algorithm convergence is usually unfeasible. Thus the integral of Eq. (4.5) cannot be performed. It is then convenient to use Eq. (4.4) and compute a potential energy difference avoiding the neighbourhood of $\lambda = 0$: the quantity we now calculate is therefore $\Delta E = \Delta T + \Delta U$, where $\Delta$ stands for a difference between energies computed with different values of $\lambda$. The absolute value of the energy can be then found by choosing a reference value.

To pursue simulations, we can rewrite Eq. (4.4) in a more convenient way:

$$\Delta U = U[\rho_\lambda] - U[\rho] = \int_1^\lambda dt\ F(t) \tag{4.39}$$

where

$$U[\rho] = U[\rho_{\lambda=1}] \tag{4.40}$$

$$F(t) = \frac{1}{t} \int dx\ 4\pi x^2\ v(t^3[\rho(x)], x/t)\ \left(3\rho(x) + \frac{\partial \rho(x)}{\partial x}\right) \tag{4.41}$$

where Eq. (4.12) has been used. This way we see the energy functional as an integral function of $\lambda$: varying the parameter and computing potentials from the IKS procedure, we can calculate the potential energy difference between the scaled system energy and the true potential energy $U[\rho]$.
Running the simulations, results are shown in Fig. 4.6a.

Looking now at the kinetic energies, the approach is more straightforward since we know the analytical expression of the kinetic functional (Eq. (2.39)) and the scaling to which it is subjected (Eq. (4.38)). Employing this last equation, the kinetic energy difference reads:

$$\Delta T = T^\lambda - T = (\lambda^2 - 1)\, T \tag{4.42}$$

To calculate the scaled kinetic energy we can proceed in two ways: the first consists in evaluating the kinetic energy for $\lambda = 1$, which is the real kinetic energy of the system,

from the minimisation of the objective function Eq. (2.43) during the IKS method, and from here apply the simple scaling $T^\lambda = \lambda^2 T$ to find $T^\lambda$. Otherwise we can directly consider the kinetic energy value obtained by the IKS technique applied to the scaled systems. We refer to the former approach as the theoretical one, since we are employing a theoretical result regarding the scaling expression of the kinetic functional, whereas we address to the second as the IKS method. The results of simulations are reported in Fig. 4.6b.

Therefore, the total energy difference can be evaluated by summing the two terms obtained above (Fig. 4.6c). We would expect to find a minimum of this functional in correspondence of $\lambda = 1$, as this value provides the real ground state of the nucleus: all the other scaled systems must have greater total energy, otherwise they would be the ground state system which exists in reality.

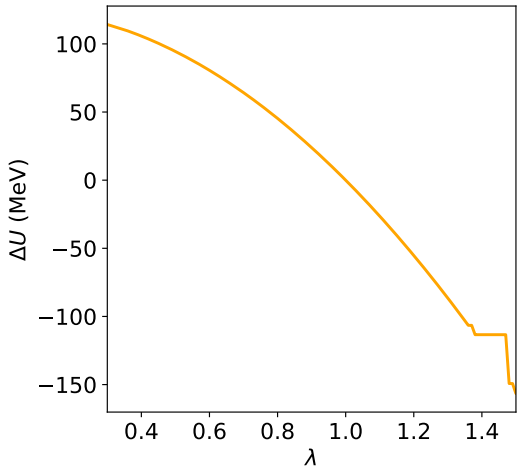


**(a)** $^{16}$O SkX potential energy difference.

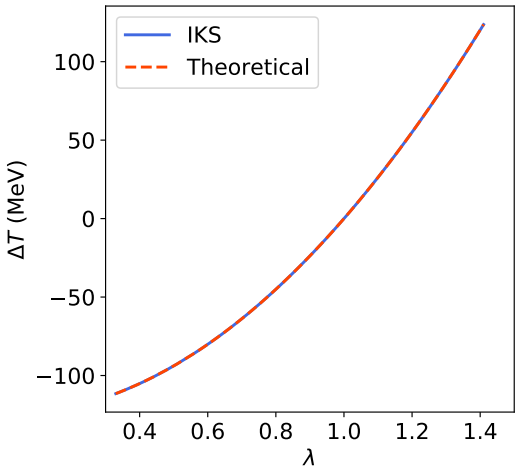


**(b)** $^{16}$O SkX kinetic energy difference.

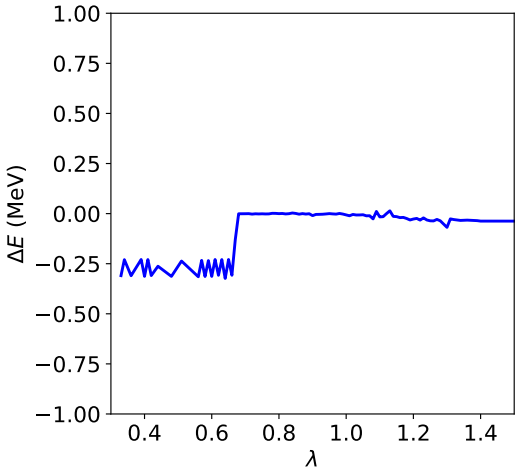


**(c)** $^{16}$O SkX total energy difference.

**Figure 4.6:** $^{16}$O nucleus simulations based on SkX interaction. (a) Potential energy difference $\Delta U$. (b) Kinetic energy difference $\Delta T$, calculated both from the theoretical scaling $T^\lambda = \lambda^2 T$ and from the IKS approach. (c) Total energy difference $\Delta E = \Delta T + \Delta U$.

From Fig. 4.6 we can first note that the two methods with which we computed the kinetic energy are in great agreement with one another. However, we see that there is no minimum of the total energy at $\lambda = 1$: the behaviour of $\Delta E$ is almost constant and close to zero. The oscillations of Fig. 4.6c have an amplitude far smaller than the magnitude of potential and kinetic difference values, and are due to numerical errors and approximations made during the IKS procedure. What we found actually asserts the conservation of the system total energy.
For the $^{40}$Ca nucleus the very same results can be obtained.

What was obtained in Fig. 4.6 proves that the total energy is constant as lambda is varied. However, this is unexpected and not intuitive: as the discussion presented previously cannot account for the resulting behaviour, further analysis is required (Sec. 4.6). To better understand the results coming from simulations we now consider a simpler nuclear model.

### 4.5.2 $(t_0, t_3)$ $^{16}$O model

The $(t_0, t_3)$ model is a simplified Skyrme model in which potential and EDF only depend on $\rho$ and not on its derivatives. We also neglect the Coulomb interaction so as to have symmetry between neutrons and protons, being able to treat the whole nucleus as if it were made of 16 neutrons. Moreover, the great advantage of this model dwells in the analytical knowledge of its EDF [49]. Since we have the exact expression of the EDF, we can use Eq. (4.1) to evaluate the potentials theoretically: this can prove useful while studying the system energy and potential using the IKS approach.

In this section we run the same simulations we performed for the $^{16}$O with SkX interaction (Sec. 4.5.1). However, as in this case we also know the analytical form of potential and energy functional, we can compare the energy difference obtained by inserting in Eq. (4.4) both the potentials computed from the IKS approach and the theoretical ones. After having studied the energies, we can also make a comparison between the theoretical and the Kohn-Sham scaled potentials.

Referring to [49], the parameters used in the simulations are:

$$\begin{gathered} t_0 = -2552.84 \quad t_1 = 0 \quad t_2 = 0 \quad t_3 = 16694.7 \\ x_0 = 0 \quad x_1 = 0 \quad x_2 = 0 \quad x_3 = 0 \\ W_0 = 0 \quad W_0' = 0 \quad t_{13} = 0 \\ \alpha = 0.20309 \end{gathered} \tag{4.43}$$

The potential energy functional of the system can be written as follows:

$$U = \int d^3r \, \mathcal{U} = \int d^3r \, (\mathcal{U}_0 + \mathcal{U}_1) \tag{4.44}$$

where

$$\mathcal{U}_0 = \frac{1}{4}t_0(2\rho^2 - (\rho_p^2 + \rho_n^2)) \tag{4.45}$$

$$\mathcal{U}_1 = \frac{1}{24}t_3\,\rho^\alpha(2\rho^2 - (\rho_p^2 + \rho_n^2)) \tag{4.46}$$

$$\rho = \rho_p + \rho_n \tag{4.47}$$

Thus, as we said, we can calculate the potential through Eq. (4.1):

$$v([\rho(\mathbf{r})], \mathbf{r}) = \frac{\delta U}{\delta \rho_q} = \frac{\partial \mathcal{U}}{\partial \rho_q} \tag{4.48}$$

The density $\rho_q$ can be both $\rho_p$ or $\rho_n$, as Eq. (4.48) holds in any case.
Choosing $\rho_q = \rho_p$ and using Eq. (4.47), we obtain:

$$v^{\mathrm{p}}_{\mathrm{Skyrme}}[\rho] = t_0\left(\rho - \frac{1}{2}\rho_p\right) + \frac{t_3}{24}\left[2\,(2+\alpha)\,\rho^{\alpha+1} - 2\rho^\alpha\rho_p - \alpha\rho^{\alpha-1}\left(\rho_p^2 + \rho_n^2\right)\right]. \tag{4.49}$$

Now employing $\rho_n = \rho_p = \rho/2$, since no coulomb interaction is present, we have:

$$\begin{aligned} v_{\mathrm{Skyrme}}[\rho] &= \frac{3t_0}{4}\rho + \frac{t_3}{24}\left[2(2+\alpha)\rho^{\alpha+1} - \rho^{\alpha+1} - \frac{\alpha}{2}\rho^{\alpha+1}\right] \\ &= \frac{3t_0}{4}\rho + \frac{t_3}{8}\left(1 + \frac{\alpha}{2}\right)\rho^{\alpha+1}. \end{aligned} \tag{4.50}$$

We can write this, schematically, as

$$v[\rho] = a\rho + b\rho^\beta. \tag{4.51}$$

We note that Eq. (4.51) is a potential of the form (4.23), for which we explicitly proved the EDF formula (4.5) in Sec. 4.3.

It is now possible to compute the $^{16}$O potential energy both from Eq. (4.44), which is the theoretical behaviour, and from the IKS minimisation procedure. To evaluate the theoretical scaled energy functional we apply $\lambda$ scaling $\rho_\lambda(\mathbf{r}) = \lambda^3\rho(\lambda\mathbf{r})$ directly to $\rho_p$ and $\rho_n$ in Eq. (4.44). Such densities are computed through the HF method in the case of the $(t_0, t_3)$ interaction.
As for the IKS approach, we compute the KS potentials with the usual CV method applied to the scaled densities $\rho_\lambda(r)$, then inserting them in Eq. (4.4). As for the kinetic energy, we can use the same technique followed in the previous section.
Proceeding with the simulations, we report results in Fig. 4.7.

Although the two kinetic energy plots show similar behaviour, it is clear that the potential energy is completely different: the only similarities lie in the neighbourhood of $\lambda = 1$. As for the theoretical case we see (Fig. 4.7d) that the total energy has the expected minimum at $\lambda = 1$: as we said this is due to the physical statement that the system with density $\rho_{\lambda=1}(r) = \rho(r)$ is the real ground state of the nucleus, therefore energies of the scaled systems must be greater.

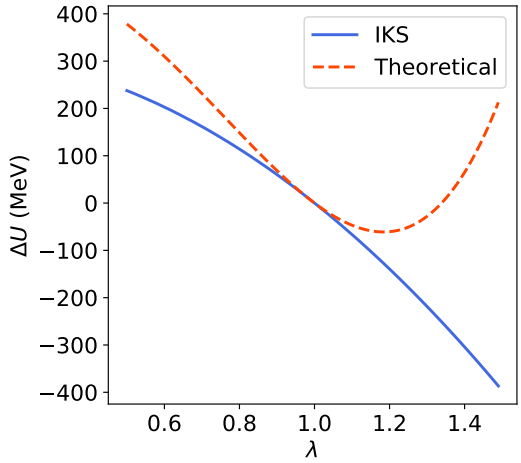


**(a)** $^{16}$O $(t_0, t_3)$ potential energy difference.

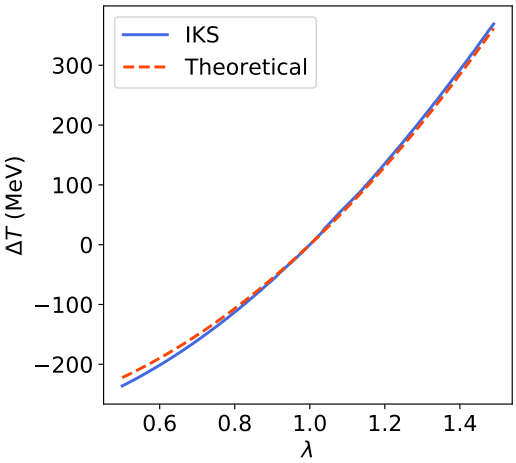


**(b)** $^{16}$O $(t_0, t_3)$ kinetic energy difference.

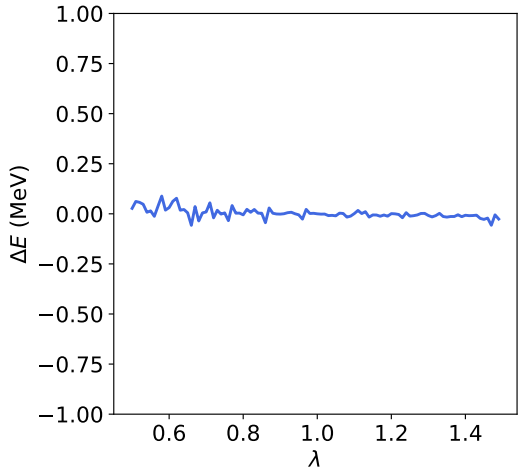


**(c)** $^{16}$O $(t_0, t_3)$ total energy difference from the IKS approach.

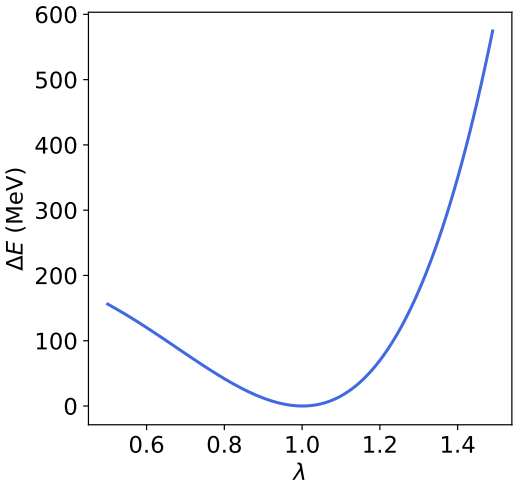


**(d)** $^{16}$O $(t_0, t_3)$ total energy difference from theoretical calculations.

**Figure 4.7:** $^{16}$O nucleus simulations based on the $(t_0, t_3)$ model without Coulomb interaction. (a) Potential energy difference $\Delta U$ computed with the IKS approach and the theoretical knowledge of the EDF. (b) Kinetic energy difference $\Delta T$, calculated both from the theoretical scaling $T^\lambda = \lambda^2 T$ and from the IKS approach. (c) Total energy difference from the IKS approach. (d) Total energy difference from theoretical calculations by using Eq. (4.44).

On the other hand, Fig. 4.7c shows the same aspects of what we found in the SkX $^{16}$O case. This is again related to the energy conservation, but at the moment we are not ready to fully explain it (see Sec. 4.6).

As the issue concerns the energy potential behaviour, it is surely related to the KS potentials computed from the IKS procedure. Employing Eq. (4.50) we can then compare the theoretical scaled potentials with the ones obtained by applying the CV method to a system whose density is $\rho_\lambda(r)$, that is the IKS approach. To find the theoretical scaled potentials we simply apply $\lambda-$scaling to the density in Eq. (4.50). Results are shown in Fig. 4.8.

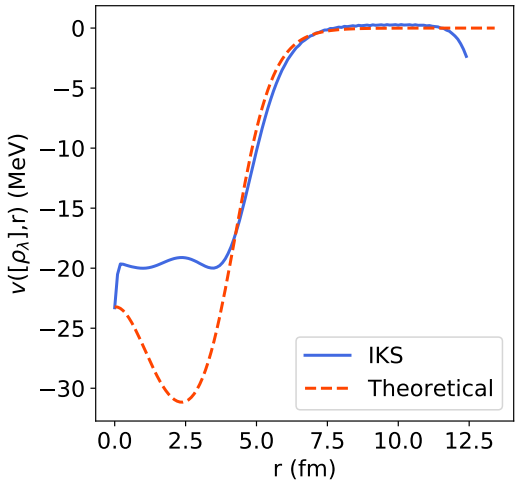


**(a)** Scaled potential with $\lambda = 0.6$

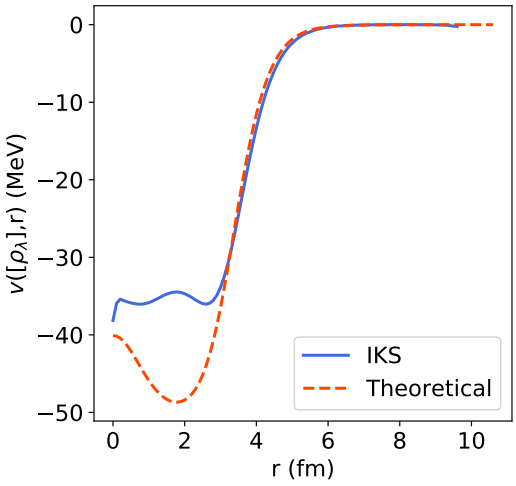


**(b)** Scaled potential with $\lambda = 0.8$

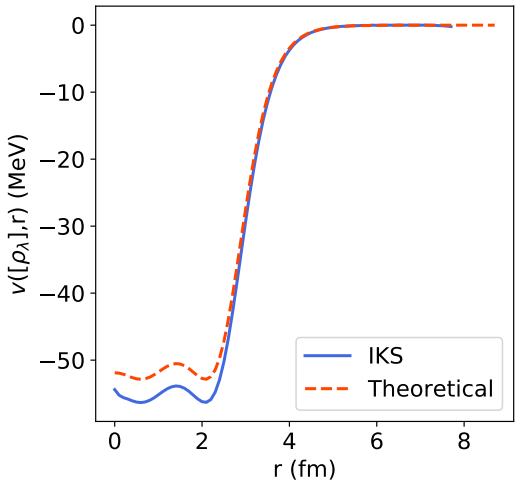


**(c)** Non scaled potential ($\lambda = 1.0$)

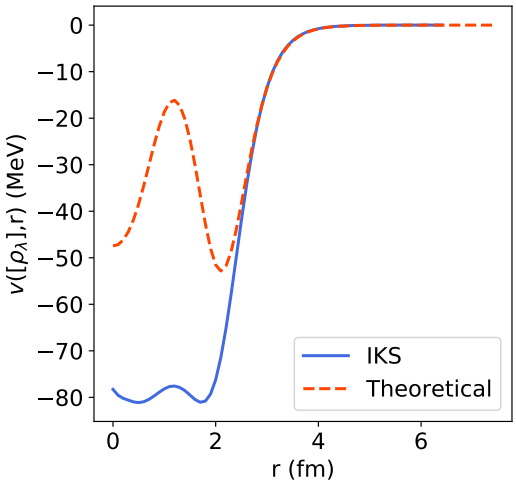


**(d)** Scaled potential with $\lambda = 1.2$

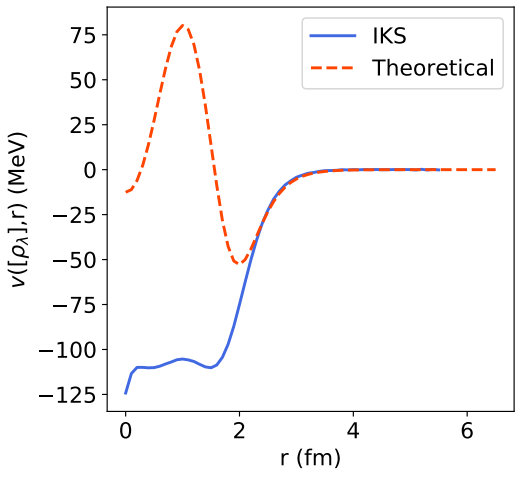


**(e)** Scaled potential with $\lambda = 1.4$

**Figure 4.8:** $^{16}$O $(t_0, t_3)$ scaled potentials for different values of $\lambda$. The IKS potentials are evaluated by applying the CV method to the scaled density $\rho_\lambda(r)$ of the system, whereas Theoretical scaled potentials are computed employing $\lambda-$scaling inside the analytical expression of the potential (4.50).

All potentials have been shifted so that $v(r) \to 0$ for $r \to \infty$. We see right away that there is a significant difference between the potentials computed with the two methods. This, as we have seen before, has serious consequences on potential energies.

In the following section we try to understand both why the potentials computed from the IKS method are different, and how this is related to the conservation of the energy.

## 4.6 Critical discussion

From the results obtained in Sec. 4.5 a question follows: can Eq. (4.4) actually be applied to gain information on the energy functional, when the potential is not known in a closed form, but is defined numerically by an inversion method? In previous sections we had assumed it was possible, but this now requires more attention.

We briefly recall the inverse Kohn-Sham method of DFT which we introduced in Chap. 2: by defining the non-interacting kinetic energy functional, i.e. the kinetic energy of a generic system of $A$ independent particles, we can pursue the following constrained variation:

$$T_s[\rho] = \inf_{\Psi \longrightarrow \rho} \langle \Psi | \hat{T} | \Psi \rangle \tag{4.52}$$

where $\Psi$ is a Slater determinant that yields the density $\rho(\mathbf{r})$. In a second stage, looking for the extrema of $T_s$ allows to determine the actual ground state density of the system.

By virtue of the Lagrange multipliers technique, the problem can be equivalently cast as a single free variation of an objective functional that incorporates extra terms to account for the constraints [13] [50]. If we require that $\rho(\mathbf{r})$ be equal to a given target density $\tilde{\rho}(\mathbf{r})$, and also fix the normalisation of $\rho(\mathbf{r})$ to the correct number of particles $A$, the objective functional reads:

$$J[\rho(\mathbf{r}); v(\mathbf{r}), \mu] = T_s[\rho] + \int d\mathbf{r} v(\mathbf{r}) \left(\rho(\mathbf{r}) - \tilde{\rho}(\mathbf{r})\right) - \mu \left( \int d\mathbf{r} \rho(\mathbf{r}) - A \right) \tag{4.53}$$

where $v(\mathbf{r})$ and $\mu$ are fixed by requiring the subsidiary condition $\rho(\mathbf{r}) = \tilde{\rho}(\mathbf{r})$ and $\int d^3r \rho(\mathbf{r}) = A$. We have seen that $v(\mathbf{r})$ is a single particle potential, whereas $\mu$ is defined as the chemical potential of the system. Now, varying $J$ with respect to $\rho$ gives the Euler equation:

$$\frac{\delta T_s[\rho]}{\delta \rho(\mathbf{r})} + v(\mathbf{r}, [\rho]) = \mu \tag{4.54}$$

We also remind that to each density $\tilde{\rho}(\mathbf{r})$ corresponds a different effective potential.

Something can be learnt by combining the Euler equation (4.54) with Eq. (4.4), as studied in [50]. Assuming that $\rho_t(\mathbf{r})$ is a number-preserving path, so that all densities are normalised to the same number of particles, we can then multiply Eq. (4.54) by

$d\rho_t/dt$ and integrate over both $t$ and $\mathbf{r}$. The right hand side vanishes, as $\mu$ is a constant and the integrals of $\rho_A$ and $\rho_B$ coincide. It is then immediate to find:

$$\Delta T_s = -\int_A^B dt \int d^3r\, v(\mathbf{r}, [\rho_t]) \frac{\mathrm{d}\rho_t(\mathbf{r})}{\mathrm{d}t}. \tag{4.55}$$

In a sense, we have found a conserved quantity along the density path. We stress that $v(\mathbf{r}, [\rho_t])$ is to be thought here as coming from an inversion method for each $t$. Unfortunately, from our perspective this result is unpleasant, since it states that what Eq. (4.4) applied to potentials extracted from IKS method yields a quite trivial result: the kinetic energy can be much more easily found by the same constrained minimisation scheme. Thus, it looks like we cannot gain information on the potential energy functional this way.

A few lines of discussion are mandatory on a subtle point. The meaning of the potential $v_{KS}(\mathbf{r})$ obtained by IKS given a target density $\tilde{\rho}(\mathbf{r})$ has to be examined. Indeed, calling $v\,[\rho]$ the functional derivative of the potential energy, while one could expect $v_{KS}(\mathbf{r})$ to be equal to $v\,[\tilde{\rho}]$, that is not the case: $v_{KS}(\mathbf{r})$ is the effective Kohn-Sham potential for the system, but it is not in general the same as $v\,[\tilde{\rho}]$, except if $\tilde{\rho}$ is the true ground state density. In the other cases, $v_{KS}$ can still be interpreted by reminding ourselves of the original DFT, in which the KS potential is made by a universal term plus an *external* potential $v_{ext}$. For us, this means that:

$$v_{KS}(\mathbf{r}) = v\,[\tilde{\rho}] + v_{ext}(\mathbf{r}) \tag{4.56}$$

where $v_{ext}(\mathbf{r})$ may vary according to the density $\tilde{\rho}$. Thus, in a general situation, we would have two unknowns for each $\tilde{\rho}$, i.e. both $v\,[\tilde{\rho}]$ and $v_{ext}(\mathbf{r})$. How to disentangle them is a further issue.

In other words, the difference between $v_{KS}(\mathbf{r})$ and $v\,[\tilde{\rho}]$ can be justified by the following argument. The ground state density of a system, be it experimental, HF, *ab initio* or deriving from any other model, is essentially unique. From a mathematical point of view, taking a density path is a sort of trick that is well-defined once $v[\rho]$ is explicitly given as a functional of $\rho$. From a physical point of view, however, such densities $\rho_t$ do have a meaning, but only if we understand them as ground state densities of a *perturbed* system. Stated otherwise, Eq. (4.4) can work only if we find a path of densities such that each $\rho_t$ is actually a ground state for the system, either its "natural" ground state or its ground state under a constraint (which is equivalent to saying that the system has been perturbed): under these hypothesises $v_{KS}(\mathbf{r})$ is indeed $v\,[\tilde{\rho}]$.

This explains why in Fig. 4.6c and 4.7c we saw the total energy as a conserved quantity for different values of $\lambda$: the IKS procedure interprets the $\rho_\lambda(\mathbf{r})$ density as a ground state density of some system, thus during the minimisation procedure the potential is evaluated so as to nullify the alteration of the kinetic part induced by the scaled orbitals, providing at last the same total energy.

However, there may be a way out, at least partially. If one employs a technique which returns the ground state density $\rho_\lambda(\mathbf{r})$ and the associated potential $v\,(\rho_\lambda(\mathbf{r}), \mathbf{r})$,

then Eq. (4.4) can be used to find the proper potential energy of the system. A first implementation along this line using Constrained Hartee-Fock calculations (CHF) is presented in Sec. 4.7.

## 4.7 Constrained Hartree-Fock calculations

The idea behind CHF calculations consists in applying an external perturbation of "monopolar" type $\mu r^2$ to the system, forcing a deformation of the radius and of the density. Considering the familiar $\lambda-$scaling, a correspondence between $\mu$ and $\lambda$ can be established, at least in an appropriate regime close to the unperturbed state, so that we can think of $\mu$ as a $\mu(\lambda)$ (App. C). As a consequence, for a given $\lambda$, the corresponding external potential is known and is given by:

$$v_{ext,\lambda} = \mu(\lambda) r^2 \tag{4.57}$$

Eventually, we are in a position to calculate $v\left[\tilde{\rho}_\lambda\right]$ by subtracting the external contribution at each $\lambda$ to the total $v_{KS}$ term, as Eq. (4.56).

To employ this technique we consider an Hartree-Fock Hamiltonian $H$ and turn it into:

$$H' = H + \mu r^2, \tag{4.58}$$

where $\mu$ is varied in small steps around 0; this parameter is to be interpreted as a Lagrange multiplier. This procedure provides the energy of the system when the mean-square radius is constrained.
In other words, the solutions of the HF equations associated with $H'$, for every $\mu$, provide a wave function $|\Phi_\mu\rangle$ that minimises $H'$ (in the space of Slater determinants). We can write:

$$\min_\Phi \langle\Phi|H'|\Phi\rangle = \langle\Phi_\mu|H'|\Phi_\mu\rangle = E_\mu + \mu\langle\Phi_\mu|r^2|\Phi_\mu\rangle. \tag{4.59}$$

In the following discussion we first consider the path of densities induced by the parameter $\mu$, be it the $\mu-$scaling. It can be shown that $\mu-$ and $\lambda-$scaling are strictly correlated, at least for certain choices of such parameters (App. C).

We now perform CHF calculations using the same simplified model of Sec. 4.5.2, that is the $(t_0, t_3)$ Skyrme model for $^{16}$O nucleus. From here, we can compute the potential energy difference $\Delta U = \Delta U_\mu - \Delta U_{\mu=0}$. On the other hand, it is possible to use Eq. (4.4), be it the *Reconstruction method*, by setting the parameters $A = 0$ and $B = \mu$ and using $\rho_\mu(\mathbf{r})$ densities and $v\left([\rho_\mu(\mathbf{r})], \mathbf{r}\right)$ potentials calculated from CHF. Thus the potential energy difference can be evaluated and compared with the previous results. This is presented in Fig. 4.9.

Fig. 4.9 shows that the two plotted behaviours are in good agreement. We have thus seen that the reconstruction method works if the correct scaled densities are considered in the line integration. To find the total energy, the kinetic term must be taken

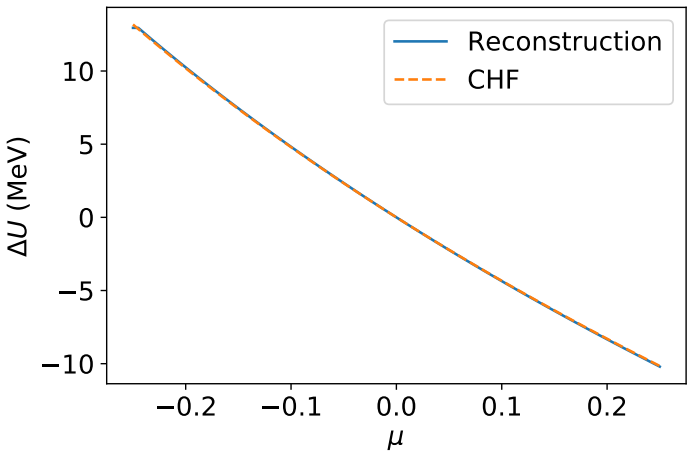


**Figure 4.9:** Comparison between the potential energy difference $\Delta U$ computed from CHF calculations and from Eq. (4.4) for $^{16}$O nucleus with $(t_0, t_3)$ interaction.

into account as well.

We can also move from $E(\mu)$ to $E(\langle r^2 \rangle)$. Formally, this is a Legendre transformation [51]:

$$\mu = \frac{\partial E_\mu}{\partial \langle r^2 \rangle}. \tag{4.60}$$

In practice, the transformation has been performed through a numerical fit of $\langle r^2 \rangle$ as a function of $\mu$. We find that we can write:

$$\langle r^2 \rangle_\mu = a\mu + b = a\mu + \langle r^2 \rangle_{\mu=0}. \tag{4.61}$$

This way we can see the energy difference behaviour in terms of $\langle r^2 \rangle$ which has a clear physical meaning.

A step forward which can suggest a practical use of this procedure consists in considering a $(t_0, t_3)$ model with several values of the parameter $\alpha$ (Eq. (4.46)). Once $\alpha$ is chosen, $t_0$ and $t_3$ parameters can be set by asking that the quantity $E/A(\rho)$ has a minimum in $\rho = 0.16$ fm$^{-3}$ equal to $-16$ MeV, which corresponds to the saturation of infinite symmetric matter. The $(t_0, t_3)$ interaction parameters now read:

$$\begin{aligned} \alpha = 0.16 \quad t_0 = -3068.63 \quad t_3 = 19578.0 \\ \alpha = 0.2 \quad t_0 = -2552.84 \quad t_3 = 16694.7 \\ \alpha = 0.32 \quad t_0 = -1851.75 \quad t_3 = 13124.4 \\ \alpha = 1.0 \quad t_0 = -1024.2 \quad t_3 = 14602.5 \end{aligned}$$

We can now run CHF simulations and study the resulting energy differences, which are shown in Fig. 4.10.

In Fig. 4.10 we see how the energy behaviour depends on the parameter $\alpha$. We look at Fig. 4.10c, which has a clear physical interpretation: as $\alpha$ increases, the system

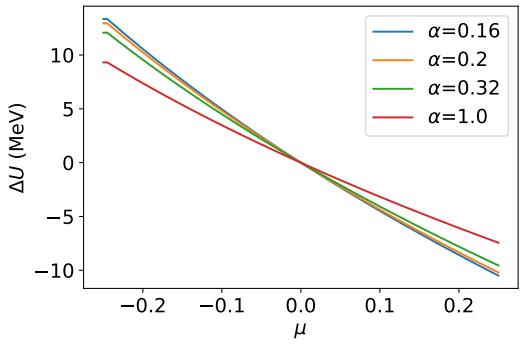


**(a)** $^{16}$O $(t_0, t_3)$ potential energy difference.

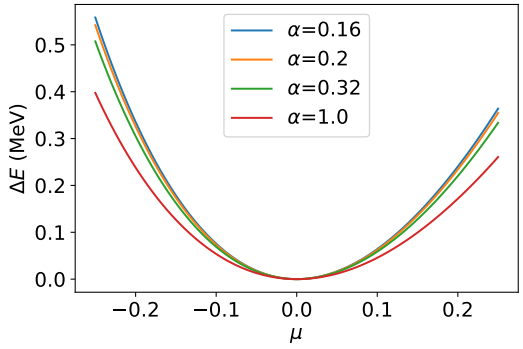


**(b)** $^{16}$O $(t_0, t_3)$ total energy difference.

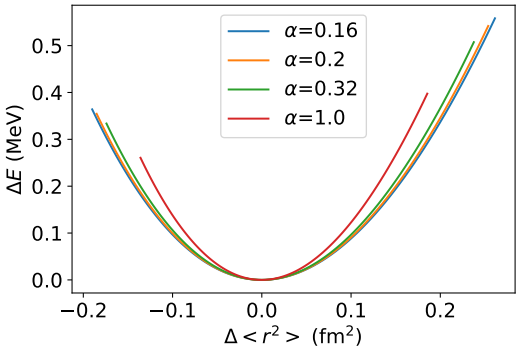


**(c)** $^{16}$O $(t_0, t_3)$ total energy difference.

**Figure 4.10:** $^{16}$O nucleus CHF simulations based on the $(t_0, t_3)$ model without Coulomb interaction. (a) Potential energy difference $\Delta U$. (b) Total energy difference $\Delta E$ as a function of $\mu$. (c) Total energy difference $\Delta E$ as a function of $\langle r^2 \rangle$.

energy shows a narrower well. Indeed, since the potential goes as $v \sim \rho^\alpha$, for larger values of $\alpha$ the potential is stiffer and more energy must be spent to move a particle inside the system. Thus, systems with greater $\alpha$ are more confined.

In principle, as there is a correspondence between $\alpha$ and the curvature of $\Delta E$ (see Fig. 4.10c), we could try to determine $\alpha$ from a potential energy curve obtained through Eq. (4.4) by using realistic densities.

To conclude, the CHF calculations allowed to compute the exact ground state density of a perturbed system as well as the potential associated to it; to find the total energy the kinetic term must be then added. This way we can employ the line integration method of Eq. (4.4) and evaluate the potential energy of the system, avoiding the ambiguities which appeared by using the IKS approach (see Sec. 4.6). The results we obtained are encouraging, albeit further studies are needed.

# Conclusions

This work aimed at finding the Energy Density Functional (EDF) of a nuclear system, starting from the knowledge of the system density. This purpose cannot be achieved without a thorough investigation of effective nuclear potentials: in the approach we followed EDF and nuclear potentials are indeed strictly related.
In Chap. 2 we introduced the DFT formalism, focusing in particular on the inverse problem of DFT, in which the system density is taken as input and physical properties are determined, and on the Kohn Sham approach. In the latter, an interacting system is mapped into a fictitious non-interacting one in an external potential. Different models have been studied to implement the inverse DFT: in this work we made use of the Constrained Variational method, based on a constrained minimisation of the kinetic energy of the system seen as a functional of the orbitals.
In Chap. 3 we detailed the implementation of the CV method applied to spherical nuclei, from both a theoretical and numerical perspective. For theoretical and experimental densities nuclear potentials were shown in the case of $^{16}$O, $^{40}$Ca and $^{208}$Pb nuclei, and were compared to benchmark behaviours. The reasonably good accuracy of the inversion has thus been verified.
Then we studied the orbitals calculated from the CV method. We showed that the method leads to non-canonical Schrödinger equations. We motivated that a diagonalisation of the eigenvalue matrix $(\epsilon_{ij})$ is required in order to determine the canonical orbitals, eigenstates of the effective potential. These were successfully compared to HF calculations, proving the correctness of such technique.

In Chap. 4 we finally dealt with the problem of reconstructing the energy density functional. A line integration formula has been considered to perform the potential to energy transition for a specific system. This approach involves considering a one-parameter family of scaled densities and their associated potentials, and perform the integration over such path of scaled densities. Physically speaking, this is equivalent to deforming the ground state of a nuclear system by applying an external perturbation, thus modifying its density. The purpose now is to calculate the scaled potential and use it to compute the EDF.
Given this setting, we have first verified the formula by testing it on analytical potentials. The initial idea was to determine the potential energy by applying the aforementioned formula to the scaled potentials computed from the CV method, then adding the kinetic term whose scaling is known analytically. Such an achievement would be of significant importance as it would allow to compute the energy functional from a potential known numerically. However, we found that this approach has a serious shortcoming. The reason is behind what the Kohn-Sham method interprets as ground

state density: the density path over which the line integration is performed must be seen as a set of ground state densities, either of the original system or of the scaled ones. However, the densities given in input to the inverse DFT problem are not actual ground state densities of any system, thus the Kohn-Sham potential differs from the quantity we were actually looking for, i.e. the nuclear effective potential (the functional derivative of the potential energy), by an extra term that plays the role of an external potential. Even though we were unable to determine the EDF, the model allowed us to study properties of scaled systems, such as their potential and their orbitals, which have indeed a well-precise physical interpretation.
A further step in this topic consisted in considering constrained calculations (CHF). In the CHF we computed the energy of the system varying the mean square radius of the Hamiltonian by applying an external one-body perturbation. Such perturbation is defined by a parameter whose variation can be shown to define a path that corresponds precisely to the path of scaled densities seen before. In this way it is possible to find the external potential term we were missing before, and compute the EDF with the approach previously introduced. The results obtained are encouraging: looking at the difference between total system energies, calculated with different values of the scaling parameter, we found a minimum corresponding to the density of the original, non scaled system. Moreover, the total energy is found to agree with our expectation.

Next steps consist in generalising the approach we followed in order to simulate nuclei with different densities between protons and neutrons, also taking into account spin-orbit, Coulomb, and non local interactions, i.e. interactions depending on $\nabla\rho$ and higher derivatives of the density. Eventually, the ultimate purpose is to apply the method to *ab initio* densities which represent real nuclear systems.
Moreover, few lines must be said to underline the importance of the inverse DFT approach and encourage its study. Although this technique still has not been widely used to face nuclear problems, it is leading to interesting improvements in the fields it is employed, e.g. in the development of Optimised Effective Potentials (OEP) [52] or in effort to improving existing EDFs perturbatively [27].

# Appendix A

# Elements of Functional Analysis

## Functional derivative

Given a manifold $M$ containing smooth functions $\rho$ and a functional $F$ so that $F\colon M \to \mathbb{R}$, we call functional derivative of $F[\rho]$ the quantity $\delta F/\delta\rho$ defined by:

$$\begin{aligned}\int \frac{\delta F}{\delta \rho}(x)\phi(x)\, dx &= \lim_{\varepsilon\to 0}\frac{F[\rho+\varepsilon\phi]-F[\rho]}{\varepsilon} \\ &= \left[\frac{d}{d\varepsilon}F[\rho+\varepsilon\phi]\right]_{\varepsilon=0},\end{aligned} \tag{A.1}$$

where $\phi$ is an arbitrary test function.
Linearity property is straightforward. As for the chain rule, considering a functional $G\colon M \to \mathbb{R}$ we have:

$$\frac{\delta F[G[\rho]]}{\delta\rho(y)} = \int dx \frac{\delta F[G]}{\delta G(x)}_{G=G[\rho]} \cdot \frac{\delta G[\rho](x)}{\delta\rho(y)} \tag{A.2}$$

Moreover, if $G$ is a differentiable function the following equation holds:

$$\frac{\delta F[G(\rho)]}{\delta\rho(y)} = \frac{\delta F[G(\rho)]}{\delta G[\rho(y)]}\,\frac{dG(\rho)}{d\rho(y)} \tag{A.3}$$

Assuming now that we can write the functional $F[\rho]$ as

$$F[\rho] = \int f(\boldsymbol{r}, \rho(\boldsymbol{r}), \nabla\rho(\boldsymbol{r}), \nabla^2\rho(\boldsymbol{r}))\, d\boldsymbol{r} \tag{A.4}$$

employing divergence theorem and boundary conditions on the arbitrary function $\phi$ of Eq. (A.1), it is possible to express the functional derivative of $F$ as:

$$\frac{\delta F}{\delta\rho(\boldsymbol{r})} = \frac{\partial f}{\partial\rho} - \nabla\cdot\frac{\partial f}{\partial\nabla\rho} + \nabla^2\cdot\frac{\partial f}{\partial\nabla^2\rho} \tag{A.5}$$

Eq. (A.5) proves more useful and convenient that the original definition (A.1). It can also be generalised if the integral function $f$ depends on higher derivatives of $\rho$.

At last, we introduce the differential of a functional. In analogy with the classical total differential of a function $f$, which reads:

$$df = \sum_{i=1}^{n} \frac{\partial f}{\partial x_i} \, dx_i \tag{A.6}$$

the functional differential, or variation, of the functional F is defined as:

$$\delta F[\rho; \phi] = \int \frac{\delta F}{\delta \rho}(x) \, \phi(x) \, dx \tag{A.7}$$

# Appendix B

# Detailed calculations of the CV method

In this appendix we conclude the implementation of the Constrained Variational approach discussed in Sec. 3.1, reporting the complete calculations of the quantities used in the construction of the algorithm.

## B.1 Kinetic functional

### B.1.1 Functional with scaled variables

In Eq. (3.14) we introduced the scaled functions $\{f_k\}$ as:

$$u_k(r) = f_k(r)\sqrt{4\pi\tilde{\rho}(r)}\, r = f_k(r)\sqrt{4\pi}A(r)\, r \tag{B.1}$$

where we defined the quantity $A(r) = r\sqrt{\tilde{\rho}(r)}$.
The kinetic term in Eq. (3.8) includes first and second derivatives of $u_k(r)$ with respect to $r$, we want to express them in terms of functions $f_k(r)$. Denoting with the dot $\dot{}$ the derivative along the radial coordinate, we have:

$$\dot{u}(r) = \sqrt{4\pi}\left(\dot{A}(r)f(r) + A(r)\dot{f}(r)\right) \tag{B.2}$$

$$\ddot{u}(r) = \sqrt{4\pi}\left(\ddot{A}(r)f(r) + 2\dot{A}(r)\dot{f}(r) + A(r)\ddot{f}(r)\right) \tag{B.3}$$

where the derivatives of $A(r)$ read:

$$\dot{A}(r) = \sqrt{\tilde{\rho}(r)} + \frac{\dot{\tilde{\rho}}(r)}{2\sqrt{\tilde{\rho}}(r)}r \tag{B.4}$$

$$\ddot{A}(r) = \frac{\dot{\tilde{\rho}}}{\sqrt{\tilde{\rho}}} + \frac{r}{2}\frac{\ddot{\tilde{\rho}}}{\sqrt{\tilde{\rho}}} - \frac{r}{4}\frac{\left(\dot{\tilde{\rho}}\right)^2}{(\tilde{\rho})^{3/2}} \tag{B.5}$$

Substituting the above expression in Eq. (3.8) we obtain the kinetic energy functional in terms of $f_k(r)$:

$$T[\{f_k\}] = -\frac{4\pi\hbar^2}{2m}\sum_k d_k \int dr \Bigg[ f_k^2(r)\left(A(r)\ddot{A}(r) - \frac{l_k(l_k+1)}{r^2}A^2(r)\right) + \\ + \frac{d}{dr}\left(A^2(r)\right) f_k(r)\dot{f}_k(r) + A^2(r) f_k(r)\ddot{f}_k(r)\Bigg] \tag{B.6}$$

Introducing then $C_0(r,k)$, $C_1(r)$, $C_2(r)$ functions, defined as:

$$C_2(r) \equiv r^2\tilde{\rho}(r) \tag{B.7}$$

$$C_1(r) \equiv \dot{C}_2(r) = r^2\dot{\tilde{\rho}}(r) + 2r\tilde{\rho}(r) \tag{B.8}$$

$$C_0(r,k) \equiv A(r)\ddot{A}(r) - \frac{l_k(l_k+1)}{r^2}A^2(r) = -l_k(l_k+1)\tilde{\rho}(r) + r\dot{\tilde{\rho}}(r) + \frac{r^2}{2} + \ddot{\tilde{\rho}}(r) - \frac{r^2}{4}\frac{(\dot{\tilde{\rho}}(r))^2}{\tilde{\rho}(r)} \tag{B.9}$$

we can write the kinetic energy functional solely in terms of $f_k(r)$ functions:

$$T_s[\{f_k\}] = \sum_k d_k \int dr \left(\left(-\frac{\hbar^2}{2m}4\pi\right)\left(C_0(r,k)f_k^2(r) + C_1(r)f_k(r)\dot{f}_k(r) + C_2(r)f_k(r)\ddot{f}_k(r)\right)\right) \tag{B.10}$$

### B.1.2 Kinetic gradient and Hessian

In Sec. 3.1.3 we saw that IPOPT needs both the gradient of the kinetic functional and the jacobian of the constraints, as well as the Hessian of the whole objective functional $J[\{u_k(r)\}]$ of Eq. (2.43).
To implement the algorithm, we divide the interval used for the inversion in $N_{points}$ (Eq. (3.23)) and discretise the scaled orbital functions. In the following approach, notation $f_i^k$ stands for the $k-th$ orbital function evaluated in the $i-th$ point of the radial grid.
We employ the Finite Difference Method (FDM) to calculate function derivatives: be $h$ the interval step, from known tables at the second order we have[1]:

$$\dot{f}_i = \frac{f_{i+1} - f_{i-1}}{2h} \tag{B.11}$$

$$\ddot{f}_i = \frac{f_{i+1} - 2f_i + f_{i-1}}{h^2} \tag{B.12}$$

We can define a new functional $I$ as:

$$I[f^k] = \int dr \left(C_0(r,k)(f^k)^2 + C_1(r)\dot{f}^k f^k + C_2(r)\ddot{f}^k f^k\right) \tag{B.13}$$

The kinetic functional then reads:

$$T[\{f^k\}] = -\frac{4\pi\hbar^2}{2m}\sum_k^{N_{orbs}} d_k I[f^k] \tag{B.14}$$

[1] https://en.wikipedia.org/wiki/Finite_difference_coefficient

This way we can focus on $I$ and calculate its derivatives with the FDM. For the following calculations we focus on a single orbital $f$, thus omitting its upper index $^k$.
Another step consists in discretising the integral of Eq. (B.13) as a sum:

$$I[f] = h \sum_{i}^{N_{points}} \left( C_0^i f_i^2 + C_1 \dot{f}_i f_i + C_2 \ddot{f}_i f_i \right) \tag{B.15}$$

We are now ready to compute derivatives. As for the first derivative, considering a generic orbital $f$ and applying partial derivative with respect to $f_k$ we have:

$$\begin{aligned}
\frac{\partial I[f]}{\partial f_k} &= h \Bigg( 2C_0^k f_k + C_1^k \dot{f}_k + C_2^k \ddot{f}_k + \frac{1}{2h}(C_1^{k-1} f_{k-1} - C_1^{k+1} f_{k+1}) + \\
&\qquad + \frac{1}{h^2} \left( C_2^{k-1} f_{k-1} - 2C_2^k f_k + C_2^{k+1} f_{k+1} \right) \Bigg) = \\
&= h \left( 2C_0^k f_k + C_1^k \dot{f}_k + C_2^k \ddot{f}_k - \frac{d}{dr}\left(C_1 f\right)\Big|_k \right) + \frac{d^2}{dr^2}\left(C_2 f\right)\Big|_k = \\
&= h \left( 2C_0^k f_k + \cancel{C_1^k \dot{f}_k} + C_2^k \ddot{f}_k - \cancel{\dot{C}_1^k f_k} - \cancel{C_1^k \dot{f}_k} + \cancel{\ddot{C}_2^k f_k} + 2\dot{C}_2^k \dot{f}_k + C_2^k \ddot{f}_k \right) = \\
&= 2h \left( C_0^k f_k + C_1^k \dot{f}_k + C_2^k \ddot{f}_k \right)
\end{aligned} \tag{B.16}$$

Where explicit dependencies of $C_0(r,k)$, $C_1(r)$, $C_2(r)$ functions have been omitted, and Eq. (B.7), (B.8), and (B.9) have been used.
We can now evaluate the second derivative following the same approach:

$$\begin{aligned}
\frac{\partial^2 I[f]}{\partial f_k \partial f_l} &= 2h \left( C_0^k \delta_k^l + C_1^k \frac{\delta_{k+1}^l - \delta_{k-1}^l}{2h} + C_2^k \frac{\delta_{k+1}^l - 2\delta_k^l + \delta_{k-1}^l}{h^2} \right) \\
&= 2h\delta_k^l \left( C_0^k - \frac{2}{h^2} C_2^k \right) + \delta_{k+1}^l \left( C_1^k + \frac{2}{h} C_2^k \right) + \delta_{k-1}^l \left( -C_1^k + \frac{2}{h} C_2^k \right)
\end{aligned} \tag{B.17}$$

At last, writing the derivatives of the original kinetic functional we have:

$$\frac{\partial T[\{f^i\}]}{\partial f_k^i} = -\frac{4\pi\hbar^2}{2m} \frac{\partial I[f^i]}{\partial f_k^i} \tag{B.18}$$

$$\frac{\partial^2 T[\{f^i\}]}{\partial f_k^i \partial f_l^j} = -\frac{4\pi\hbar^2}{2m} \frac{\partial^2 I[f^i]}{\partial f_k^i \partial f_l^j} \delta_i^j \tag{B.19}$$

## B.2 Constraints

Considering now the constraint conditions, we evaluate both the first and the second derivatives.
Using the notation introduced above, the density contraint written in terms of the scaled $\{f^k\}$ orbitals reads:

$$g(r) = \sum_{k=1}^{N_{orbs}} d_k (f^k)^2(r) \tag{B.20}$$

Evaluated at the $l-th$ of the grid point function $g$ is:

$$g_l = \sum_{k=1}^{N_{orbs}} d_k (f_l^k)^2 \tag{B.21}$$

Applicating the FDM to calculate the derivatives we have:

$$\frac{\partial g_l}{\partial f_n^k} = 2 d_k f_l^k \delta_{nl} \tag{B.22}$$

$$\frac{\partial^2 g_l}{\partial f_n^k \partial f_m^j} = 2 d_k \delta_{ml} \delta_{nl} \delta^{jk} \tag{B.23}$$

As for the orthonormality constraints between scaled functions, we have seen in Sec. 3.1 that they are only needed if generalised spherical harmonics are not orthogonal, that is, if we have $l_i = l_j$, $j_i = j_j$ $\forall i, j = 1, ..., N_{orbs}$. We can then start by listing the $(i, j)$ couples for which the constraint must be applied, and then proceed to calculate its derivatives.
Using the $k$ index to indicate the couple of orbitals $(i, j)$, and following the same considerations made above, we have:

$$G_k[f] = \int dr \, 4\pi r^2 \tilde{\rho} f^{i_k} f^{j_k} \tag{B.24}$$

Discretising the equation we obtain:

$$G_k[f] = h \sum_{n=1}^{N_{points}} 4\pi r_n^2 \tilde{\rho}_n f_n^{i_k} f_n^{j_k} \tag{B.25}$$

Computing the derivatives:

$$\frac{\partial G_k[f]}{\partial f_n^q} = 4\pi r_n^2 h \, \tilde{\rho}_n \left( f_n^{i_k} \delta^{j_k q} + f_n^{j_k} \delta^{i_k q} \right) \tag{B.26}$$

$$\frac{\partial^2 G_k[f]}{\partial f_m^q \partial f_n^p} = 4\pi r_n^2 h \, \delta_{mn} \tilde{\rho}_n \left( \delta^{j_k p} \delta^{i_k q} + \delta^{i_k p} \delta^{j_k q} \right) \tag{B.27}$$

This expressions can be now turned into code and be implemented in the CV algorithm.

# Appendix C

# Relation between $\mu-$ and $\lambda-$scaling

Referring to Sec. 4.7, to understand the relation between $\mu-$ and $\lambda-$scaling we start by noting that in the $\lambda$-scaling we have:

$$\langle r^2 \rangle_\lambda = \frac{1}{\lambda^2} \langle r^2 \rangle_{\lambda=1}. \tag{C.1}$$

If $\lambda$ is not varied too much around 1, namely $\lambda \approx 1 + \epsilon$, then Eq. (C.1) becomes

$$\langle r^2 \rangle_\lambda = \langle r^2 \rangle_\epsilon = \frac{1}{(1+\epsilon)^2} \langle r^2 \rangle_{\epsilon=0} \approx (1 - 2\epsilon) \langle r^2 \rangle_{\epsilon=0}. \tag{C.2}$$

By comparing the latter equation with Eq. (4.61), we easily obtain

$$\begin{aligned} \epsilon &= -\frac{a\mu}{2\langle r^2 \rangle_{\epsilon=0}}, \\ \lambda &= 1 - \frac{a\mu}{2\langle r^2 \rangle_{\epsilon=0}}. \end{aligned} \tag{C.3}$$

Remarkably, the densities found by the CHF calculations at a given $\mu$, and the scaled densities with $\lambda$ provided by (C.3), are almost equal. Therefore, the $\lambda$-scaling may be a good choice for a density path, since it suggests the possibility to extract the contribution $v\,[\tilde{\rho_\lambda}]$ through the inversion. In an optimistic perspective, at any $\lambda$ the "external" part of the KS potential can be found. Then, the knowledge of $\tilde{\rho}(\mathbf{r})$ would allow to define the whole path of potentials $v\,[\tilde{\rho_\lambda}]$, and hence enable the use Eq. (4.4).

# Bibliography


[1] A. Das, T. Ferbel *Introduction Nuclear and Particle Physics*. World Scientific Publishing 2003.

[2] K. S. Krane. *Introductory nuclear physics*. Wiley, 1988.

[3] E. Rutherford. *The scattering of alpha and beta particles by matter and the structure of the atom*. Philosophical Magazine, volume 21 (1911), pages 669-688.

[4] R. Hofstadter. *Electron Scattering and Nuclear Structure*. Rev. Mod. Phys 28 p.214 (1956).

[5] G. Colò. *Nuclear Physics*. Lecture notes, University of Milan, 2014-15.

[6] N. Takigawa , K. Washiyama. *Fundamentals of nuclear physics*. Springer, 2016.

[7] B. A. Brown. *New Skyrme interaction for normal and exotic nuclei*. Phys. Rev. C 58, 220 (1998).

[8] D. Gogny, P. L. Lions *Hartree-Fock theory in nuclear physics*. RAIRO – Modélisation mathématique et analyse numérique, tome 20, no 4 (1986), p. 571-637.

[9] R. Machleidt, D.R. Entem *Chiral effective field theory and nuclear forces* Physics Reports. 503 (1): 1–75, (2011)

[10] P. Benzoni *Potenziali nucleari dall'inversione delle equazioni di Kohn-Sham con metodi iterativi*. Bachelor's Thesis, unpublished, 2020.

[11] I. Cucchetti *Da densità ab initio a potenziali efficaci nucleari*. Bachelor's Thesis, unpublished, 2020.

[12] R.M. Dreizler, E.K.U., Gross. *Density Functional Theory*. Springer-Verlag, 1990.

[13] R. G. Parr, W. Yang. *Density functional theory of atoms and molecules*. Oxford University Press, 1989.

[14] R. M. Martin. *Electronic Structure: Basic Theory and Practical Methods* Cambridge University Press (2012).

[15] N. Schunck. *Energy Density Functional Methods for Atomic Nuclei*. IOP Publishing Ltd 2019.

[16] M. Bender, P. H. Heenen, P. G. Reinhard. *Self-consistent mean-field models for nuclear structure*. Rev. Mod. Phys., 75:121–180, Jan 2003.

[17] Paul C. Martin and Julian Schwinger. *Theory of Many-Particle Systems. I.* Phys. Rev. 115, 1342 (1959) – Published 15 September 1959

[18] P. Hohenberg, W. Kohn. *Inhomogeneous electron gas.* Phys. Rev., 136:B864-B871, November 1964.

[19] E. K. U. Gross, E. Runge, O. Heinonen. *Many-particle Theory.* A. Hilger, Bristol, 1991.

[20] M. Levy. *Universal variational functionals of electron densities, first-order density matrices, and natural spin-orbitals and solution of the v-representability problem.* Proc. Natl. Acad. Sci. U.S.A., 76, 1979.

[21] H. Lieb. *Density functionals for coulomb systems.* International Journal of Quantum Chemistry, 24(3):243-277.

[22] W. Kohn, L. J. Sham. *Self-consistent equations including exchange and correlation effects.* Phys. Rev., 140:A1133-A1138, Nov 1965.

[23] D. S. Jensen, A. Wasserman. *Numerical methods for the inverse problem of Density Functional Theory.* International Journal of Quantum Chemistry, 118(1):e25425.

[24] K. Burke *Perspective on density functional theory.* The Journal of chemical physics 136, 150901 (2012)

[25] P. Verma, D. G. Truhlar *Status and challenges of density functional theory.* Trends in Chemistry 2, 302–318 (2020).

[26] G. Accorto, P. Brandolini, F. Marino, A. Porro, A. Scalesi, G. Colò, X. Roca-Maza, E. Vigezzi *First step in the nuclear inverse Kohn-Sham problem: From densities to potentials.* Phys. Rev. C, 101:024315, Feb 2020.

[27] G. Accorto, T. Naito, H. Liang, T. Niksic, D. Vretenar *Nuclear energy density functionals from empirical ground-state densities.* Phys. Rev. C 103, 044304 (2021)

[28] T. Naito, D. Ohashi, H. Liang *Improvement of functionals in density functional theory by the inverse Kohn–Sham method and density functional perturbation theory.* J. Phys. B: At. Mol. Opt. Phys. 52 (2019) 245003

[29] G. Colò *Nuclear density functional theory.* Advances in Physics: X, 5:1, 1740061 (2020).

[30] R. Romano *Contributo dell'energia di correlazione all'equazione di stato della materia nucleare.* Bachelor's Thesis, unpublished, 2015.

[31] P. C. Sabatier. *Inverse problems - an introduction.* Inverse Problems, 1(1), 1985.

[32] L. C. Evans *Partial differential equations* Second Edition (Graduate Studies in Mathematics), 2010.

[33] J. Kaipio, E. Somersalo. *Statistical and computational inverse problems.* Springer, 2005.

[34] F. Marino. *Formulazione variazionale del problema inverso della DFT.* Bachelor's Thesis, unpublished, 2018.

[35] G. Accorto. *A Constrained-Minimization Method for the Solution of the Inverse Kohn-Sham Problem in Nuclei*. Master's Thesis, unpublished, 2018.

[36] R. van Leeuwen, E. J. Baerends *Exchange-correlation potential with correct asymptotic behavior*. Phys. Rev. A, 49:2421 2431, Apr 1994.

[37] J. Zenihiro, H. Sakaguchi, T. Murakami, M. Yosoi, Y. Yasuda, S. Terashima, Y. Iwao, H. Takeda, M. Itoh, H. P. Yoshida, M. Uchida. *Neutron density distributions of Pb deduced via proton elastic scattering at E= 295 mev*. Phys. Rev. C, 82:044611, Oct 2010. p204;206;208

[38] H. D. Vries, C. D. Jager, C. Vries *Nuclear charge-density-distribution parameters from elastic electron scattering*. Atomic Data and Nuclear Data Tables, 1987.

[39] A. P. Gaiduk. *Theory of Model Kohn-Sham Potentials and its Applications*. The University of Western Ontario, PhD Thesis, unpublished. 2013

[40] A. P. Gaiduk, S. K. Chulkov, V. N. Staroverov. *Reconstruction of Density Functionals from Kohn-Sham Potentials by Integration along Density Scaling Paths*. J. Chem. Theory Comput., 5, 699–707, 2009

[41] R. van Leeuwen and E. J. Baerends. *Energy expressions in density-functional theory using line integrals*. Phys. Rev. A 51, 170 (1995).

[42] S. Liu and R. G. Parr. *Expansion of the correlation-energy density functional $E_c[\rho]$ and its kinetic-energy component $T_c[\rho]$ in terms of homogeneous functionals*. Phys. Rev. A 53, 2211 (1996).

[43] G. K.-L. Chan and N. C. Handy. *Kinetic-energy systems, density scaling, and homogeneity relations in density-functional theory*. Phys. Rev. A 59, 2670 (1999).

[44] A. Nagy. *Density scaling and exchange-correlation energy*. J. Chem. Phys. 123, 044105 (2005).

[45] M. Levy and J. P. Perdew. *Hellmann–Feynman, virial, and scaling requisites for the exact universal density functionals. Shape of the correlation potential and diamagnetic susceptibility for atoms*. Phys. Rev. A 32, 2010 (1985).

[46] H. Ou-Yang and M. Levy. *Theorem for exact local exchange potential*. Phys. Rev. Lett. 65, 1036 (1990).

[47] J. P. Perdew, L. A. Constantin, and E. Sagvolden. *Relevance of the slowly varying electron gas to atoms, molecules, and solids*. Phys. Rev. Lett. 97, 223002 (2006).

[48] A. Scalesi *Teoria del funzionale della densità: dalla sezione d'urto sperimentale al potenziale di Kohn-Sham*. Bachelor's Thesis, unpublished, 2018.

[49] E. Chabanat, E. Bonche, E. Haensel, J. Meyer, R. Schaeffer. *A Skyrme parametrization from subnuclear to neutron star densities*. Nuclear Physics A 627 (1997) 710-746

[50] V. Karasiev, R. Lòpez-Boada. *Energy differences between densityfunctional-theory functional values for the near-exact and the HartreeFock densities by the line-integral method*. Phys. Rev. A 58 (3 Sept.1998), pp. 1954–1959.

[51] R. K. P. Zia, F. Redish, Edward, R. McKay, Susan *Making sense of the Legendre transform* American Journal of Physics, 2009.

[52] Y. Shi, A. Wasserman *Inverse Kohn-Sham Density Functional Theory: Progress and Challenges.* arXiv:2103.04238 (physics.chem-ph), 2021.